JPRS-UMS-92-011
28 JULY 1992

JPRS Report

Science & Technology

Central Eurasia: Materials Science

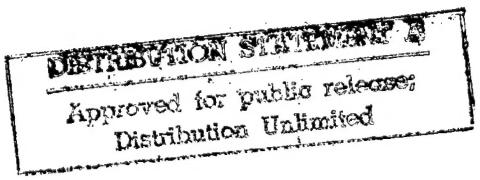

Science & Technology
Central Eurasia: Materials Science

JPRS-UMS-92-011 CONTENTS *28 July 1992*

ANALYSIS AND TESTING

Internal Structure Characteristics of Synthetic Diamond Single Crystals With Filamentary Inclusions
[Sh.A. Kurdadze, N.T. Loladze, et al.; ROSSIYSKAYA AKADEMIYA NAUK: NEORGANICHESKIYE MATERIALY, Vol 28 No 5, May 92] 1

Crystalline Structure of $Li_{12}Mg_3Si_4$ and $Li_{12}Al_3Si_4$ Compounds
[V.V. Pavlyuk, O.I. Bodak; ROSSIYSKAYA AKADEMIYA NAUK: NEORGANICHESKIYE MATERIALY, Vol 28 No 5, May 92] 1

Crystalline Structure of $Li_2Ni_{12}P_7$ and $Li_2Co_{12}P_7$ Compounds
[V.V. Pavlyuk, O.I. Bodak; ROSSIYSKAYA AKADEMIYA NAUK: NEORGANICHESKIYE MATERIALY, Vol 28 No 5, May 92] 1

Study of Thermal Transitions in $M_5Nb_3OF_{18}$ (M=NH_4, K, Rb) Ferroelectrics
[N.F. Sidorov, V.M. Mitrofanov, et al.; ROSSIYSKAYA AKADEMIYA NAUK: NEORGANICHESKIYE MATERIALY, Vol 28 No 5, May 92] 1

Study of $Cu_{2-\delta}Se$ in Solid and Liquid States by EMF Method
[V.M. Berezin, G.P. Vyarkin, et al.; ROSSIYSKAYA AKADEMIYA NAUK: NEORGANICHESKIYE MATERIALY, Vol 28 No 5, May 92] 2

Behavior of Structure and Properties of Hard Alloy Tools With Titanium Nitride Coat as Function of Ion Beam Heating During Spraying
[F.I. Shchedrina, A.A. Sklyarov, et al.; METALLURGICHESKAYA I GORNORUDNAYA PROMYSHLENNOST, No 4 (162), Oct-Dec 91] 2

Effect of Water Vapors on Electric Discharge
[V.K. Koyekin; ELEKTRONNAYA OBRABOTKA MATERIALOV, No 6 (162), Nov-Dec 91] 2

Electric Transport in Europium Oxide With CaO and ZrO_2 Additions
[V.B. Balakireva, V.P. Gorelov, et al.; ROSSIYSKAYA AKADEMIYA NAUK: SERIYA NEORGANICHESKIYE MATERIALY, Vol 28 No 4, Apr 92] 3

Isothermal Cross Section of ZrO_2-Y_2O_3-Al_2O_3 System Constitution Diagram at 1,250°C
[L.M. Lopato, L.V. Nazarenko, et al.; ROSSIYSKAYA AKADEMIYA NAUK: SERIYA NEORGANICHESKIYE MATERIALY, Vol 28 No 4, Apr 92] 3

Electron Structure of $Bi_{12}GeO_{20}$
[A.N. Kalinkin, V.M. Skorikov, et al.; ROSSIYSKAYA AKADEMIYA NAUK: SERIYA NEORGANICHESKIYE MATERIALY, Vol 28 No 3, Mar 92] 3

Relaxation Time Spectrum of Vitreous B_2O_3 in β-Transition Region
[G.M. Bartenev, V.A. Lomovskoy; ROSSIYSKAYA AKADEMIYA NAUK: SERIYA NEORGANICHESKIYE MATERIALY, Vol 28 No 3, Mar 92] 4

Electrophysical and Magnetoelectric Properties of Piezoelectric-Ferrite Type Magnetic Materials
[T.G. Lupeyko, I.B. Lopatina, et al.; ROSSIYSKAYA AKADEMIYA NAUK: SERIYA NEORGANICHESKIYE MATERIALY, Vol 28 No 3, Mar 92] 4

Effect of Film on Surface Vacancy Concentration in Crystals
[S.I. Masharov, A.S. Rybalko, et al.; POVERKHNOST: FIZIKA, KHIMIYA, MEKHANIKA, No 4, Apr 92] 4

Investigation of Effect of Ordered Target Structure in Ion-Electron Emission
[B.A. Brusilovskiy; POVERKHNOST: FIZIKA, KHIMIYA, MEKHANIKA, No 4, Apr 92] 5

On Layer-by-Layer Analysis of Chemically Active Gas Ion Impurity Profiles
[G.V. Kornich, L.O. Kornilova, et al.; POVERKHNOST: FIZIKA, KHIMIYA, MEKHANIKA, No 4, Apr 92] 5

Characteristics of X-Radiation Transport in Curved Ribbon-Shaped Waveguide
[V.A. Bushuyev, M.N. Orudzhaliyev, et al.; POVERKHNOST: FIZIKA, KHIMIYA, MEKHANIKA, No 4, Apr 92] ... 5

Assessing Reactivity of Various Types of Solid Carbon-Containing Fuel
[L.Yu. Nazyuta, T.A. Kargina, et al.; METALLURGICHESKAYA I GORNORUDNAYA PROMYSHLENNOST, No 1 (163), Jan-Mar 92] 5

Study of Nitrogen-Containing Chromium-Manganese Austenitic Steels Using Inelastic Slow Neutron Scattering
[V.G. Gavrilyuk, S.A. Danilkin, et al.; METALLOFIZIKA, Vol 13 No 12, Dec 91] 6

COATINGS

Co-Fe Coat Deposition on Aerosil by Chemical Reduction From Solution in Order to Optimize Magnetic Properties
[N.A. Khritokhin, D.V. Milchenko, et al.; ROSSIYSKAYA AKADEMIYA NAUK: NEORGANICHESKIYE MATERIALY, Vol 28 No 5, May 92] 7

Electrospark Coats on Fastening Surfaces of Ag-Ni-Graphite Contacts
[T.A. Dontsova, Ye.A. Zaytsev, et al.; ELEKTRONNAYA OBRABOTKA MATERIALOV, No 6 (162), Nov-Dec 91] . 7
Outlook for Using Electrospark Coats for Electric Contact Fastening
[L.A. Kryachko, S.P. Kokhanovskiy, et al.; ELEKTRONNAYA OBRABOTKA MATERIALOV, No 6 (162), Nov-Dec 91] 7
Combined Hard Facing of Tungsten-Free Hard Alloys by Electrospark and Thermal Diffusion Methods
[A.D. Verkhoturov, V.B. Balov, et al.; ELEKTRONNAYA OBRABOTKA MATERIALOV, No 6 (162), Nov-Dec 91] . 8
Study of Heat Exchange During Coat Deposition by Plasma Flow Condensation in Vacuum
[A.K. Vershina; ELEKTRONNAYA OBRABOTKA MATERIALOV, No 6 (162), Nov-Dec 91] 8
Mass Spectrometry Investigation of Ionized Nitrogen During Titanium Nitride Coat Synthesis
[Zh.A. Mrochek, I.A. Romanchuk, et al.; ELEKTRONNAYA OBRABOTKA MATERIALOV, No 6 (162), Nov-Dec 91] 8
Electrohydraulic Fracture of Pig Iron-Containing Slags
[V.B. Vishnevskiy, I.N. Godovannaya, et al.; ELEKTRONNAYA OBRABOTKA MATERIALOV, No 6 (162), Nov-Dec 91] 9
Production of Pyrolytic Samarium-Doped Indium Oxide Films
[M.Ya. Rakhlin, V.Ye. Rodionov, et al.; ROSSIYSKAYA AKADEMIYA NAUK: SERIYA NEORGANICHESKIYE MATERIALY, Vol 28 No 4, Apr 92] 9
Certain Structural Characteristics of $TiSi_2$ Films Produced by Annealing in Vacuum
[O.B. Yatsenko, L.Ya. Tverdokhlebova, et al.; ROSSIYSKAYA AKADEMIYA NAUK: SERIYA NEORGANICHESKIYE MATERIALY, Vol 28 No 3, Mar 92] 9
Making $B_2Sr_2CaCu_2O_x$ Films by Layer-by-Layer Spraying
[V.A. Vlasov; ROSSIYSKAYA AKADEMIYA NAUK: SERIYA NEORGANICHESKIYE MATERIALY, Vol 28 No 3, Mar 92] 10

CORROSION

Resistance of Pseudofused Titanium Carbide Powders in Sulfuric Acid and Hydrogen Peroxide Solution
[G.N. Komratov, I.D. Chausskaya, et al.; ROSSIYSKAYA AKADEMIYA NAUK: SERIYA NEORGANICHESKIYE MATERIALY, Vol 28 No 4, Apr 92] 11
Corrosion Behavior of Heterophase Sintered Materials of TiN-Cr and TiN-Ni Systems in Sulfuric Acid Solution
[T.V. Chukalovskaya, N.D. Tomashov, et al.; ZASHCHITA METALLOV, Vol 28 No 1, Jan-Feb 92] 11
Corrosion Behavior of Steel 45 Surface Alloyed With Chromium in Sulfuric and Hydrochloric Acid Solutions
[S.G. Babich, V.M. Knyazheva, et al.; ZASHCHITA METALLOV, Vol 28 No 1, Jan-Feb 92] 11
Corrosion-Electrochemical Behavior of Nickel in Aqueous Acetonitryl Perchlorate Media in Presence of Organic Bases and Acids *[V.V. Ekilik, Ye.N. Balakshina, et al.; ZASHCHITA METALLOV, Vol 28 No 1, Jan-Feb 92]* 12
Mechanism of Abnormal Corrosion Behavior of Aluminum Alloys in Concentrated Acetic Acid
[S.G. Polyakov, G.M. Grigorenko, et al.; ZASHCHITA METALLOV, Vol 28 No 1, Jan-Feb 92] 12
Protection From Two-Metal Corrosion in Steel-Titanium Pair by Microarc Oxidizing
[P.S. Gordiyenko, T.M. Skorobogatova, et al.; ZASHCHITA METALLOV, Vol 28 No 1, Jan-Feb 92] 12
Effect of Heat Treatment and Blueing on Corrosion Behavior of Sheet Steel
[V.I. Spivakov, L.V. Bogomolova, et al.; ZASHCHITA METALLOV, Vol 28 No 1, Jan-Feb 92] 13
Corrosion Rate in Electric Power Plant Pressure Tunnels
[Yu.Z. Shikhaliyev; ZASHCHITA METALLOV, Vol 28 No 1, Jan-Feb 92] 13
On Issue of Copper-Steel Clad Metal Etching
[T.S. Devyatkina, N.P. Zaykova; ZASHCHITA METALLOV, Vol 28 No 1, Jan-Feb 92] 13
High-Alloy Surfaced Layer Behavior During Low-Temperature Hydrogen Absorption
[V.M. Leybzon, V.L. Mirochnik, et al.; ZASHCHITA METALLOV, Vol 28 No 1, Jan-Feb 92] 14
St3 and Iron Electroreflection Spectra and Issue of Distinguishing Their Anodic Dissolution Kinetics
[R.M. Lazorenko-Manevich, Ye.G. Kuznetsov; ZASHCHITA METALLOV, Vol 28 No 2, Mar-Apr 92] 14
Corrosion-Electrochemical Behavior of Nickel in Sulfuric Acid Solutions
[A.E. Kozachinskiy, A.P. Pchelnikov, et al.; ZASHCHITA METALLOV, Vol 28 No 2, Mar-Apr 92] 14
Corrosion-Electrochemical Behavior of Al-Fe-Ni Bronze in Chloride Solution
[V.N. Chervyakov, L.V. Kharkova, et al.; ZASHCHITA METALLOV, Vol 28 No 2, Mar-Apr 92] 15
Effect of Lithium Doping on Aluminum's Corrosion Properties
[V.S. Sinyavskiy, A.M. Semenov, et al.; ZASHCHITA METALLOV, Vol 28 No 2, Mar-Apr 92] 15
Effect of Diamond Burnishing on Steel Kh17N15 Resistance to Chloride Corrosion Cracking
[V.S. Koropachev, V.P. Pogodin, et al.; ZASHCHITA METALLOV, Vol 28 No 2, Mar-Apr 92] 15
Electrodeposition of Ni-Re Alloys From Acetate Electrolytes
[S.I. Berezina, T.D. Keshner, et al.; ZASHCHITA METALLOV, Vol 28 No 2, Mar-Apr 92] 16
On Possibility of Using High-Intensity Electron Beam Pulses to Produce Fe-Si-Based Protective Coats
[V.I. Kolotyrkin, M.Yu. Tomashpolskiy, et al.; ZASHCHITA METALLOV, Vol 28 No 2, Mar-Apr 92] 16
Surface Composition of Ti-W Alloys After Corrosion
[I.V. Kasatkina, R.Kh. Zalavutdinov, et al.; ZASHCHITA METALLOV, Vol 28 No 2, Mar-Apr 92] 16
Effect of HCl and Molasses on Steel 12Kh18N10T Corrosion in Phosphoric Acid Solutions
[D.Kh. Kopeliovich, V.I. Ivlev; ZASHCHITA METALLOV, Vol 28 No 2, Mar-Apr 92] 17

Anodic Protection of Inner Tube Cavity of Heat Exchangers
[I.V. Bochkareva, V.T. Ivanov, et al.; ZASHCHITA METALLOV, Vol 28 No 2, Mar-Apr 92] 17
Potentiometric Sulfuric Acid Monitoring in Chemical Polishing Electrolyte
[A.I. Turashev, A.I. Samosova, et al.; ZASHCHITA METALLOV, Vol 28 No 2, Mar-Apr 92] 17
Aluminum and TsAM4-1 Alloy Corrosion in Nickel-Plating Electrolyte
[V.P. Artamonov; ZASHCHITA METALLOV, Vol 28 No 2, Mar-Apr 92] 17
Effect of Iron Impurities on Electrolytic Nickel Precipitate Structure and Properties
[G.M. Yashina, Z.S. Martemyanova, et al.; ZASHCHITA METALLOV, Vol 28 No 2, Mar-Apr 92] 18
Laser Stimulated Electrolytic Precipitation of Sn-Bi Alloy
[Yu.V. Seryanov, L.V. Aravina; ZASHCHITA METALLOV, Vol 28 No 2, Mar-Apr 92] 18

FERROUS METALS

Principal Zinc Behavior Patterns in Blast Furnaces *[Yu.P. Shchukin, V.S. Novikov, et al.; STAL, No 2, Feb 92]* 19
Development of Multijet Injectors of Natural Gas Into Blast Furnace Tuyere
[Yu.P. Mityushin, Yu.V. Fedulov, et al.; STAL, No 2, Feb 92] 19
Development of 7KhNM Steelmaking Process in Open Hearth Furnaces
[N.F. Bakhcheyev, A.F. Sarychev, et al.; STAL, No 2, Feb 92] 19
Argon Blasting of Ingot Header of Rimmed Chemically Capped Steel
[G.P. Burakovskiy, V.P. Andreyev, et al.; STAL, No 2, Feb 92] 19
Improving Killed Steel Ingot Quality *[V.P. Vozhdayev, Yu.N. Selivanov, et al.; STAL, No 2, Feb 92]* 20
Improving Steel Quality for Cold Rolled Band by Degassing
[V.I. Frolov, V.F. Sarychev, et al.; STAL, No 2, Feb 92] 20
Lowering Ferromanganese Outlays in Steelmaking *[A.I. Blokhin, Yu.N. Volshchukov, et al.; STAL, No 2, Feb 92]* ... 20
Improving Rimmed Chemically Capped Steel Quality During Casting by Using Intensifying Briquettes
[G.P. Burakovskiy, V.S. Ploshkin, et al.; STAL, No 2, Feb 92] 21
Material Balance of Ferrosilicon Smelting With Vanadium
[N.V. Tolstoguzov, S.S. Zhilyakov, et al.; STAL, No 2, Feb 92] 21
Making Steel 08Yu of Higher Drawability Classes *[S.A. Bratus, V.A. Maslennikov, et al.; STAL, No 2, Feb 92]* 21
New Type of Steel Making Vessel
[N.M. Skorokhod, N.A. Antonov, et al.; METALLURGICHESKAYA I GORNORUDNAYA PROMYSHLENNOST, No 4 (162), Oct-Dec 91] 22
Confidence Coefficient of Blast Furnace Zone Balance Analysis Data
[K.M. Bugayev; METALLURGICHESKAYA I GORNORUDNAYA PROMYSHLENNOST, No 4 (162), Oct-Dec 91] 22
Liquid Steel Treatment in Ingot Mold by Powder Wire
[V.A. Vikhlevshchuk, V.M. Chernogritskiy, et al.; METALLURGICHESKAYA I GORNORUDNAYA PROMYSHLENNOST, No 4 (162), Oct-Dec 91] 22
Mastering Alloyed Steel Steel Smelting in 350 Ton Converters Using Liquid Alloying Compositions and Ladle Refining
[L.F. Kosoy, S.I. Yaburov, et al.; METALLURGICHESKAYA I GORNORUDNAYA PROMYSHLENNOST, No 4 (162), Oct-Dec 91] 23
Metal Desulfurization in Ladle by Active Slag Mixtures
[M.A. Pozhivanov, P.M. Semenchenko, et al.; METALLURGICHESKAYA I GORNORUDNAYA PROMYSHLENNOST, No 4 (162), Oct-Dec 91] 23
Effect of Ion Irradiation on Composition and Atomic Structure of Fe-Ni System Alloys
[M.A. Vasilyev, S.D. Gorodetskiy; POVERKHNOST: FIZIKA, KHIMIYA, MEKHANIKA, No 4, Apr 92] 23
Abnormal Mass Transfer in $Fe_{70}Ni_{27}Mn_3$ Alloy Under Low-Energy Proton Irradiation
[V.A. Tsurin, A.M. Sorkin, et al.; POVERKHNOST: FIZIKA, KHIMIYA, MEKHANIKA, No 4, Apr 92] 24
Blast Furnace Restart Blowing After Extended Shutdown
[G.G. Vasyura, V.N. Dementyev, et al.; METALLURGICHESKAYA I GORNORUDNAYA PROMYSHLENNOST, No 1 (163), Jan-Mar 92] 24
Ferromanganese Smelting Using Burden With Decreased Manganese Content
[V.A. Gordiyenko, G.G. Vasyura, et al.; METALLURGICHESKAYA I GORNORUDNAYA PROMYSHLENNOST, No 1 (163), Jan-Mar 92] 24
Assimilation of Commercial Plant for Measuring Coke Combustibility at Dneprovskiy Integrated Iron and Steel Works
[A.D. Dzhigota, F.N. Moskalina, et al.; METALLURGICHESKAYA I GORNORUDNAYA PROMYSHLENNOST, No 1 (163), Jan-Mar 92] 24
Improving Quality of 8.5-Ton Killed Steel Ingots Cast With Hot Top Insulated by Heat Resistant Concrete
[M.Ya. Zavadskiy (deceased), A.Yu. Konoplyanik, et al.; METALLURGICHESKAYA I GORNORUDNAYA PROMYSHLENNOST, No 1 (163), Jan-Mar 92] 25
Lowering Top Discards of 24-Ton Killed Steel Ingots Cast With Hot Top Insulated by Heat Resistant Concrete
[Ye.G. Gryzlov, A.I. Belkin, et al.; METALLURGICHESKAYA I GORNORUDNAYA PROMYSHLENNOST, No 1 (163), Jan-Mar 92] 25

NONFERROUS METALS AND ALLOYS; BRAZES AND SOLDERS

Successive Phase Transition Kinetics in InSb Films Made by Pulse Condensation
[V.I. Petrosyan, O.I. Vasin; ROSSIYSKAYA AKADEMIYA NAUK: NEORGANICHESKIYE MATERIALY, Vol 28 No 5, May 92] 26
Electrocapillary Phenomena on Liquid Lead in Chloride Melt With Lithium and Potassium Nitrate Additions
[T.V. Valuyeva, V.B. Patrov, et al.; IZVESTIYA VYSSHIKH UCHEBNYKH ZAVEDENIY: TSVETNAYA METALLURGIYA, No 3, Jun 91] 26
Optimization of Low-Temperature Guinea Bauxite Leaching Process
[V.M. Alkatseva, V.F. Kokayeva, et al.; IZVESTIYA VYSSHIKH UCHEBNYKH ZAVEDENIY: TSVETNAYA METALLURGIYA, No 3, Jun 91] 26
Microstructure and Mechanical Properties of 20-100 kg Br013 Tin Bronze Ingots
[Yu.V. Yefimov, L.A. Ryabtsev (deceased), et al.; IZVESTIYA VYSSHIKH UCHEBNYKH ZAVEDENIY: TSVETNAYA METALLURGIYA, No 3, Jun 91] 26
Structural Recrystallization Detection During Titanium Alloy Heating in β-Region
[V.K. Portnoy, N.L. Anikanov, et al.; IZVESTIYA VYSSHIKH UCHEBNYKH ZAVEDENIY: TSVETNAYA METALLURGIYA, No 3, Jun 91] 27
On Morphology of α-Phase Plates in α+β-Ti Alloys
[T.N. Roshchina, L.A. Bunin, et al.; IZVESTIYA VYSSHIKH UCHEBNYKH ZAVEDENIY: TSVETNAYA METALLURGIYA, No 3, Jun 91] 27
Superplasticity of Al-Zn-Mg-Zr-Sc System Alloy
[A.M. Diskin, A.A. Alalykin; IZVESTIYA VYSSHIKH UCHEBNYKH ZAVEDENIY: TSVETNAYA METALLURGIYA, No 3, Jun 91] 28
On Issue of Selecting Rotary Tube Kiln Diameter
[A.M. Davidson, M.I. Akatsev; IZVESTIYA VYSSHIKH UCHEBNYKH ZAVEDENIY: TSVETNAYA METALLURGIYA, No 3, Jun 91] 28
On One Erroneous Statement Made on Book on Molten Salt Electrolysis
[A.A. Revazyan; IZVESTIYA VYSSHIKH UCHEBNYKH ZAVEDENIY: TSVETNAYA METALLURGIYA, No 3, Jun 91] 28
Er(Tm)-Fe-Ge Systems
[O.I. Bodak, O.Ya. Oleksin, et al.; ROSSIYSKAYA AKADEMIYA NAUK: SERIYA NEORGANICHESKIYE MATERIALY, Vol 28 No 3, Mar 92] 28
Investigation of Electric Properties of Bi_2Te_3 Single Crystals Doped With V and Tm
[P.N. Sherov, Kh. Mukhiddinov, et al.; ROSSIYSKAYA AKADEMIYA NAUK: SERIYA NEORGANICHESKIYE MATERIALY, Vol 28 No 3, Mar 92] 29
Niobium, Molybdenum, and Tungsten Diselenide Intercalation With Copper, Zinc, and Gallium
[L.M. Kulikov, A.A. Semenov-Kobzar, et al.; ROSSIYSKAYA AKADEMIYA NAUK: SERIYA NEORGANICHESKIYE MATERIALY, Vol 28 No 3, Mar 92] MATERIALY, Vol 28 No 3, Mar 92] 29

NONMETALLIC MATERIALS

Low-Temperature Oxidation of Zinc Sulfide Phosphor
[A.O. Dmitriyenko, L.V. Abramova, et al.; ROSSIYSKAYA AKADEMIYA NAUK: NEORGANICHESKIYE MATERIALY, Vol 28 No 5, May 92] 30
New Crystalline Phase in Li_2O-Al_2O_3-SiO_2 System and Transparent Glass Crystalline Materials on its Basis
[O.S. Dymshits, A.A. Zhilin, et al.; ROSSIYSKAYA AKADEMIYA NAUK: NEORGANICHESKIYE MATERIALY, Vol 28 No 5, May 92] 30
Effect of Hydrothermal Treatment and Subsequent Sintering on Strength of Titanium Dioxide Ceramics Prepared by Sol-Gel Method
[V.M. Chertov, T.F. Makovskaya, et al.; ROSSIYSKAYA AKADEMIYA NAUK: NEORGANICHESKIYE MATERIALY, Vol 28 No 5, May 92] 30
Concrete Effectiveness and Reliability at Elevated Activated Coarse Aggregate Consumption
[V.I. Selivanova, G.I. Zharycheva; BETON I ZHELEZOBETON, No 5 (446), May 92] 30
Crack Resistance and Strength of End Sections of Prestressed Elements With Cable Reinforcement
[N.A. Markarov, R.Sh. Sharipov, et al.; BETON I ZHELEZOBETON, No 5 (446), May 92] 31
Practical Oblique Section-Based Reinforced Concrete Wall and Beam Strength Analysis Method
[K.G. Ashkinadze; BETON I ZHELEZOBETON, No 5 (446), May 92] 31
Effect of Colmating Water-Dispersing Film-Forming Compositions on Protective Pipe Coat Quality
[G.V. Topilskiy, V.I. Melikhov, et al.; BETON I ZHELEZOBETON, No 5 (446), May 92] 31
Effect of Additives on Corrosion Resistance of Building Mortars in Man-Made Media
[V.V. Goncharov, A.M. Rozhanskaya; BETON I ZHELEZOBETON, No 5 (446), May 92] 32
Tasks of Improving Domestic Structural Design Standards
[N.A. Markarov, V.D. Grinev; BETON I ZHELEZOBETON, No 5 (446), May 92] 32
Joining of Ceramic Parts From Reaction-Bonded Silicon Nitride
[V.V. Vikulin, I.N. Kurskaya; OGNEUPORY, No 5, May 92] 32

Sialon-Containing Silicon Carbide Refractories *[N.V. Pitak, R.M. Fedoruk, et al.; OGNEUPORY, No 5, May 92]* ... 32
Resistance of Silicon Nitride-Based Hot Compacted Materials to High-Temperature Oxidation
[V.D. Borzilova, I.I. Tkacheva; OGNEUPORY, No 5, May 92] ... 33
Grinding of Certain Composition Particles in $(Al_2O_3-ZrO_2)-Y_2O_3$ System Produced by High-Speed Melt Quenching
[Yu.S. Vilk, Ye.A. Ilin, et al.; OGNEUPORY, No 5, May 92] ... 33
Making Products of Complex Configuration With Expanded Polystyrene Cores
[V.A. Ustichenko, V.V. Primachenko, et al.; OGNEUPORY, No 5, May 92] ... 33
Certification Track Record of Refractory Enterprise Technologies
[S.G. Dolgikh, A.K. Karklit; OGNEUPORY, No 5, May 92] ... 34
Mullite-Silica Glass Fiber Refractories Production and Application Analysis and Outlook for Increasing Their Output at Seversk Dolomite Plant *[I.G. Subochev, L.A. Dergaputskaya, et al.; OGNEUPORY, No 5, May 92]* ... 34
Thermal Power Plant Ash Waste-Based Facing Glass Materials
[O.A. Golozubov, N.G. Kisilenko, et al.; STEKLO I KERAMIKA, No 5, May 92] ... 34
Interrelation of Thermal and Mechanical Soda-Lime Sheet Glass Properties and Molding Parameters
[V.F. Solinov, T.V. Kaplina, et al.; STEKLO I KERAMIKA, No 5, May 92] ... 35
Characteristics of Inelastic Strain of Glass Band on Molten Metal
[V.B. Seltser, V.S. Guryanov; STEKLO I KERAMIKA, No 5, May 92] ... 35
Temperature- and Strain-Induced Optical Element Shape Distortions During Machining
[A.A. Frolov; STEKLO I KERAMIKA, No 5, May 92] ... 35
Elasticity of Silicon Nitride-Based Ceramics
[V.N. Yakovkin, V.A. Kuzmenko; STEKLO I KERAMIKA, No 5, May 92] ... 36
Silicon Nitride Milling Media for Fine Grinding of Ceramic Materials
[B.I. Kislov, L.V. Vodopyanova; STEKLO I KERAMIKA, No 5, May 92] ... 36
Porcelain Cullet as Filtering Material
[B.U. Barshchevskiy, V.M. Logvinov; STEKLO I KERAMIKA, No 5, May 92] ... 36
Characteristics of GaAs Deposition on Si Substrates From Superthin Liquid Phase in Temperature Gradient
[V.V. Dorogan, V.A. Kosyak, et al.; ROSSIYSKAYA AKADEMIYA NAUK: SERIYA NEORGANICHESKIYE MATERIALY, Vol 28 No 4, Apr 92] ... 36
$Tl_4AsS_2-As_2S_3$ System, Constitution Diagrams, and Vitrification in Some Chalcogenide Systems
[Yu.I. Vorobyev, N.G. Velikova, et al.; ROSSIYSKAYA AKADEMIYA NAUK: SERIYA NEORGANICHESKIYE MATERIALY, Vol 28 No 4, Apr 92] ... 37
Single Crystal Growth and Photoelectric Properties of New Lamellar $AgGa_{2.5}In_{2.5}S_8$ Compound
[N.A. Moldovyan; ROSSIYSKAYA AKADEMIYA NAUK: SERIYA NEORGANICHESKIYE MATERIALY, Vol 28 No 4, Apr 92] ... 37
Photoelectric and Optical Properties of $Mg_{0.5}Ga_2InS_5$ Single Crystals
[N.A. Moldovyan; ROSSIYSKAYA AKADEMIYA NAUK: SERIYA NEORGANICHESKIYE MATERIALY, Vol 28 No 4, Apr 92] ... 37
Determining Solid Solution Single Crystal Composition of $Bi_2Te_3-Sb_2Te_3-Bi_2Se_3$ System
[L.D. Ivanova, Yu.V. Granatkina, et al.; ROSSIYSKAYA AKADEMIYA NAUK: SERIYA NEORGANICHESKIYE MATERIALY, Vol 28 No 4, Apr 92] ... 38
Production of Disperse Silicon Carbide Powders by Carbothermy Method
[A.P. Petrov, V. Kevorkian, et al.; ROSSIYSKAYA AKADEMIYA NAUK: SERIYA NEORGANICHESKIYE MATERIALY, Vol 28 No 4, Apr 92] ... 38
Solid Solution Formation in SiC-BeO System During Hot Ceramics Compaction
[G.K. Safaraliyev, Yu.M. Tairov, et al.; ROSSIYSKAYA AKADEMIYA NAUK: SERIYA NEORGANICHESKIYE MATERIALY, Vol 28 No 4, Apr 92] ... 38
Using Mechanical Activation for Synthesizing High-T_c Semiconductors
[N.G. Khaynovskiy, Yu.T. Pavlyukhin, et al.; ROSSIYSKAYA AKADEMIYA NAUK: SERIYA NEORGANICHESKIYE MATERIALY, Vol 28 No 4, Apr 92] ... 39
Thermal Stability of Y-Ba-Cu-O System High-T_c Semiconductor Ceramics in Amorphous State
[V.D. Okunev, Z.A. Zamoylenko; ROSSIYSKAYA AKADEMIYA NAUK: SERIYA NEORGANICHESKIYE MATERIALY, Vol 28 No 4, Apr 92] ... 39
Interaction of $YBa_2Cu_3O_{7-\delta}$ Ceramics With $SrTiO_3$, MgO, ZrO_2 Substrates at 1,170-1,470K
[A.Yu. Musatenko, R.B. Turovskiy, et al.; ROSSIYSKAYA AKADEMIYA NAUK: SERIYA NEORGANICHESKIYE MATERIALY, Vol 28 No 4, Apr 92] ... 40
Effect of Growth Buildup Conditions on Stoichiometry in GaAs-Autoepitaxial Layer Boundary Area
[A.A. Krasnov, A.A. Akmarov, et al.; ROSSIYSKAYA AKADEMIYA NAUK: SERIYA NEORGANICHESKIYE MATERIALY, Vol 28 No 4, Apr 92] ... 40
Certain Optical Properties of $YbGa_2S_4$ Single Crystals
[G.M. Niftiyev, O.B. Tagiyev, et al.; ROSSIYSKAYA AKADEMIYA NAUK: SERIYA NEORGANICHESKIYE MATERIALY, Vol 28 No 4, Apr 92] ... 40
Bi-Containing Oxide High-T_c Semiconductors
[G.Ye. Nikiforova, V.B. Lazarev, et al.; ROSSIYSKAYA AKADEMIYA NAUK: SERIYA NEORGANICHESKIYE MATERIALY, Vol 28 No 3, Mar 92] ... 40

Epitaxial Si Layers Grown by Crystallization From Sn-Based Solution Melts
[D.I. Brinkevich, N.M. Kazyuchits, et al.; ROSSIYSKAYA AKADEMIYA NAUK: SERIYA NEORGANICHESKIYE MATERIALY, Vol 28 No 3, Mar 92] 41
Effect of Ge on Defect Formation Processes in Si
[D.I. Brinkevich, N.I. Gorbachev, et al.; ROSSIYSKAYA AKADEMIYA NAUK: SERIYA NEORGANICHESKIYE MATERIALY, Vol 28 No 3, Mar 92] 41
Effect of Growth Reagent Ratio in Vapor Phase on Nucleation Process During Epitaxial GaAs Growth on Si in $Ga(CH_3)_3$-AsH_3-H_2 System
[A.A. Krasnov, R.V. Kudryavtseva, et al.; ROSSIYSKAYA AKADEMIYA NAUK: SERIYA NEORGANICHESKIYE MATERIALY, Vol 28 No 3, Mar 92] 41
Epitaxial Growth of $InAs_{1-x-y}Sb_xBi_y$ on InSb Substrates From Bismuth Solutions
[R.Kh. Akchurin, T.V. Sakharova, et al.; ROSSIYSKAYA AKADEMIYA NAUK: SERIYA NEORGANICHESKIYE MATERIALY, Vol 28 No 3, Mar 92] 42
Production and Properties of $CuInS_3$ Semiconductor Films
[V.P. Panov, O.G. Movchan, et al.; ROSSIYSKAYA AKADEMIYA NAUK: SERIYA NEORGANICHESKIYE MATERIALY, Vol 28 No 3, Mar 92] 42
Microstructure and Superconducting Properties of $YBa_2Cu_3O_{7-x}$ Fused Ceramics With Silver Additions
[B.P. Mikhaylov, G.Ye. Nikiforova, et al.; ROSSIYSKAYA AKADEMIYA NAUK: SERIYA NEORGANICHESKIYE MATERIALY, Vol 28 No 3, Mar 92] 42
Effect of Surface Phases and Critical State Occurrence on Ceramic Formation
[Yu.P. Korostikov, V.S. Strykanov; ROSSIYSKAYA AKADEMIYA NAUK: SERIYA NEORGANICHESKIYE MATERIALY, Vol 28 No 3, Mar 92] 43
Use of Cd-Containing Fused Silica Glass in High-Temperature Thermodynamic Studies by Electromotive Force Method
[V.A. Leybov; ROSSIYSKAYA AKADEMIYA NAUK: SERIYA NEORGANICHESKIYE MATERIALY, Vol 28 No 3, Mar 92] 43
Luminescence of Cadmium Diarsenide Single Crystals
[S.F. Marenkin, A.V. Mudryy, et al.; ROSSIYSKAYA AKADEMIYA NAUK: SERIYA NEORGANICHESKIYE MATERIALY, Vol 28 No 3, Mar 92] 43
Stimulated Emission Under Electron Excitation of $ZnAs_2$ Single Crystals
[S.F. Marenkin, D.I. Pishchikov, et al.; ROSSIYSKAYA AKADEMIYA NAUK: SERIYA NEORGANICHESKIYE MATERIALY, Vol 28 No 3, Mar 92] 43
Deformation Effect in Exoemission of Dielectric Glass With Modified Surface
[L.B. Glebov, A.F. Zatsepin, et al.; POVERKHNOST: FIZIKA, KHIMIYA, MEKHANIKA, No 4, Apr 92] 44
Surface Periodic Structures in Polycrystalline Silicon Layers Recrystallized by Nanosecond Pulsed Laser Radiation
[A.V. Demchuk, V.A. Labunov; POVERKHNOST: FIZIKA, KHIMIYA, MEKHANIKA, No 4, Apr 92] 44

PREPARATION

Thermal GaAs Oxidation in 'Dopantless' and Dopant Atmosphere
[I.Ya. Mittova; ROSSIYSKAYA AKADEMIYA NAUK: NEORGANICHESKIYE MATERIALY, Vol 28 No 5, May 92] 45
Production and Study of Electrophysical Properties of $CuInSe_2$ Crystals and Films
[M.A. Abdullayev, Dzh.Kh. Amirkhanova, et al.; ROSSIYSKAYA AKADEMIYA NAUK: NEORGANICHESKIYE MATERIALY, Vol 28 No 5, May 92] 45
Thermal and Laser-Thermal Titanium Oxidation Within 773-973K Temperature Range
[L.V. Bareukova, A.M. Khoviv, et al.; ROSSIYSKAYA AKADEMIYA NAUK: NEORGANICHESKIYE MATERIALY, Vol 28 No 5, May 92] 45
Magnetic Material Films Grown by Molecular Beam Epitaxy Method
[Ye.P. Vasilyeva, L.I. Vershinina, et al.; ROSSIYSKAYA AKADEMIYA NAUK: NEORGANICHESKIYE MATERIALY, Vol 28 No 5, May 92] 46
Continuous Wave 3-μm Stimulated Emission of BaY_2F_8-Er^{3+} Crystals at Room Temperature With Semiconductor Laser Pumping
[A.A. Kaminskiy, D. Wandt, et al.; ROSSIYSKAYA AKADEMIYA NAUK: NEORGANICHESKIYE MATERIALY, Vol 28 No 5, May 92] 46

TREATMENT

$La_{1.8}Sr_{0.2}CuO_{4-\delta}$ Hydrothermal Treatment at 200-300°C and 10-70 MPa
[E.N. Korytkova, N.I. Nesterchuk, et al.; ROSSIYSKAYA AKADEMIYA NAUK: NEORGANICHESKIYE MATERIALY, Vol 28 No 5, May 92] 47
Development and Implementation of New Wide Strip Hot Rolling Process
[A.I. Starikov, V.M. Salganik, et al.; STAL, No 2, Feb 92] 47
Automation of Continuous Cold Rolling Mills *[S.I. Belov, I.V. Zalesskiy, et al.; STAL, No 2, Feb 92]* 47

Lateral Strain in Thin Strip Rolled in Twenty-High Mill
[P.I. Denisov, R.V. Fayzullina, et al.; STAL, No 2, Feb 92] 47
Decreasing Metal Losses During Rolled Stock Cutting in Section Mills
[A.G. Averchenko, A.P. Khamlov, et al.; STAL, No 2, Feb 92] 48
Making Drilling Pipes With Welded Tool Joints From Low Carbon Steel
[V.A. Rodnikov, I.G. Pogorelova; STAL, No 2, Feb 92] 48
Crack Resistance Analysis of Steel for Cold Upsetting and Extrusion
[V.N. Urtsev, V.A. Maslennikov, et al.; STAL, No 2, Feb 92] 48
Comparing Requirements for Vehicle Cardan Shaft Pipes and Ways of Improving Their Quality
[G.I. Gulyayev, K.I. Shkabatur, et al.; METALLURGICHESKAYA I GORNORUDNAYA PROMYSHLENNOST, No 4 (162), Oct-Dec 91] 49
Study of Possibility of Railroad Wheel Roll Surface Laser Hardening. In Two Parts. Part 1. Pulsed Laser Treatment
[Yu.N. Taran, V.P. Yesaulov, et al.; METALLURGICHESKAYA I GORNORUDNAYA PROMYSHLENNOST, No 4 (162), Oct-Dec 91] 49
Computer Simulation of Certain Problems of Electrochemical Machining to Size
[L. Dambrowski, E. Kozak; ELEKTRONNAYA OBRABOTKA MATERIALOV, No 6 (162), Nov-Dec 91] 49
Behavior of Quartz and Phenakite Crystals' Exoemission Properties During Radiative Transformation of Surface Structure
[A.F. Zatsepin, V.S. Kortov, et al.; POVERKHNOST: FIZIKA, KHIMIYA, MEKHANIKA, No 4, Apr 92] 50
Study of Possibility of Railroad Wheel Roll Surface Laser Hardening. Part 2: Continuous Wave Laser Emission
[Yu.N. Taran, V.P. Yesaulov, et al.; METALLURGICHESKAYA I GORNORUDNAYA PROMYSHLENNOST, No 1 (163), Jan-Mar 92] 50

WELDING, BRAZING AND SOLDERING

Thin-Walled Electric-Welded Tubes for Automotive Cardan Shafts
[K.I. Shkabatur, F.D. Davydov, et al.; METALLURGICHESKAYA I GORNORUDNAYA PROMYSHLENNOST, No 1 (163), Jan-Mar 92] 51

EXTRACTIVE METALLURGY AND MINING

Transfer Hopper Charge Level Control System of Sinter Machine
[I.M. Salnikov, V.D. Getalo, et al.; METALLURGICHESKAYA I GORNORUDNAYA PROMYSHLENNOST, No 4 (162), Oct-Dec 91] 52
Ways of Improving Deep Floor Mining Efficiency at Ingulets Ore Dressing Combine Quarry
[A.V. Krivosheyev; METALLURGICHESKAYA I GORNORUDNAYA PROMYSHLENNOST, No 4 (162), Oct-Dec 91] 52
Using Biolocation in Mining in Krivoy Rog Basin
[G.A. Libster, A.I. Chirva; METALLURGICHESKAYA I GORNORUDNAYA PROMYSHLENNOST, No 4 (162), Oct-Dec 91] 52
Detonation Wiring Network Which Expands Short-Delay Blasting Capabilities
[V.R. Dyadyushko, V.A. Zayarnyuk, et al.; METALLURGICHESKAYA I GORNORUDNAYA PROMYSHLENNOST, No 4 (162), Oct-Dec 91] 52
Ways of Improving Mining Surveys of Ore Deposits Under Cost Accounting Conditions
[B.Ye. Povnyy; METALLURGICHESKAYA I GORNORUDNAYA PROMYSHLENNOST, No 1 (163), Jan-Mar 92] 53
On Using Draglines for Hoisting Rock in Deep Quarries
[L.M. Solodovnik, S.A. Stepchenkov, et al.; METALLURGICHESKAYA I GORNORUDNAYA PROMYSHLENNOST, No 1 (163), Jan-Mar 92] 53
Underground Ore Dressing Mill Under 'Gigant' Mine Conditions
[V.I. Karamzin, S.G. Borisenko, et al.; METALLURGICHESKAYA I GORNORUDNAYA PROMYSHLENNOST, No 1 (163), Jan-Mar 92] 53

MISCELLANEOUS

Ecology of Massive Explosions in Collieries
[E.I. Yefremov, V.D. Petrenko; METALLURGICHESKAYA I GORNORUDNAYA PROMYSHLENNOST, No 4 (162), Oct-Dec 91] 54
Effect of Sociopsychological Factors on Occupational Safety
[V.T. Britan, Yu.Ye. Shulga, et al.; METALLURGICHESKAYA I GORNORUDNAYA PROMYSHLENNOST, No 4 (162), Oct-Dec 91] 54
New Diode-Pumped CW Lasers Based on Compounds With Structure of Calcium Gallogermanate With Nd^{3+} Ions
[A.A. Kaminskisy, H.R. Verdun, et al.; IZVESTIYA AKADEMII NAUK SSSR: SERIYA NEORGANICHESKIYE MATERIALY, Vol 28 No 1, Jan 92] 54

Spectral-Luminescent Properties of Laser-Active Phosphorus Oxide Chloride Based Fluids Under Excitation by Nuclear Reaction Products
[Ye.A. Seregina, P.P. Dyachenko, et al.; IZVESTIYA AKADEMII NAUK SSSR: SERIYA NEORGANICHESKIYE MATERIALY, Vol 28 No 1, Jan 92] 54
$Cu_4Rb_{0.5}K_{0.5}Br_3I_2$ Superion Conductor
[V.V. Ivanov; IZVESTIYA AKADEMII NAUK SSSR: SERIYA NEORGANICHESKIYE MATERIALY, Vol 28 No 1, Jan 92] 55

Internal Structure Characteristics of Synthetic Diamond Single Crystals With Filamentary Inclusions

927D0189E Moscow ROSSIYSKAYA AKADEMIYA NAUK: NEORGANICHESKIYE MATERIALY in Russian Vol 28 No 5, May 92 pp 969-981

[Article by Sh.A. Kurdadze, N.T. Loladze, V.P. Martovitskiy, Georgian Engineering University; UDC 529.26;548.73]

[Abstract] The importance of classifying diamond materials by their sets of topomorphous properties in various fields of science and engineering is stressed and the concepts of synthetic diamond with filamentary inclusions as crystals with a dendritic structure are examined and developed. An attempt is made to classify such synthetic diamonds by the peculiar features of their internal structure. The experimental procedure based on the method of section X-ray topography which makes it possible to study the images of the defect structure of a 10-15 μm thin crystal layer by nondestructive techniques is outlined. Electron microscope photographs and X-ray section topograms of crystals with octahedral, cubic, and cubic octahedral habits with filamentary inclusions in Mo*K* and CuK_{ga} radiation are presented. An analysis of synthetic diamonds grown in the area of thermodynamic stability and their defect structure makes it possible to identify the leading role of filamentary inclusions in the process of crystal formation. It is shown that the (100), (111), and (110) filamentary growth directions may be combined with several types of in-growth of the areas between them; moreover, one predominant filamentary direction in the crystal may change to another, as a result of which the crystals with the same habit may have several types of internal structure, depending on the growth conditions. The authors are grateful to N.A. Bulyenkov and M.I. Samoylovich for interest in the study and A.S. Vishnevskiy for providing the electron microscope photograph. Figures 5; references 21: 12 Russian, 9 Western.

Crystalline Structure of $Li_{12}Mg_3Si_4$ and $Li_{12}Al_3Si_4$ Compounds

927D0189F Moscow ROSSIYSKAYA AKADEMIYA NAUK: NEORGANICHESKIYE MATERIALY in Russian Vol 28 No 5, May 92 pp 988-990

[Article by V.V. Pavlyuk, O.I. Bodak, Lvov State University imeni I. Franko; UDC 548.736.4]

[Abstract] The $Li_{12}Mg_3Si_4$ and $Li_{12}Al_3Si_4$ compounds which crystallize as the $Cu_{15}Si_4$ structural type discovered in examining the phase equilibria in Li-Mg(Al)-Si systems at a 470K temperature whose Debye patterns are similar to those of the $Li_{15}Ge_4$ binary germanide are discussed and their structure is interpreted. To this end, samples are prepared by fusing a charge consisting of pure components in an electric arc furnace in an atmosphere of purified argon with subsequent diffusion annealing at 470K for 300 h; the crystalline structure is investigated by the powder method, diffraction patterns are plotted by a DRON-2.0 diffractometer in Fe- and Cu*K* radiation; the lattice cell parameters are refined by the least squares method (MNK); all calculations are made on an Elektronika MS-0585 computer. The atomic parameters and interatomic spacing are summarized. It is noted that smaller atoms (Mg, Al, Si) are characterized by an icosahedral coordination; the lattice constants are a=1.0688(3) nm for the compound with lithium and a=1.0620(4) nm for the compound with aluminum. Tables 3; references 3: 1 Russian, 2 Western.

Crystalline Structure of $Li_2Ni_{12}P_7$ and $Li_2Co_{12}P_7$ Compounds

927D0189G Moscow ROSSIYSKAYA AKADEMIYA NAUK: NEORGANICHESKIYE MATERIALY in Russian Vol 28 No 5, May 92 pp 991-994

[Article by V.V. Pavlyuk, O.I. Bodak, Lvov State University imeni I. Franko; UDC 548.736.4]

[Abstract] The $Li_2Ni_{12}P_7$ and $Li_2Co_{12}P_7$ isostructural compounds produced in examining the phase equilibria in Li-Ni(Co)-P systems are investigated. To this end, samples are synthesized by fusing a charge consisting of batches of pure Ni and an alloying composition of Li with P in electric arc furnace in an atmosphere of purified argon with subsequent diffusion annealing at 470K for 300 h. A single crystal is then pulled from the melt. The crystals are examined by the photographic method using RKV-86 and RGNS-2 cameras in Mo- and Cu*K* radiation, revealing a crystal structure with the lattice constants of a=0.9037(2) mm and c=0.3584(4) nm. The crystal structure is subsequently investigated by the powder method and the diffraction patterns are plotted using a DRON-3 diffractometer in Cu*K* radiation. The triangular prismatic structure packing with P atoms at the prism centers with 4Ni(Co) and 2Li in the apices of the crystalline samples is shown and the atomic parameters and interatomic spacing in the crystals are summarized. Figures 1; tables 3; references: 2 Western.

Study of Thermal Transitions in $M_5Nb_3OF_{18}$ (M=NH_4, K, Rb) Ferroelectrics

927D0189L Moscow ROSSIYSKAYA AKADEMIYA NAUK: NEORGANICHESKIYE MATERIALY in Russian Vol 28 No 5, May 92 pp 1096-1102

[Article by N.F. Sidorov, V.M. Mitrofanov, S.Yu. Stefanovich, A.F. Gutsol, V.T. Kalinnikov, Rare Elements and Mineral Raw Materials Chemistry and Technology Institute at the Kola Scientific Center of Russia's Academy of Sciences; UDC 546.882]

[Abstract] The temperature behavior of $M_5Nb_3OF_{18}$ (where M=NH_4, K, Rb) ferroelectrics is investigated by the methods of oscillatory spectroscopy and X-ray diffraction analysis in order to determine the characteristics of these compounds' structure and ordering. To this end, the infrared absorption spectra are recorded by a

Specord-M80 spectrometer, the Raman scattering (KR) spectra are excited by the 514.5 nm line of an ILA-120 Ar laser and recorded by a DFS-24 spectrometer; the lattice cell parameters are measured at various temperatures using a Sinteks R1 diffractometer. Raman scattering and infrared absorption spectra of ferroelectric polycrystals at room temperature, Raman scattering spectra in polarized radiation at 293K, and the temperature dependence of the lattice cell parameters are plotted and a fragment of the oxofluorniobate chain in a Rb-based crystal is drawn. The oscillatory spectrum frequencies are calculated and measured experimentally and the values of force constants of the oxofluorniobate chain before and after the phase transition are determined. The findings make it possible to state that the ferroelectric crystal destruction under external exposure starts in the oxofluorniobate chains and is accompanied by their rupture due to the breaking of Nb-O-Nb bridge bonds with subsequent chemical transformations. The destructive transition is also accompanied by a reversible ferroelectric phase transition at a 600K temperature. Pyrohydrolysis occurs at room temperature due to an interaction with moisture. The authors are grateful to M.B. Smirnov for making available spectrum analysis routines. Figures 5; tables 2; references 6.

Study of $Cu_{2-\delta}Se$ in Solid and Liquid States by EMF Method

927D0189M Moscow ROSSIYSKAYA AKADEMIYA NAUK: NEORGANICHESKIYE MATERIALY in Russian Vol 28 No 5, May 92 pp 1109-1110

[Article by V.M. Berezin, G.P. Vyarkin, P.I. Karikh, Chelyabinsk State Engineering University; UDC543.25]

[Abstract] The advantages and limitations of the electromotive force method (EDS) in studying copper selenide—a *p*-type semiconductor with one of the highest values of thermoelectric activity parameter at medium and high temperatures—are discussed and $Cu_{2-\delta}Se$ is examined in the liquid and solid state by the EMF method. To this end, a high-temperature solid electrolyte is produced and compact ceramic pellets are made; then the ionic and electron conduction components are measured within a broad temperature range. Data on coulometric titration of copper selenide produced at a 673K temperature in an atmosphere of argon at a 1.1×10^5 Pa pressure and the temperature dependence of the electromotive force are plotted. The break observed on the *E(T)* curve near 850 is attributed to a blurred phase transition established by Glazov *et al* while the second break near the melting point is explained as the copper reference electrode melting. The jump-like change in the EMF at the melting point is probably due to the melting enthalpy. It is noted that at low temperature, the coulometric titration curves produced with the $CuTi_2(PO_4)_3$ solid electrolyte and with the commonly used CuBr electrolyte coincide quite well. Figures 2; references 10: 7 Russian, 3 Western.

Behavior of Structure and Properties of Hard Alloy Tools With Titanium Nitride Coat as Function of Ion Beam Heating During Spraying

927D0175J Dnepropetrovsk METALLURGICHESKAYA I GORNORUDNAYA PROMYSHLENNOST in Russian No 4 (162), Oct-Dec 91 pp 50-51

[Article by F.I. Shchedrina, A.A. Sklyarov, I.V. Shevtsova, V.A. Margolius, Ferrous Metal Mechanization Scientific Production Association; UDC 669.14.018.25:539.4.015.1]:[621.78.062.26-97:669.295.5.867]

[Abstract] The behavior of the hard alloy tool structure and properties when it is heated by an ion beam during the titanium nitride coat spraying is investigated within a 800-800°C temperature range. To this end, tools are tested under plant conditions whereby the optimum ion beam heating conditions which make it possible to deposit a coat in a Bulat unit with the maximum resistance are determined. Tools made from the VK-6, T5K10, and T15K6 hard alloys are tested and metallographic, X-ray diffraction, X-ray spectral microanalysis, and fractographic studies are conducted to determine the reason for the increased tool wear. The tests demonstrate that the optimum ion beam heating temperature ranges for depositing titanium nitride coats on these tools are 650-670°C for the T5K10 and T15K6 hard alloys and 670-700°C for the VK-6 alloy. Tables 1.

Effect of Water Vapors on Electric Discharge

927D0174H Chisinau ELEKTRONNAYA OBRABOTKA MATERIALOV in Russian No 6 (162), Nov-Dec 91 pp 38-41

[Article by V.K. Koyekin, Kovrov Instrument Making Plant]

[Abstract] The effect of electric fields (EP) on hydrogen-containing molecules and their associates, particularly molecules with such polar groups as H_2O and the effect of water vapor on electric discharge are discussed. An experimental unit for examining the effect of H_2O vapor on electric discharge at an atmospheric pressure consisting of an UPU-10 high-voltage source with analog voltage control within a 0-10 kV range, an M265M microammeter, and an S-196 kilovoltmeter is described, its block diagram is cited, and its operating principle is outlined. Point-point (O-O) and point-plate (O-P) electrodes are used in the experiment. The voltage-current characteristics of the discharge at +20°C for both types of electrodes at low and saturation H_2O concentrations and the dependence of the ionization coefficient ratio to the gas pressure and electric field strength on the electric field strength to pressure ratio are plotted. Schematic diagrams of the electrode configurations are cited. Three mechanisms of knocking out electrons from the molecules are considered: by an electron impact, by an ion impact, and by light quanta, i.e., photoionization. An analysis of the findings obtained at a 4 mm gap between

pure carbon and iron electrodes without condensation shows that electron impact is the principal source of electrons and positive ions in gaseous discharges and determines, as a rule, the possibility of the discharge process itself; ionization by the ion impact is likely only at energies of several keV while photoionization is also unlikely due to the limited size of the lab installation. The results can be used in atmospheric electricity physics for explaining the mechanism of space charge accumulation in the cloud as well as commercial units for enhancing the process of heat and mass transfer by electric fields. Figures 4; references 7.

Electric Transport in Europium Oxide With CaO and ZrO_2 Additions

927D0173J Moscow ROSSIYSKAYA AKADEMIYA NAUK: SERIYA NEORGANICHESKIYE MATERIALY in Russian Vol 28 No 4, Apr 92 pp 822-825

[Article by V.B. Balakireva, V.P. Gorelov, Ye.M. Bernikova, Electrochemistry Institute at the Urals Department of Russia's Academy of Sciences; UDC 541.135.4]

[Abstract] The origin of ion transport in europium oxide with 0.1-5.0 percent CaO and 0.3-3.0 percent ZrO_2 additions is investigated allowing for the possibility of the proton conduction appearance due to the interaction of the material with the hydrogen-containing atmosphere; to this end, conductivity is measured at a 550-1,050°C temperature within an oxygen pressure range of 2.1 x 10^{-1}-10^{-11} Pa and a water vapor pressure range of 0.6-7.0 kPa. The mixtures for the study are prepared from the EvO-1 europium oxide with OSCh 17-2-grade calcium carbonate or pure-grade zirconium dioxide. Isothermal curves of the total electric conductivity and its ion and proton components at various temperatures and pressures, the temperature dependence of conductivity and the ion and proton components of europium oxide with CaO and ZrO_2 in the air at various temperatures and pressures, the dependence of the total conductivity on the water vapor pressure of europium oxide with CaO and ZrO_2 additions in various concentrations, and the dependence of conductivity on the oxygen pressure for the same compositions are plotted. The dependence of the proportion of proton conduction on the sample temperature and composition in the air is summarized. An analysis of the cubic *C*-solid solutions forming due to the dissolution of calcium and zirconium oxide shows that in the air, samples with ZrO_2 additions are mixed ion-hole semiconductors with an up to 50 percent ion transport at 1,000°C while in a reducing atmosphere they are *n*-type semiconductors; moreover, proton conduction is not found within the entire temperature range. Samples with CaO additions in the air are largely *p*-type semiconductors while proton conduction reaches 50 percent in a reducing medium. The maximum proton conduction reaches 1.13 x 10^{-3} siemens/cm. A weak dependence of *p*-type conduction on the water vapor pressure is noted. Figures 4; tables 2; references 5: 4 Russian, 1 Western.

Isothermal Cross Section of ZrO_2-Y_2O_3-Al_2O_3 System Constitution Diagram at 1,250°C

927D0173K Moscow ROSSIYSKAYA AKADEMIYA NAUK: SERIYA NEORGANICHESKIYE MATERIALY in Russian Vol 28 No 4, Apr 92 pp 835-839

[Article by L.M. Lopato, L.V. Nazarenko, G.I. Gerasimyuk, A.V. Shevchenko, Institute of Materials Science Problems imeni I.N. Frantsevich at the Ukrainian Academy of Sciences; UDC 546.651/659]

[Abstract] The outlook for using the ZrO_2-Y_2O_3-Al_2O_3 system for developing materials with elevated physical and mechanical characteristics and the seeming inadequacy of available data on the isothermal cross sections of the system's constitution diagram due to obvious violations of Gibbs's rule prompted an investigation of phase equilibria in the system at a 1,250°C temperature—a point at which ceramic materials are usually annealed. A phase equilibria diagram of the system at 1,250°C, the lattice constant behavior of fluorite-type *C*-oxide solid solutions of rare earth elements (RZE) as a function of the solution composition, and X-ray patterns of samples annealed at 1,250°C for 1,800 h are plotted and the phase composition of the system is tabulated. Phase field boundaries are determined by the annealing and hardening method. At a >33 percent Y_2O_3 concentration, phase equilibria in the system do not differ from those at 1,650°C. As in a binary system, the Z_3Y_2 compound does not have a homogeneity domain. Altogether, the isothermal cross section of the ZrO_2-Y_2O_3-Al_2O_3 system at 1,250°C is characterized by seven two-phase and six three-phase regions while no new phases are discovered in the system. Figures 3; tables 1; references 5: 2 Russian, 3 Western.

Electron Structure of $Bi_{12}GeO_{20}$

927D0172K Moscow ROSSIYSKAYA AKADEMIYA NAUK: SERIYA NEORGANICHESKIYE MATERIALY in Russian Vol 28 No 3, Mar 92 pp 558-562

[Article by A.N. Kalinkin, V.M. Skorikov, A.A. Soldatov, General and Inorganic Chemistry Institute imeni N.S. Kurnakov at Russia's Academy of Sciences; UDC 537.37]

[Abstract] Extensive uses of $Bi_{12}GeO_{20}$ single crystals in optoelectronics and holography due to their high photosensitivity, piezoelectric properties, and optical activity prompted a cluster analysis of $Bi_{12}GeO_{20}$ by means of relativistic self-consistent *X* analysis by the relativistic values (RV) method. Atomic orbitals (AO) are calculated in the Dirac-Slater approximation. A $Bi_{12}GeO_{20}$ cluster in an *xy*-projection, electron spectra of $Bi_{12}GeO_{20}$ clusters and BiO_7^{-11} clusters, and electron state density, reflection spectrum, and imaginary part of dielectric permittivity of $Bi_{12}GeO_{20}$ are plotted. The analysis of clusters with a dot symmetry in germanosillenite and a study of the effective charge on the atoms and the

character of hybrid orbitals attest to strong hybridization in the Bi-O(1) sublattice which is responsible for the optical properties of $Bi_{12}GeO_{20}$. Analytical doublets of the Bi and Ge ground levels are consistent with the atomic values and XPS spectrum. Figures 3; tables 3; references 12: 7 Russian, 5 Western.

Relaxation Time Spectrum of Vitreous B_2O_3 in β-Transition Region

927D0172L Moscow ROSSIYSKAYA AKADEMIYA NAUK: SERIYA NEORGANICHESKIYE MATERIALY in Russian Vol 28 No 3, Mar 92 pp 622-628

[Article by G.M. Bartenev, V.A. Lomovskoy, Physical Chemistry Institute at Russia's Academy of Sciences; UDC 539.21.213]

[Abstract] The vitreous structure of B_2O_3—a linear inorganic polymer—and its difference from the SiO_2 reticular structure and the internal friction spectra of vitreous boron oxide are discussed and an attempt is made to find the continuous relaxation time spectrum corresponding to β-relaxation on the basis of the internal friction spectrum. A formula is derived for the temperature dependence of the tgδ loss factor in the β-relaxation region and the internal friction spectra of vitreous B_2O_3 at various frequencies in a vacuum, the temperature-frequency diagram of vitreous B_2O_3, and a segment of the internal friction spectrum in the β-transition region are plotted. Continuous relaxation time spectra of the β- and δ-processes in vitreous B_2O_3 at various frequencies are constructed. A change in frequency leads to a spectral curve reordering. It is noted that β- and α-relaxation spectra tend to a δ-function; while α-relaxation is due to the mobility of large boron-oxygen chain segments, β-relaxation is related to the small-scale movement of small chain fragments. The lower the frequency and temperature, the wider the α- and β-relaxation time spectra, the clearer their delineation, and the greater their shift toward longer time values. Figures 4; references 14: 8 Russian, 6 Western.

Electrophysical and Magnetoelectric Properties of Piezoelectric-Ferrite Type Magnetic Materials

927D0172M Moscow ROSSIYSKAYA AKADEMIYA NAUK: SERIYA NEORGANICHESKIYE MATERIALY in Russian Vol 28 No 3, Mar 92 pp 632-636

[Article by T.G. Lupeyko, I.B. Lopatina, I.V. Kozyreva, L.A. Derbaremdiker, Rostov State University and Scientific Research Institute of Physical and Organic Chemistry; UDC 537.228.1]

[Abstract] Interest in piezoelectric-magnetostrictive ferrite composites, e.g., lead zirconate titanate (TsTS), as magnetic field transducers which are also capable of an inverse electric signal to magnetic field transformation is discussed and the electrophysical and magnetoelectric properties if Ni-Co-Fe-O and lead zirconate titanate composites, e.g., PKR-7m and TsTS-36, are studied. The experimental specimens are produced by hot compaction of components which are synthesized beforehand by the ceramic method. To prevent cracking and lower the sintering temperature, 1-10 percent glass is added to the composition. The sample phase composition is monitored by X-ray phase analysis using a DRON-2.0 diffractometer in Cu*K* radiation while the composite microstructure is examined by the replica method under an EMV-100LV electron microscope. The microprobe analysis is carried out in an REMMA-200 scanning electron microscope and the electrophysical properties are examined pursuant to GOST 12370-80. The magnetoelectric sensitivity is measured by a special transducer. The microstructure of the ceramic composite with a $(1-x)BaTiO_3+xNi_{0.9}Co_{0.1)etFe_2}O_4$ composition at various x is cited and the concentration dependence of resistivity, dielectric loss tangent, and dielectric permittivity of various composite materials, the dependence of the piezoelectric moduli, Poisson ratio, speed of sound, elastic pliability, and Young modulus of various composites, and the concentration dependence of the magnetoelectric sensitivity are plotted. An analysis of the findings shows that the use of lead zirconate titanate materials in magnetoelectric composite materials ensures their high sensitivity to alternating magnetic fields while the chemical interaction of piezoelectric materials with ferrites complicates the deliberate component selection for highly efficient magnetoelectrics. The above materials are also characterized by a noticeable piezoelectric effect. Figures 4; references 4: 1 Russian, 3 Western.

Effect of Film on Surface Vacancy Concentration in Crystals

927D0171A Moscow POVERKHNOST: FIZIKA, KHIMIYA, MEKHANIKA in Russian No 4, Apr 92 pp 26-30

[Article by S.I. Masharov, A.S. Rybalko, D.A. Safarov, Urals Polytechnic Institute, Yekaterinburg; UDC 548.313.3:541.123]

[Abstract] The effect of the surface state of solids on their physical, chemical, and mechanical properties is discussed and the vacancy concentration on the film/crystal interface and the film itself is calculated. The problem is characterized in that the film/crystal system is not thermodynamically in an equilibrium state since equilibrium is realized in the system only in the case of a uniform spatial distribution of the film and crystal atoms; in our case, there is a slow interdiffusion of atoms. The particular case where the film is applied to the surface of a monoatomic crystal is considered and the analysis is performed in the framework of a triplanar film model and a uniplanar model of the interface assuming that the film and the crystal have the same crystal structure. The conditions are formulated under which the presence of film on the surface leads to a change in surface vacancies

in both directions. The conclusion is drawn that deposition onto the surface crystal of a film from a substance with a higher vacancy formation energy leads to a decrease in the defect level on the surface. References 4.

Investigation of Effect of Ordered Target Structure in Ion-Electron Emission

927D0171B Moscow POVERKHNOST: FIZIKA, KHIMIYA, MEKHANIKA in Russian No 4, Apr 92 pp 31-37

[Article by B.A. Brusilovskiy, Scientific Research Institute of Nuclear Physics at the Moscow State University imeni M.V. Lomonosov; UDC 537.534.9]

[Abstract] The study of the patterns of kinetic ion-electron emission from the surface of ordered solids (*Zhurnal tekhnicheskoy fiziki* Vol. 44 No. 1, 1974 and Vol. 46 No. 11, 1976 and *Poverkhnost* Nos. 3 and 4, 1987, No. 2, 1988, No. 8, 1990, and No. 2, 1991) is continued. The mechanism by which the ordered target structure affects the electron emission and the issue of the crystallographic directions and planes which have a special relation to the electron emission are discussed. It is noted that the theory of ion-electron emission used in describing the patterns of electron emission from the surface of single crystals under ion irradiation has too many parameters which are picked empirically. The angular dependence of the ion-electron emission coefficient of a Mo single crystal is examined and the $\gamma(\beta, \varphi)$, $\Gamma(\beta, \varphi)$, and $\Gamma(\psi_p, \varphi)$ surfaces of the ion electron emission coefficient and the $\Gamma(d)$ dependence are plotted an an experimental unit which made it possible to rotate the target around two perpendicular axes is described. A comparison of the experimental results and theoretical data reveals that both the experimental and theoretical relations are an increasing function of the atomic series parameter; it is speculated that some conclusions drawn in the theory of ion-electron emission based on the crystal transparency model relative to the incident beam are consistent with the experiment. Figures 4; references 10: 9 Russian, 1 Western.

On Layer-by-Layer Analysis of Chemically Active Gas Ion Impurity Profiles

927D0171C Moscow POVERKHNOST: FIZIKA, KHIMIYA, MEKHANIKA in Russian No 4, Apr 92 pp 38-42

[Article by G.V. Kornich, L.O. Kornilova, S.V. Teplov, Donetsk State University; UDC 620.193.6:533.924]

[Abstract] The increasing importance of quality control of multilayered structures due to their miniaturization and a multielement integrated circuit development trend prompted an investigation of a phenomenological model of the layer-by-layer ion analysis by means of oxygen atoms which takes into account the binding of the magnesium impurity atoms by the bombarding ions in the silicon matrix. The model is described and the profile evolution of the two-layered impurity Mg system in a Si matrix as a result of layer-by-layer analysis by O^+ and Ne^+ ions at various flux densities is plotted. The findings obtained in the framework of the proposed model are quite consistent with Hues's and Willams's data according to which the use of oxygen ions makes it possible noticeably to improve the attenuation depth for the Ca-Si and Mg-Si two-layered system due to the higher Ca and Mg affinity for oxygen that Si. It is speculated that the use of oxygen will thus improve the resolution and sensitivity of the layer-by-layer analysis method. The authors are grateful to R.P. Webb for providing the SUSPRE routine. Figures 2; references 21: 7 Russian, 14 Western.

Characteristics of X-Radiation Transport in Curved Ribbon-Shaped Waveguide

927D0171F Moscow POVERKHNOST: FIZIKA, KHIMIYA, MEKHANIKA in Russian No 4, Apr 92 pp 69-75

[Article by V.A. Bushuyev, M.N. Orudzhaliyev, S.R. Sarkisov, E.R. Sarkisov, Moscow State University imeni M.V. Lomonosov and All-Union Scientific Research Institute of Engineering Physics and Radio Engineering Measurements, Moscow; UDC 548.732]

[Abstract] The need for efficient X-ray optics designs capable of bending and rotating hard X-radiation at a wavelength of close to 1 angstrom by utilizing the multiple total external reflection (PVO) phenomenon prompted a study of X-radiation transport in curved ribbon-shaped waveguides (LV); to this end, the dependence of the ribbon-shaped waveguide transmissivity on the turning angle, the angle of the beam incidence upon the outlet face, on the ribbon-shaped waveguide channel width, and on the root mean square profile roughness height of the waveguide walls is investigated. The angular dependence of the Mo*K* radiation intensity on the outlet of the curved slotless collimator is manifestly nonmonotonic. A comparison of experimental and theoretical data shows that the use of ribbon waveguides and X-ray optics systems is preferable to capillary systems in a number of cases; moreover, transporting a slightly diverging X-ray beam with the help of numerous ribbon-type waveguides is a simpler task than that in a capillary system. It is shown that in addition to the above task, ribbon waveguides may be used for examining the real structure of the smooth surface. Figures 4; references 13.

Assessing Reactivity of Various Types of Solid Carbon-Containing Fuel

927D0170F Dnepropetrovsk METALLURGICHESKAYA I GORNORUDNAYA PROMYSHLENNOST in Russian No 1 (163), Jan-Mar 92 pp 20-23

[Article by L.Yu. Nazyuta, T.A. Kargina, O.V. Filonov, V.S. Chuprina, Mariupol Metallurgy Institute, Ukrainian State Metallurgy and Coal Industry Directorate,

and InFOU at Ukrainian Academy of Sciences; UDC 669.184:[662.64/.66:543.878.003.12]

[Abstract] The use of various carbon-containing additional heat and mass transfer agents—the carbonizers—in steelmaking, e.g., coke, graphite, and secondary carbonaceous materials, especially in the converter process, and the role of these agents' reactivity in characterizing the properties of equipment are discussed. A block diagram of a plant for measuring the reactivity of coke is cited and the chemical composition and data of technical analysis of various types of fuel as well as the reactivity of some carbon-containing solid fuel are summarized. Fuel reactivity (RS) is studied using differential thermogravimetric (DTGA) analysis whereby the specific rate (or rate constant) and activation energy of the process of solid carbonaceous fuel gasification by CO_2 are used as criteria for estimating reactivity. The effect of the process temperature and metamorphism on the carbon-containing fuel reactivity is demonstrated and it is shown that at a 1,000°C standard analysis temperature, solid fuel reactivity decreases with an increase in the metamorphism degree, i.e., the ordering of the carbon structure, while at the converting temperature, reactivity becomes steady and is determined by the coke residue structure. Figures 2; tables 2; references 2.

Study of Nitrogen-Containing Chromium-Manganese Austenitic Steels Using Inelastic Slow Neutron Scattering

927D0127A Kiev METALLOFIZIKA in Russian Vol 13 No 12, Dec 91 pp 29-34

[Article by V.G. Gavrilyuk, S.A. Danilkin, V.P. Minayev, V.V. Sumin, Yu.N. Yagodzinskiy, Institute of Physics of Metals at the Ukrainian Academy of Sciences, Energy Physics Institute, Obninsk, and Department of the Physicochemical Institute imeni L.Ya. Karpov, Obninsk; UDC 539.2]

[Abstract] Applications of inelastic slow neutron scattering (NRN) for studying the phonon spectrum of crystals and then reconstructing the force interaction or interaction potential in the metal-metal, metal-nitrogen, and nitrogen-nitrogen systems in steel are discussed and the interatomic force interaction is investigated in the Cr-Mn austenite as a function of the N and Mn concentration. To this end, phonon spectra of steels Kh18AG10 with 0.4 percent N by mass, Kh18AG15 with 0.6 percent N by mass, and Kh18AG20 with 1.14 percent N by mass are recorded by the inelastic slow neutron scattering method and the composition, structure, and basic spectral characteristics of these steels are summarized. The effect of nitrogen on the metallic bond and the characteristics of the metal-nitrogen and nitrogen-nitrogen interaction are established. It is shown that the metal-nitrogen force constant in Cr-Mn austenite is 50 percent higher than the metal-carbon constant in Fe-Mn or Fe-Ni austenite while the addition of nitrogen weakens the metal-metal bond according to Grueneisen law due to the austenite lattice expansion. It is speculated that the concentration dependence of the local mode half-power width cannot be attributed solely to the indirect strain interaction and that direct interaction and other factors, such as Cr-N and Mn-N interactions, also contribute to the local nitrogen oscillation broadening; the need for further studies of nitrogen and carbon behavior within the same lattice cell is emphasized. Figures 1; tables 1; references 12.

Co-Fe Coat Deposition on Aerosil by Chemical Reduction From Solution in Order to Optimize Magnetic Properties

927D0189H Moscow ROSSIYSKAYA AKADEMIYA NAUK: NEORGANICHESKIYE MATERIALY in Russian Vol 28 No 5, May 92 pp 995-999

[Article by N.A. Khritokhin, D.V. Milchenko, A.A. Kudryavtsev, A.Ya. Yuffa, Tyumen State University; UDC 621.793.3]

[Abstract] The shortcomings of halide sorption from the gaseous phase with subsequent reduction by hydrogen for the purpose of metallizing the aerosil surface due to the insufficient volatility of a number of transition metal halides prompted a study which established that disperse silica, e.g., aerosil, can be metallized with the help of sodium borohydride even without preliminary activation by sorption of palladium compounds. Attempts to optimize the magnetic properties of silica, particularly aerosil, used in metal-polymer composites, by depositing Co-Fe coats from a solution by chemical reduction whereby the coercive force H_c serves as the optimization variable are described. Sodium borohydride is used as the hydrogen-containing reducing agent while aerosil with a specific surface of 180 m^2/g is used as the substrate. The initial metallization solution is similar to the one used for depositing Ni-Fe coats. The ferromagnetic characteristics are investigated by by the hysteresis loop produced in a 60 kA/m field at a 50 Hz frequency. A 2^8 factorial experiment is conducted and a regression analysis is carried out on an Iskra 1030 II microcomputer (PK); two factors are manipulated in the experimental design: the annealing duration and temperature. The samples' ferromagnetic characteristics, i.e., the dependence of the coercive force and hysteresis loop rectangularity (PPG) on the annealing temperature is plotted. A threefold coercive force increase is attained as a result of optimization. The findings demonstrate that annealing of metallized aerosil to 200-350°C additionally increases the coats' magnetic hardness. Figures 1; tables 5; references 6: 4 Russian, 2 Western.

Electrospark Coats on Fastening Surfaces of Ag-Ni-Graphite Contacts

927D0174B Chisinau ELEKTRONNAYA OBRABOTKA MATERIALOV in Russian No 6 (162), Nov-Dec 91 pp 15-17

[Article by T.A. Dontsova, Ye.A. Zaytsev, G.N. Braterskaya, Institute of Materials Science Problems at the Ukrainian Academy of Sciences, Kiev]

[Abstract] The need to save precious metals used for making contacts in switching devices, e.g., the KMK-A10, KMK-A-20, KMK-A32, and KMK-A10M electric contacts which contain a pure Ag sublayer necessary for ensuring the strength of the welded joint with the contact holder, prompted an examination of the possibility of applying an Ag-containing sublayer by the electrospark alloying (EIL) method; the study is carried out at the Institute of Materials Science Problems at the Ukrainian Academy of Sciences (IPM). Consequently, the possibility of using electrospark coats as the backing layer on Ag-Ni-graphite electric contact materials is investigated. To this end, the Ni content in a series of such materials is manipulated within 5-50 percent by mass and the graphite content—within 3-5 percent. The materials are made by powder metallurgy. The effect of additives to the contact materials (the base) and electrodes which form the backing on the characteristics of mass transport during electrospark alloying in an Elitron-22 unit is analyzed and the behavior of the cathode mass as a function of the base composition with changes in the electrode content and a bar chart of the dependence of the cathode mass change on the electrode material, electrospark current, and graphite concentration in the Ag+30 percent Ni+graphite base are plotted. A microphotograph of the coats is cited and their energy spectra during electrospark alloying of a Ag+30 percent Ni+graphite base are plotted. It is noted that the use of Ni-based composites makes it possible to increase the mass transfer by two- to threefold compared to pure Ni electrodes and reduce the coat thickness. Pilot tests of contact assemblies show that composite coats in place of pure silver backing make it possible to ensure the strength stability of the welded joint. The use of electrospark coats makes it possible not only to save silver but also ensure the strength of the welded and soldered contact joints with the holder. Figures 4; references 2.

Outlook for Using Electrospark Coats for Electric Contact Fastening

927D0174C Chisinau ELEKTRONNAYA OBRABOTKA MATERIALOV in Russian No 6 (162), Nov-Dec 91 pp 18-20

[Article by L.A. Kryachko, S.P. Kokhanovskiy, V.A. Korobskiy, Institute of Materials Science Problems at the Ukrainian Academy of Sciences, Kiev]

[Abstract] Successful experience in substituting the silver backing of electric contacts with nickel for fastening contacts from a Ag-CdO composite is discussed and the conditions necessary for applying electrospark coats to 6 mm dia. contacts from Ag-CuO and Ag-Ni-C composites prepared from a mechanical mixture of components during alloying with Ag and Ni electrodes with a 2 mm diameter in Elitron-12, Elitron-22, and Yelfa-541 units are investigated. To this end, the cathode and anode mass variation is recorded with the help of VLA-200-M scales at a 0.5 min alloying interval over a 2 min process, the coat thickness and its adhesion are monitored in metallographic sections under a Neophot-2 microscope, and the surface morphology is examined by a Stereoscan S4-10 scanning electron microscope. The dependence of the total cathode mass gain and mass transport coefficient on the duration of Ag-CuO composite contact alloying by a silver electrode is plotted and the behavior of the cathode and anode mass during electrospark alloying of Ag-Ni-C composite contacts by a nickel electrode are summarized. The contact assemblies are

tested for the welded force (shear strength): it ranges from 1,200 N for Ag-Ni-C to 2,400 N for Ag-CuO, regardless of the coat material. The surface morphology and contact microstructure are shown. The findings confirm the possibility of expanding the range of electric contacts with electrospark coats for welded joints, including silverless, making it possible not only to save precious metals but also improve the adhesion quality of the contact and the base and increase the operating reliability of electrical devices. Figures 3; tables 2; references 2.

Combined Hard Facing of Tungsten-Free Hard Alloys by Electrospark and Thermal Diffusion Methods

927D0174D Chisinau ELEKTRONNAYA OBRABOTKA MATERIALOV in Russian No 6 (162), Nov-Dec 91 pp 12-16

[Article by A.D. Verkhoturov, V.B. Balov, D.S. Guzanov, N.M. Potapova, Machine Science and Metallurgy Institute at the Far Eastern Department of Russia's Academy of Sciences, Komsomolsk-na-Amure]

[Abstract] The increasing scarcity of tungsten-containing sources and the resulting need for tungsten-free or low-tungsten tool materials Ti(C; N)-based steels and hard alloys, e.g., KNT, as well as the poor endurance properties of KNT-type alloys prompted a study of comprehensive processing of KNT-type alloys by means of electrospark hard-facing of the alloy surface with carbon or metals in order to saturate the surface with these elements, develop their structure, and produce the necessary metal state for facilitating diffusion during subsequent chemical heat treatment. This treatment makes it possible to build up the coat thickness and continuity by creating wear resistant and temperature resistant phases and relaxing internal stresses. Cutting tips from the KNT-16 hard alloy are hardened according to GOST 19052-80. The Elitron-22 unit is used for primary hard facing. Subsequent tip treatment is performed by diffusion hardening by the contact method in mixtures containing additions of the PN77Kh15S3R5 Cr-containing powder. The microhardness distribution in the surface layer of the KNT-16 hard alloy after various stages of additional treatment, the specific sample mass variation during the KNT-16 hard alloy heating to 650°C after additional treatment, and the endurance behavior of the KNT-16 alloy with and without additional treatment during face turning of steel 45 are plotted. The study confirms the possibility of improving the performance of the KNT-16 tungstenless alloy by using comprehensive working surface treatment consisting of electrospark hard facing with carbon and subsequent diffusion hardening with Cr powder under heating to 1,000-1,025°C. The use of a combination of the above methods makes it possible to control the wear resistance of hard alloy tools and improve the tool accuracy. Figures 3; references 6.

Study of Heat Exchange During Coat Deposition by Plasma Flow Condensation in Vacuum

927D0174E Chisinau ELEKTRONNAYA OBRABOTKA MATERIALOV in Russian No 6 (162), Nov-Dec 91 pp 21-24

[Article by A.K. Vershina, Engineering Physics Institute at the Belarussian Academy of Sciences, Minsk]

[Abstract] The expanding applications of, and improving prospects for using various coats in different branches of industry warrant an investigation of coat application by condensing plasma flows in a vacuum onto a base heated to a certain temperature. The problem of determining the temperature field in the base/coat system allowing for the coat thickness buildup is considered and the buildup conditions are studied. A mathematical model of the heat transfer process in the base/coat system is derived and the behavior of the temperature on the coat and base contact during the base rotation at a 2 RPM speed in a carousel for various deposited coat depths, the contact temperature behavior at various rotation speeds for a 10^{-4} m thick coat, and the contact temperature behavior as a function of the speed of the base spinning around its axis as a function of the carousel rotation speed are plotted. The problem of finding the temperature pattern in the base and the coat is reduced to solving a system of first-order ordinary differential equations. Figures 3; references 6.

Mass Spectrometry Investigation of Ionized Nitrogen During Titanium Nitride Coat Synthesis

927D0174F Chisinau ELEKTRONNAYA OBRABOTKA MATERIALOV in Russian No 6 (162), Nov-Dec 91 pp 25-28

[Article by Zh.A. Mrochek, I.A. Romanchuk, M.M. Semenkevich, Engineering Physics Institute at the Belarussian Academy of Sciences, Minsk]

[Abstract] The effect of the processes occurring in the bulk and on the electrodes during the coat deposition by the electric arc method on the temperature and coat deposition rate as well as the physical and mechanical properties of the coat is discussed and the shortcomings of existing mass spectrometry methods used for analyzing the metallic ion component in the vacuum arc plasma are noted. A new mass spectrometry method of studying the metal and gaseous ionized components using plasma transport in a curvilinear plasma guide is described and the intensity of ionized atomic N and Ti lines as a function of the reaction gas pressure is measured. The experiment is conducted in a VU-1 unit using an MX7303 RF monopole mass spectrometer whose sensor is evacuated by an NMDO-0.16 magnetic pump. The dependence of the singly and doubly charged Ti ion current on the plasma guide potential at various static plasma guide magnetic fields and current densities, the dependence of the singly and doubly charged Ti ion current on the magnetic field strength inside the plasma

guide at various plasma guide potentials, and the dependence of the singly and doubly charged Ti ion current, atomic N ion current, and the coat growth rate on the nitrogen pressure are plotted. The correlation of the ion current and titanium nitride coat growth rate with the nitrogen pressure points toward the active role of ionized nitrogen atoms in the coat forming; it is shown that an unambiguous conclusion about the effect of any single type of active particle calls for measuring the quantities of these particles and the coat growth rate under identical experimental conditions. Figures 3; references 8.

Electrohydraulic Fracture of Pig Iron-Containing Slags

927D0174G Chisinau ELEKTRONNAYA OBRABOTKA MATERIALOV in Russian No 6 (162), Nov-Dec 91 pp 29-30

[Article by V.B. Vishnevskiy, I.N. Godovannaya, N.M. Parkhomenko, A.I. Chuyko, Institute of Materials Science Problems at the Ukrainian Academy of Sciences, Kiev]

[Abstract] The shortcomings and limitations of traditional methods of mechanical slag grinding using conventional equipment, e.g., crushers and screens, the difficulty of breaking up slag lumps larger than 1,000-1,200 mm in size, and the large amount of dust generated in the process are outlined and the results of fracture tests of slag conglomerates in water with subsequent sorting of the metallic and ceramic components by separation are discussed. Pig iron-containing slag is used in the experiment whereby the slag conglomerate size does not exceed 88-100 mm. Electric exposition with a pulse energy of 0.8-1.0 kJ is used to break up the lumps. The behavior of the working media resistivity as a function of the slag:water ratio and the number of pulses, the behavior of the CaO concentration in the slurry as a function of the slag:water ratio and the number of pulses, the magnetic component content in pig iron-containing slag conglomerate fractions at 1:1 and 1:3 slag:water ratios, and the particle size distribution and the conglomerate distribution by fractions after the electrohydraulic processing at 1:1 and 1:3 slag:water ratios are plotted. The results show that 95-100 percent of particles larger than 95-100 percent consist of metal; as the particle size decreases, the metal content drops to 70 percent. The total amount of metal recovered from the slag is at least 80 percent and its refining degree is 90 percent. Thus, the electrohydraulic effect may be used successfully for ferrous metal recovery from slag; this is especially important in the secondary pig iron production where the metal content in the slag reaches 50-60 percent. Figures 4; references 3.

Production of Pyrolytic Samarium-Doped Indium Oxide Films

927D0173I Moscow ROSSIYSKAYA AKADEMIYA NAUK: SERIYA NEORGANICHESKIYE MATERIALY in Russian Vol 28 No 4, Apr 92 pp 800-804

[Article by M.Ya. Rakhlin, V.Ye. Rodionov, A.K. Savin, T.G. Sokolova, Semiconductors Institute at the Ukrainian Academy of Sciences; UDC 546.682:546.659]

[Abstract] The shortcomings of the group II metal sulfides as radiating materials in electroluminescence structures prompted an investigation of the possibility of producing luminescent films of indium oxide doped with Sm during the growth by the pyrolytic method. Activated and nonactivated indium oxide films are prepared by pyrolysis of an organic solution of indium acetylacetonate in dimethylformamide. The films are sprayed onto glass substrates covered with a transparent conducting tin oxide layer; the film thickness is monitored by a MII-4 microinterferometer while the film phase composition and structure are examined radiographically in a DRON-2.0 unit in Cu*K* radiation. The film photoluminescence (FL) is examined at room temperature in the visible spectrum under LGI-21 laser excitation. Diffraction patterns of the In_2O_3 powder and In_2O_3(Sm) film and the photoluminescence spectra of Sm-doped indium oxide films with various compositions, both annealed and nonannealed, are plotted; radiographic data on Sm-activated indium oxide films and photoluminescence bands of In_2O_3(Sm) films are summarized. An analysis of the oxygen-containing chelate indium complexes shows that Sm atoms penetrate the indium oxide's crystal lattice while the structure and symmetry of the original samarium complexes affect the concentration of the activating dopant in the films and their luminescent properties. In activating indium oxide with samarium in order to attain a predominantly red emission band characteristic of the Sm^{3+} ion, highly symmetric samarium complexes must be heat treated. Figures 2; tables 2; references 6: 5 Russian, 1 Western.

Certain Structural Characteristics of $TiSi_2$ Films Produced by Annealing in Vacuum

927D0172J Moscow ROSSIYSKAYA AKADEMIYA NAUK: SERIYA NEORGANICHESKIYE MATERIALY in Russian Vol 28 No 3, Mar 92 pp 536-540

[Article by O.B. Yatsenko, L.Ya. Tverdokhlebova, E.A. Sadygov, Voronezh State University; UDC 621.315.592:539.216.2]

[Abstract] The use of disilicides of refractory metals, e.g., titanium, as integrated circuit bonding materials and various methods of producing such $TiSi_2$ films are discussed. The structure and phase composition of films produced as a result of solid phase interaction of titanium with single crystal and polycrystalline silicon under vacuum annealing conditions at a 800°C temperature, a 6×10^{-5} Pa pressure, and a 30 min exposure are investigated by radiographic and electron diffraction pattern analyses, electron Auger spectroscopy, and scanning electron microscopy in combination with layer-by-layer and selective etching. Ti films (40-50 nm thick) are deposited by the magnetron spraying method on KDB-10 (111) single crystal Si wafers and poly-Si/mono-Si and poly-Si/SiO_2/mono-Si heterostructures on its basis. Fragments of the electron diffraction patterns of the initial Ti film and heterostructures annealed as 800°C and Auger

profiles of the principal and impurity element distribution in the surface layer before and after annealing are plotted and microphotographs of the silicide film surfaces are shown. The results indicate that a stable C54 $TiSi_2$ phase develops due to vacuum annealing; an orientational dependence of the $TiSi_2$ layer growth and manifestations of the long-range interaction effect of the single crystal substrate on the film structure formation are discovered. The silicide formation process is accompanied by an impurity gettering not only from the annealing chamber atmosphere but also from the Si layer. A local inhomogeneity formation mechanism is proposed and is confirmed by experimental data. It is shown that the structural defects have a matrix origin and are due to the presence of *B*-defects in Si crystals. Figures 3; references 7: 5 Russian, 2 Western.

Making $B_2Sr_2CaCu_2O_x$ Films by Layer-by-Layer Spraying

927D0172S Moscow ROSSIYSKAYA AKADEMIYA NAUK: SERIYA NEORGANICHESKIYE MATERIALY in Russian Vol 28 No 3, Mar 92 pp 685-686

[Article by V.A. Vlasov, High-Pressure Physics Institute imeni L.F. Vereshchagin at Russia's Academy of Sciences; UDC 546.87'56'42'41]

[Abstract] Layer-by-layer spraying deposition of elements with subsequent high-temperature annealing of the resulting coats in the air as a means of making high-T_c superconducting (VTSP) films is discussed and it is stated that in addition to the apparent simplicity of the equipment it requires, the method makes it possible to produce virtually single-phase $B_2Sr_2CaCu_2O_x$ oriented films with sufficiently good characteristics. The diffraction pattern of the film and its temperature dependence of resistivity are plotted. The films are produced by vaporizing the elements from a single tantalum evaporator heated by an electron beam. The outcome of an effort to deposit multilayer films of the $B_2Sr_2CaCu_2O_x$ (2-2-1-2) phase is described. The best films—with the least amount of low- (2-2-0-1) and high-temperature (2-2-2-3) phases—are produced by using three-stage annealing. The diffraction pattern confirms the absence of these phases' peaks. The study demonstrates that the method makes it possible to produce such multilayer films with a zero conductivity at 80K. The author is grateful to Ye.S.Itskevich for help. Figures 2; references 1.

Resistance of Pseudofused Titanium Carbide Powders in Sulfuric Acid and Hydrogen Peroxide Solution

927D0173F Moscow ROSSIYSKAYA AKADEMIYA NAUK: SERIYA NEORGANICHESKIYE MATERIALY in Russian Vol 28 No 4, Apr 92 pp 776-781

[Article by G.N. Komratov, I.D. Chausskaya, L.V. Kustova, Structural Macrokinetics Institute at Russia's Academy of Sciences; UDC 546.261:620.193]

[Abstract] Decomposition of titanium carbide (KT) in aqueous solutions of H_2O_2 and H_2SO_4 which is characterized by the $[Ti(H_2O_2)]^{4+}$ stained complex formation is discussed and the dependence of the rate of powdered titanium carbide reaction with a sulfuric acid solution of hydrogen peroxide on the mean fraction grain size and the process temperature is investigated. The pseudofused titanium carbide powder is synthesized at the Donetsk chemical reagent plant pursuant to TU 6-09-4704-79. The rate curves of the titanium concentration behavior in the solution during the pseudofused titanium carbide powder decomposition at 80K for various graininess, rate curves of the Ti ion accumulation in the solution during the pseudofused and furnace titanium carbide powder decomposition at various temperatures, the temperature dependence of $\lg W_0$ on $1/T$ for pseudofused and furnace titanium carbide where $\lg W_0$ is the initial decomposition rate, the dependence of the initial decomposition rate on the original powder surface at various temperatures, and the dependence of the lattice constant a on the mean titanium carbide particle size at various temperatures are plotted. The elemental composition of pseudofused titanium carbide fractions and the granulometric composition of various titanium carbide powder fractions are summarized. The conclusion is drawn that the lattice constant a is a function of not only the mean powder particle size but also the nature and concentration of the liquid phase components as well as the decomposition temperature. An analysis of the rate curves made it possible to establish the activation energy of both types of powders (21+/-3 to 52+/-4 for pseudofused and 28+/-4 to 53+/-6 kJ/mole for the furnace powder, depending on the grain size) and certain kinetic parameters of the process. Figures 5; tables 4; references 6.

Corrosion Behavior of Heterophase Sintered Materials of TiN-Cr and TiN-Ni Systems in Sulfuric Acid Solution

927D0168A Moscow ZASHCHITA METALLOV in Russian Vol 28 No 1, Jan-Feb 92 pp 62-69

[Article by T.V. Chukalovskaya, N.D. Tomashov, F.F. Yegorov, Physical Chemistry Institute at Russia's Academy of Sciences; UDC 620.193.4]

[Abstract] The development of new heterophase titanium nitride-based composites for use as nonconsumable welding and electrospark alloying electrodes is discussed and the corrosion behavior of TiN-Cr and TiN-Ni system materials as a function of their composition and structure is investigated. Samples for the study are made by cold compaction of the corresponding powder mixtures with a 5-60 percent Cr and 5-40 percent Ni volume concentration with subsequent sintering within a 1,650-1,900°C temperature range and a 2-90 min exposure to argon. The corrosion tests are carried out in a 0.5 M H_2SO_4 solution at room temperature (20-22°C). The total corrosion is determined by the mass loss method. The dependence of the general corrosion rate, titanium dissolution rate, and titanium yield coefficient on the chromium content in the TiN-Cr and TiN-Ni materials and the general corrosion kinetics, titanium dissolution kinetics, and titanium yield coefficient for the TiN-5 percent Cr, TiN-20 percent Cr, TiN-5 percent Ni, and TiN-20 percent Ni materials are plotted. The phase composition of the TiN-Cr and TiN-Ni samples after sintering is summarized. The effect of the sintering temperature and duration on the general corrosion rate is examined. The results of 200 h long corrosion tests of alloys in 1 N H_2SO_4 solution at room temperature are cited. The conclusion is drawn that complex heterophase structures consisting of TiN and a metallic matrix (binder)—a solid solution of Ti in Cr or Ni+intermetallic compounds of Cr or Ni and chromium nitride—form during the sintering of materials in an Ar atmosphere. The amount of intermetallic compounds rises with an increase in the sintering temperature and duration. The materials of the TiN-Cr system are stably passive and dissolve at very low rates; in TiN-Ni samples, nickel phases are in an active state under corrosion. The TiN-Cr corrosion rate drops sharply with an increase in the metallic component but increases in TiN-Ni under the same conditions. The corrosion resistance of both alloys increases with an increase in the sintering temperature and duration. Figures 3; tables 3; references 17.

Corrosion Behavior of Steel 45 Surface Alloyed With Chromium in Sulfuric and Hydrochloric Acid Solutions

927D0168B Moscow ZASHCHITA METALLOV in Russian Vol 28 No 1, Jan-Feb 92 pp 70-76

[Article by S.G. Babich, V.M. Knyazheva, I.I. Zayets, Yu.Ye. Roginskaya, L.Ye. Alekseyenko, Ye.F. Koloskova, Physical Chemistry Scientific Research Institute imeni L.Ya. Karpov; UDC 620.193.2]

[Abstract] The possibility of using certain metallic chromium compounds, particularly carbide and carbonitrides, as corrosion-resistant coats on steel is discussed and the corrosion resistance ability of coats consisting mostly of chromium carbides in the outer layer and a solid solution of Cr in α-Fe on the boundary with the base in H_2SO_4 and HCl solutions is investigated. The samples of steel 45 under study are surface alloyed with chromium by the thermal diffusion method; before the

tests, the samples are degreased with ethanol and washed twice in distilled water; the solutions are analyzed by a Perkin-Elmer 503 spectrometer; the phase composition of the samples is examined by a DRON-3 diffractometer; the elemental composition of the coat is identified by the Auger electron spectrometry method in a Varian (USA) spectrometer. The anode potentiodynamic curves of chrome- and boron and chrome-plated steel 35 in 0.1 *N* H_2SO_4 at a 20°C temperature and the dependence of the steady-state carbonitride metal sublattice dissolution rate on the potential in 1 *N* H_2SO_4, the anode potentiodynamic curves of chrome- and boron and chrome-plated steel 45 as well as the steady-state iron dissolution rate in chrome-plated and boron and chrome-plated steel 45 in *N* HCl at 20°C, and the behavior of the corrosion potential of chrome-plated steel 45 during a 1 h long corrosion test in oleum are plotted. The findings indicate that chrome-plating increase the corrosion resistance of steel 45 by 2-3 orders of magnitude within a broad range of potential in hydrochloric and sulfuric acid solutions while boron-chrome-plating increases it further by 2-3 times. Successful extended operation of chrome- and boron and chrome-plated steel in acid reducing media is complicated by the base dissolution through the coat's microdefects whose impact decreases greatly within a 0.6-1.05 V potential range where passivation becomes possible. The possibility of considerably increasing the corrosion resistance of coats by changing their composition from carbonitrides to chromium carbides is shown. Figures 3; tables 1; references 12: 10 Russian, 2 Western.

Corrosion-Electrochemical Behavior of Nickel in Aqueous Acetonitryl Perchlorate Media in Presence of Organic Bases and Acids

927D0168C Moscow ZASHCHITA METALLOV in Russian Vol 28 No 1, Jan-Feb 92 pp 77-82

[Article by V.V. Ekilik, Ye.N. Balakshina, L.D. Popov, Rostov State University and Physical and Organic Chemistry Scientific Research Institute at the Rostov State University; UDC 541.138]

[Abstract] The substantially different effect of organic bases (azoles) on the anodic dissolution of Ni in aqueous and organic media prompted a study of their effect on the electrochemical behavior of metal in aqueous organic systems in the presence of phosphonic acids. Potentiostatic measurements are taken on N-1 nickel in Ar-saturated water-acetonitryl solutions of *x*M $HClO_4$+(0.05-*x*) M $LiClO_4$ containing 0.6 and 20 percent mol. water using various additives. The dependence of the corrosion rate and diffusion current on pH at both water contents, the dependence of the Ni dissolution rate on pH at various potentials, and the dependence of the adsorption factor and pH factor on the concentration of the β-imino-α-oximinoacetoacetarylamid at various corrosion potentials are plotted and the total dependence of the surfactant (PAV) action on the additive concentration and potential is summarized. It is shown that with an addition of *N*-containing compounds, the pH factor plays a dominant role while the process is inhibited due to adsorption in the passive state. These patterns are reversed for phosphonic acids: their adsorption properties are manifested to a greater extent near the corrosion potential. The mutual behavior of inhibiting and enhancing additives is analyzed. The authors are grateful to Yu.B. Polikanova for help with the experiments. Figures 3; tables 3; references 8.

Mechanism of Abnormal Corrosion Behavior of Aluminum Alloys in Concentrated Acetic Acid

927D0168D Moscow ZASHCHITA METALLOV in Russian Vol 28 No 1, Jan-Feb 92 pp 83-87

[Article by S.G. Polyakov, G.M. Grigorenko, O.D. Smiyan, M.B. Kladnitskaya, G.Ye. Boyeva, A.A. Trofimov, Electric Welding Institute imeni Ye.O. Paton at the Ukrainian Academy of Sciences; UDC 620.193:669.71]

[Abstract] The peculiar behavior of aluminum alloys in bubbling acetic acid and other aliphatic first noted in 1916 is discussed and the mechanism of the corrosion behavior of aluminum and its alloys in concentrated acetic acid containing less than 0.5 percent H_2O is investigated. To this end, ADO aluminum and the AMg3 alloy samples machined to a 1.25 μm roughness, pickled in a 10 percent NaOH solution for 0.5-1 min at 50-60°C, rinsed in cold water, and bleached in a 25 percent HNO_3 solution at room temperature for 5 min are tested for 3-1,000 h in chemically pure glacial acetic acid within a 25-118°C temperature range. The chemical composition and texture of the surface are examined by an MS-156 mass spectrometer made by Riber (France) and a Stereoscan-733 X-ray microanalyzer. The results show that the character of corrosion in concentrated acid changes with a drop in the water concentration below 0.51 percent from uniform to enhanced along the grain boundaries; within a 25-60° range, pitting is observed while uniform corrosion is dominant at 118°. The effective reaction order for water molecules is equal to six while the corrosion activation energy for the ADO at [H_2O]=0.51 percent corresponds to the diffusion control within the entire temperature range. A change in the limiting stage is observed for the AMg3 at 60°. To prevent corrosive failure of aluminum alloys in contact with acetic acid, it is necessary to ensure that the water concentration is at least 0.5 percent. Figures 2; tables 1; references 16: 10 Russian, 6 Western.

Protection From Two-Metal Corrosion in Steel-Titanium Pair by Microarc Oxidizing

927D0168E Moscow ZASHCHITA METALLOV in Russian Vol 28 No 1, Jan-Feb 92 pp 117-121

[Article by P.S. Gordiyenko, T.M. Skorobogatova, O.A. Khrisanfova, A.G. Zavidnaya, M.P. Kandinskiy, Chemistry Institute at the Far Eastern Branch of Russia's Academy of Sciences; UDC 620.193.4:669.295]

[Abstract] The shortcomings of corrosion-preventive thermal oxidizing of titanium and titanium alloy products and the advantages of microarc oxidizing (MDO) of titanium alloys in aqueous electrolyte solutions prompted an attempt to compare the effect of various microarc oxide coats on titanium on the severity of its galvanic corrosion in a pair with steel St3. Cast VT1-0 titanium sheets mechanically ground and chemically polished for 3-5 s in a 1:3 mixture of concentrated hydrofluoric and nitric acids at 80° are used in the tests. The process is conducting at the arcing voltage with electrolyte stirring and cooling using a titanium plate cathode. The phase composition of the coat layer is examined by a DRON-2.0 diffractometer in Cu*K* radiation; the elemental composition is studied by an electron microprobe in an IXA-5A X-ray spectral microanalyzer at a 20 kV accelerating voltage and a 48 nA current. The galvanic corrosion current density in oxidized titanium and the galvanic titanium corrosion current after microarc oxidizing in a pair with St3 in various electrolytes are summarized; a block diagram of the two-metal corrosion measurement unit is cited. An analysis demonstrates that the corrosion protection properties of microarc oxide coats on Ti largely depend on the electrolyte composition. The galvanic corrosion current in a pair with St3 decreases in the following MDO coat series: thermal rutile, MDO rutile, anatase, anatase+rutile, amorphous Al, Ti, P, and Na-Zr oxide phases, titanate, spinels, Ta oxides. Figures 1; tables 2; references 6: 5 Russian, 1 Western.

Effect of Heat Treatment and Blueing on Corrosion Behavior of Sheet Steel

927D0168F Moscow ZASHCHITA METALLOV in Russian Vol 28 No 1, Jan-Feb 92 pp 132-134

[Article by V.I. Spivakov, L.V. Bogomolova, L.L. Lyakhovetskaya, Ferrous Metallurgy Institute, Dnepropetrovsk; UDC 620.193.2]

[Abstract] The need to supplement heat treatment of plate and sheet steel with other methods in order to remove scale while preventing the metal from corrosion, e.g., by blueing, is stressed and the corrosion susceptibility of steel 09G2S after various types of heat treatment with and without blueing is assessed. Steel 50 x 50 x 5 mm samples are tested after the following: water quenching at 920°+tempering for 10 min at 600°; normalizing at 950° for 10 min; hardening + tempering + blueing; normalizing+blueing; and hot-rolling + blueing. Corrosion tests are carried out in a steam chamber for 2 weeks at 50° and a 95 percent relative humidity and in a corrosion test bench under atmospheric conditions. An analysis of the corrosive mass loss of the samples shows that hardened, tempered, and blued samples have the lowest losses while normalized samples—the highest (more than 300 mg). Moreover, the ferrite+pearlite heterogeneous structure is more susceptible to corrosion than the homogeneous structure. Thermal oxidizing of steel sheets and plates by oil cooling at the tempering temperature may used directly in the continuous-type production line as a means of temporary corrosion protection. Figures 2; references 1.

Corrosion Rate in Electric Power Plant Pressure Tunnels

927D0168G Moscow ZASHCHITA METALLOV in Russian Vol 28 No 1, Jan-Feb 92 pp 137-140

[Article by Yu.Z. Shikhaliyev, Azeri Petroleum and Chemistry Institute imeni M. Azibekov; UDC 620.193.2]

[Abstract] The dependence of the water pressure tunnel corrosion rate on the water flow velocity, oxygen concentration, and temperature is investigated using the author's method described in *Zashchita metallov* Vol. 18 No. 2, 1982. The waveguide [sic] corrosion rate is selected as the criterion function while the flow velocity, O_2 concentration in the water, and water temperature—as factors. The 2^3-type full factorial experiment method (PFE) is used to derive the regression equations. A curve of the corrosion rate and potential in steel St3 in the river Kura water and the anodic and cathodic polarization resistance ratio on the flow velocity in the pressure tunnel is plotted. It shows that among other factors, the water velocity has the greatest effect on the corrosion rate. The specific features of the river Kura water, such as the high silicate and carbonate content, have a low impact in a fast flow with restricted oxygen access. Ferrous hydroxides accumulating on the steel surface in stagnant water with restricted oxygen access are washed away by faster than 4.5 m/s flows; this increases the corrosion rate. A certain increase in the corrosion rate at a velocity above 6 m/s may be attributed to cavitation or erosion phenomena. Figures 1; tables 2; references 5.

On Issue of Copper-Steel Clad Metal Etching

927D0168H Moscow ZASHCHITA METALLOV in Russian Vol 28 No 1, Jan-Feb 92 pp 147-150

[Article by T.S. Devyatkina, N.P. Zaykova, Urals Scientific Research Institute of Tube Making Industry; UDC 620.103.2]

[Abstract] Etching of the copper-steel clad metal rolled stock, usually conducted in H_2SO_4 whereby copper is contact-deposited on the steel surface, is discussed and the electrochemical behavior of steel St20 and M1 copper as well as steel-copper clad metal with and without scale in sulfuric acid solutions with chelation agent and surfactant (PAV) additions is examined. According to X-ray structural analysis, scale securely bonded to the base has a wuestite-magnetite structure and is 30-40 μm thick on steel and has a CuO-nonoxidized copper structure and is 20-25 μm thick on copper. The steel, copper, and clad metal polarization dissolution curves in various acid solutions and the polarization dissolution curves of scale on copper and steel in various acid solutions are plotted and the dependence of the corrosion activity of the clad metal etching

solution on the component origin and concentration at a 65° temperature is summarized. An analysis of the clad metal behavior makes it possible to recommend that the etching solution base in which both clad metal components are soluble be selected. It is shown that the chelation agent capable of producing complex compounds with a more stable metal should be selected; it is suggested that the steady-state metal dissolution potentials be brought closer by controlling the ratio of the surfactant and chelation agent in the etching solution. Figures 2; tables 1; references 2.

High-Alloy Surfaced Layer Behavior During Low-Temperature Hydrogen Absorption

927D0168I Moscow ZASHCHITA METALLOV in Russian Vol 28 No 1, Jan-Feb 92 pp 155-157

[Article by V.M. Leybzon, V.L. Mirochnik, T.A. Pisarenko, A.A. Simakova, All-Union Scientific Research and Design Institute of Chemical and Petroleum Engineering; UDC 620.194:621.791.92]

[Abstract] Corrosion cracking of wellhead fittings from high alloy steel and nickel alloys by the hydrogen embrittlement mechanism prompted a study of surfacing alloys and the methods of their deposition. To this end, a surfaced metal layer deposited in an Ag-He mixture by EP-758U welding wire according to TU 14-1-3685-80 specifications onto the inside surface of the wellhead gate valves from steel 20KhMA pursuant to RD RTM 26-16-31-84, GOST 4543-71 is investigated after tempering at 580° for 4 h. The surface metal has the following composition: 21.4 percent Cr, 64.7 percent Ni, 9 percent Mo, 4 percent Nb, 0.4 percent Al, and 0.4 percent Ti. Specification require that the surfacing metal be resistant to hydrogen sulfide corrosion cracking (SVK) at a stress of at least 420 MPa. The hydrogen sulfide corrosion cracking resistant is tested by the MSKR-01-85 procedure in a NACE medium; all samples passed the tests at 420 MPa. Hydrogen penetration is examined in 4 mm thick clad metal sheet samples with a 1.5-2.5 mm thick 30KhMA surface layer. The dependence of the (222) X-ray diffraction line width on the exposure duration after cathode hydrogenation for 8 h and in the initial state is plotted. During the cathode polarization in the presence of a hydrogen absorption enhancer, hydrogen penetrates the surfaced layer. The hydrogen diffusivity is calculated for a 168 h exposure at a 0.032 mm mean depth: D=8.4 x 10^{-12} cm^2 x s^{-1}. Since the minimum surfacing layer depth according to specifications is 3 mm, it would take 169.8 years for hydrogen to penetrate through the layer. Thus, in this case hydrogen diffusion is virtually insignificant. Figures 1; references 8: 6 Russian, 2 Western.

St3 and Iron Electroreflection Spectra and Issue of Distinguishing Their Anodic Dissolution Kinetics

927D0167A Moscow ZASHCHITA METALLOV in Russian Vol 28 No 2, Mar-Apr 92 pp 185-190

[Article by R.M. Lazorenko-Manevich, Ye.G. Kuznetsov, L.A. Sokolova, Physical Chemistry Scientific Research Institute imeni L.Ya. Karpov and Public Utilities Academy imeni K.D. Panfilov; UDC 620.193.01]

[Abstract] The difference in the rate characteristics of the reactions of anodic dissolution of steel St3 and iron due to the difference in these metals' surface adsorption properties and the lack of classified spectroscopic electroreflection (EO) data on St3 are discussed and the electroreflection spectra of iron and St3 are compared for the purpose of determining on this basis the reason for the difference in the corrosion behavior of these metals and establishing the correlation between the state of the metal surface and its corrosion behavior. The relation between the electroreflection spectra of iron and chemisorption of water in the form of surface complexes with charge transfer (PKPZ) is examined. A comparison of Re($\Delta R/R$) and Im($\Delta R/R$) spectra of air-passivated iron and steel St3 makes it possible to draw the conclusion about the presence on the steel surface of more activated adsorbed water molecules than on iron; this leads to an increase in the adsorbed hydroxyl group concentration and the proportion of the passivated surface and to a decrease in the apparent order of the dissolution reaction for OH^--ions. This is indirectly confirmed by the fact that in a weakly acid acetate solution, the charge transfer band (PPZ) energy decreases by more than 0.5 eV due to the acetate ion interaction with the adsorbed water; this is accompanied by a decrease in the anodic iron dissolution by at least two orders of magnitude. Figures 4; references 5: 4 Russian, 1 Western.

Corrosion-Electrochemical Behavior of Nickel in Sulfuric Acid Solutions

927D0167B Moscow ZASHCHITA METALLOV in Russian Vol 28 No 2, Mar-Apr 92 pp 191-195

[Article by A.E. Kozachinskiy, A.P. Pchelnikov, Ya.B. Skuratnik, V.V. Losev, Physical Chemistry Scientific Research Institute imeni L.Ya. Karpov; UDC 620.193.41/546.74]

[Abstract] It is speculated that ionization of hydrogen implanted in nickel and the inhibition of nickel's anodic dissolution under the effect of adsorbed hydrogen should be observed during the anodic dissolution of nickel after its corrosion beforehand in acid solutions where the metal dissolution is accompanied by hydrogen liberation. The corrosion-electrochemical behavior of nickel in a 1 N deaerated H_2SO_4 solution is studied at 20° by combined electrochemical and radiometric measurements so as to determine the partial Ni dissolution rates and the ionization rate of the implanted hydrogen simultaneously. The cathode and anode potentiodynamic curves and the behavior of the solution radioactivity and electrode potential, corrosion potential, and corrosion rate are plotted. The study demonstrates that hydrogen implanted in nickel decreases the rate of its anodic dissolution due to the blocking of active centers on the dissolving nickel surface by its atoms. The conclusion is drawn that due to a change in the electrochemical nickel

behavior during corrosion, data on its corrosion loss may be obtained only by using direct solution analysis methods. Such an approach is also valid for other metals actively interacting in the process of their corrosion with hydrogen. The effect of the KI-1 cation inhibitor on the corrosion and hydrogen absorption is examined. Figures 3; references 7: 6 Russian, 1 Western.

Corrosion-Electrochemical Behavior of Al-Fe-Ni Bronze in Chloride Solution

927D0167C Moscow ZASHCHITA METALLOV in Russian Vol 28 No 2, Mar-Apr 92 pp 196-201

[Article by V.N. Chervyakov, L.V. Kharkova, B.P. Aravin, A.P. Pchelnikov, Physical Chemistry Scientific Research Institute imeni L.Ya. Karpov and Prometey Central Scientific Research Institute of Structural Materials; UDC 620.193/669.35.6]

[Abstract] The process of selective dissolution (SR) of individual phases of aluminum bronze in sea water and the reverse precipitation of the copper passed to the solution are discussed and the role of the structural alloy components in the corrosion behavior of Br. AZhNMTs 9-4-4-1 bronze (Cu with 9 percent Al, 4 percent Fe, 4 percent Ni, and 1 percent Mn) is investigated. Cast samples annealed at 900° for 1 h and tempered at 600° (condition 1) or 350° (condition 2) are examined. Corrosion tests are conducted at 80° for 5 and 2,000 h after which metallographic sections are prepared. The free corrosion potential of cast Br. AZhNMTs 9-4-4-1 bronze, partial corrosion rates of its components, polarization curves, and steady-state polarization curves of its structural components are plotted. The integral selective dissolution potentials of heat treated Br. AZhNMTs 9-4-4-1 bronze are summarized. The findings indicate that heat annealing and tempering substantially lower the bronze susceptibility to pitting. The optimum heat treatment condition is recommended for improving the corrosion resistance: 1 h long annealing at 900° + 1 h long tempering; this eliminates both selective phase dissolution and the secondary selective dissolution due to the reverse copper precipitation. The coulometric method makes it possible to assess the susceptibility of copper alloys to this type of selective dissolution. The authors are grateful to V.V. Losev for valuable remarks. Figures 4; tables 2; references 13: 7 Russian, 6 Western.

Effect of Lithium Doping on Aluminum's Corrosion Properties

927D0167D Moscow ZASHCHITA METALLOV in Russian Vol 28 No 2, Mar-Apr 92 pp 210-217

[Article by V.S. Sinyavskiy, A.M. Semenov, V.D. Valkov, All-Union Light Alloys Institute Scientific Production Association; UDC 620.193./546.621]

[Abstract] The search for new Li-doped aluminum alloys prompted by lithium's role in substantially increasing the modulus of elasticity while lowering the alloy density is outlined and an attempt is made directly to determine the corrosion rate in Al-Li alloys and establish a broader correlation between the electrochemical and corrosion characteristics and the chemical composition, structure, and other service properties of the alloys under study. Compacted strips of three Al-Li alloys with 0.8, 1.9, and 2.3 percent Li by mass and 0.1 percent Zr are tested for layer corrosion resistance (RSK), intercrystalline corrosion resistance (MKK), general corrosion resistance, and corrosion cracking (KR). The position of the alloys under study in the Al-Li constitution diagrams, the behavior of the corrosion mass loss, corrosion potential, and mechanical properties as a function of the Li concentration (aging at 170° for 16 h), and the polarization diagram of alloy 3 (aging at 170° for 16 h) are plotted. An analysis reveals that all alloys, both underaged and aged to maximum strength, have a high corrosion cracking, layer corrosion, and intercrystalline corrosion resistance due to the absence of electrochemical heterogeneity of the grain body and boundaries. A correlation is established between the Li concentration in Al and the corrosion mass loss rate: this rate in pure Al is 30 times lower than in Al +0.8 percent Li. The alloys' electrochemical characteristics are determined as a function of the lithium concentration and artificial aging conditions: when up to 2.3 percent Li is added, the corrosion, pitting, and repassivation potentials become negative; as the artificial aging duration is prolonged to 144 h, all these electrochemical parameters shift in the negative direction almost identically. Figures 5; tables 4; references 8: 5 Russian, 3 Western.

Effect of Diamond Burnishing on Steel Kh17N15 Resistance to Chloride Corrosion Cracking

927D0167E Moscow ZASHCHITA METALLOV in Russian Vol 28 No 2, Mar-Apr 92 pp 218-222

[Article by V.S. Koropachev, V.P. Pogodin, L.A. Khvorostukhin, V.A. Gashenko, All-Union Scientific Research Institute of Inorganic Materials imeni A.A. Bochvar; UDC 620.194]

[Abstract] The inadequacy of available data on the effect of diamond burnishing on the corrosion properties of metals and alloys prompted a study of its effect on thin-walled ($\leq$0.5 mm) tubes from steel Kh17N15. Planar, annular, and tubular samples of austenitic steel Kh17N15 polished beforehand in a H_3PO_4+CrO_3 solution are tested. The potentiodynamic polarization curves in water and $FeCl_3$ of steel after various types of austenizing treatment and diffraction patterns of the austenized steel with and without additional treatment are plotted. The characteristic features of the thin-walled product working and treatment and the effect of burnishing and loading conditions on the electrochemical and corrosion behavior in an aqueous chloride solution are investigated. The findings make it possible to conclude that diamond burnishing at a $<$100 N force may be used for machining the surface of thin-walled products in order to increase their chloride corrosion cracking resistance given that the loads on the metal are below the

yield point. The use of diamond burnishing for more stressed structures is not recommended. Figures 2; tables 3; references 7.

Electrodeposition of Ni-Re Alloys From Acetate Electrolytes

927D0167F Moscow ZASHCHITA METALLOV in Russian Vol 28 No 2, Mar-Apr 92 pp 282-286

[Article by S.I. Berezina, T.D. Keshner, V.T. Ivanov, Organic and Physical Chemistry Institute imeni A.Ye. Arbuzov at the Kazan Scientific Center of Russia's Academy of Sciences; UDC 541.135]

[Abstract] The unique physical and chemical properties of rhenium and its alloys and the possibility of joint reduction of rhenate ions with iron family metal ions from various electrolytes are discussed and the results of experiments with electrodeposition of Ni-Re alloys from electrolytes with various compositions at a 1-16 A/dm^2 current density without stirring at room temperature are presented. The possibility of electrolytic precipitation of Ni-Re alloys from acetate electrolytes is established. The potentiodynamic total polarization curves of the Ni-Re alloy, Ni, and Re electrodeposition from various electrolytes, total galvanostatic polarization curves of the Ni-Re alloy precipitation and H_2 liberation, partial polarization curves (PK) of hydrogen liberation and alloy, Re, and Ni precipitation, partial galvanostatic polarization curves of individual nickel and rhenium precipitation, and polarization curves of Ni and alloys with various Re concentrations in a 0.5 M H_2SO_4 solution are plotted. Stimulated Re precipitation in acetate electrolytes is discovered and it is noted that the Re precipitation is accompanied by depolarization while the Ni precipitation—by considerable overpolarization. Individual Re precipitation from such solutions occurs with a current efficiency (VT) of $\leq$1 percent while given a [Ni(II)]:[Re(VII)]=1:10 ratio, the Re concentration in the alloy reaches 98 percent and the current efficiency—43 percent. Light dull sediments have an elevated microhardness and corrosion resistance and have a good adhesion to copper and brass bases. The best pH range for making the alloys is 3.6-4.2 while the best current density is 5-16 A/dm^2; a close-to-equimolar component ratio is recommended. Figures 4; tables 3; references 12: 7 Russian, 5 Western.

On Possibility of Using High-Intensity Electron Beam Pulses to Produce Fe-Si-Based Protective Coats

927D0167G Moscow ZASHCHITA METALLOV in Russian Vol 28 No 2, Mar-Apr 92 pp 287-294

[Article by V.I. Kolotyrkin, M.Yu. Tomashpolskiy, B.A. Demidov, V.M. Knyazheva, M.V. Ivkin, V.A. Petrov, N.G. Shirina, Physical Chemistry Scientific Research Institute imeni L.Ya. Karpov and Atomic Energy Institute imeni I.V. Kurchatov; UDC 621.9.048:620.193.41]

[Abstract] The advantages of corrosion-resistant microcrystalline Fe-Si alloys with a high ($\geq$25 percent) Si concentration made by rapid quenching and the limited applications of such rapidly quenched foils are discussed and the possibility of using high-intensity electron beam pulses for producing Fe-Si corrosion-resistant alloy coats is investigated. To this end, an experiment is carried out using a high-current Kalmar accelerator with electrical sheet steel and steel St3 as the base. Cast Fe-Si alloy pellets with 32.50 and 75 percent Si are used as the coat materials. The surface microstructure is examined by scanning electron microscopy using a JEOL JSM35F instrument in the secondary electron emission mode at a 20 kV accelerating voltage. The potentiodynamic anode curves of electrical sheet iron, cast Fe-Si alloy (50:50), and iron samples with Fe-Si coats are plotted. The findings confirm the possibility of increasing the corrosion resistance of Fe and St3 by such pulse treatment and establish that sprayed coats without an additional treatment have an elevated level of pore and microcrack defects which make it difficult to attain a good corrosion resistance. Silicon depletion from Fe-Si coats which lowers the protective efficiency is noted and the possibility of improving the protective properties by fusing is demonstrated. The outlook for developing multilayer Fe-Si-based protective coats with additional Pb sublayers from ductile low-melting metals and alloys which are corrosion-resistant in various media is evaluated. Figures 4; tables 2; references 6: 5 Russian, 1 Western.

Surface Composition of Ti-W Alloys After Corrosion

927D0167H Moscow ZASHCHITA METALLOV in Russian Vol 28 No 2, Mar-Apr 92 pp 295-297

[Article by I.V. Kasatkina, R.Kh. Zalavutdinov, A.I. Shcherbakov, Physical Chemistry Institute at Russia's Academy of Sciences; UDC 620.193.01]

[Abstract] The predominant Ti dissolution and surface enrichment with W due to corrosion of Ti-W alloys in 2.5 M H_2SO_4 and the factors affecting the properties and composition of the layer under the loose W-enriched layer in which the W concentration reaches a steady-state level quickly are discussed and it is speculated that the tungsten concentration in this sublayer depends on the alloy composition which controls the rate of its dissolution. To check this Ti-W alloy dissolution model, the surface layer composition is analyzed directly. To this end, the composition of the body and surface of binary Ti-W alloys is investigated by the X-ray spectral microanalysis (RSMA) using Camebax (France) instruments. The dependence of the W*M* radiation on the Ti-W alloy polarization duration in 2.5 M H_2SO_4 solution and the dependence of the radiation intensity and corrosion rate of a Ti+5 percent W alloy on the 2.5 M H_2SO_4 solution temperature at a -0.4 V potential and a 3 h test duration are plotted. The findings show that the dissolution rate within a 30-70° temperature range changes roughly by two orders of magnitude while the W*M* radiation intensity—merely by twofold, i.e., the W

accumulation on the surface is almost independent of the dissolution rate and depends only on the initial W concentration. These data confirm the assumption of a certain surface W-enrichment degree for each alloy composition. As the exposure and corrosive severity of the medium increase, the proportion of efficiently working tungsten decreases. Figures 2; tables 2; references 3: 2 Russian, 1 Western.

Effect of HCl and Molasses on Steel 12Kh18N10T Corrosion in Phosphoric Acid Solutions

927D0167I Moscow ZASHCHITA METALLOV in Russian Vol 28 No 2, Mar-Apr 92 pp 308-312

[Article by D.Kh. Kopeliovich, V.I. Ivlev, Mayak Production Association, Chelyabinsk; UDC 620.193.41]

[Abstract] The corrosive effect of the combination of phosphoric acid used as a flux and molasses used as a reducing agent on steel 12Kh18N10T during the hardening of the radioactive chemical production waste is discussed and likely causes of the elevated corrosiveness of the molasses mixture with H_3PO_4 are investigated. The effect of the phosphoric acid and molasses concentration on the anodic polarization of steel 12Kh18N10T and the behavior of the anodic polarization of steel 12Kh18N10T in a mixture of H_3PO_4 and HCl at various concentrations and temperatures are plotted and the corrosion rate of steel in the H_3PO_4+HCl and 50 percent H_3PO_4 solutions at various temperatures are summarized. An analysis demonstrates that although the danger of steel corrosion is enhanced by molasses, corrosion already exists in dry-process phosphoric acid, so efforts to prevent these two components from mixing do not solve the problem fully. Reliable corrosion protection may be ensured by shifting the potential to the passive domain. For anodic protection, the conditions are favorable since in cold solutions containing less than 1 g/l of HCl, the passive bandwidth is close to 1 V and the current density drops sharply; thus, e.g., in a solution of 75 percent H_3PO_4 and 0.3 gffl of HCl at 40° it drops to 10^{-2} A/m^2 after 15-30 min. Figures 2; tables 2; references 10: 8 Russian, 2 Western.

Anodic Protection of Inner Tube Cavity of Heat Exchangers

927D0167J Moscow ZASHCHITA METALLOV in Russian Vol 28 No 2, Mar-Apr 92 pp 312-316

[Article by I.V. Bochkareva, V.T. Ivanov, V.A. Makarov, V.S. Novitskiy, Bashkir State University, Physical Chemistry Scientific Research Institute imeni L.Ya. Karpov, and State Scientific Research and Design Institute of the Methanol Industry; UDC 620.193]

[Abstract] Protection of the inner tube cavity of heat exchangers with the help of auxiliary electrodes placed in the shells of the shell and tube heat exchangers on both sides is discussed and heat exchanger passivation performed at a low temperature and very low current densities is described. A formula is derived for calculating the passive length, i.e., anodic protection length, for the completely passive state as a function of the tube radius, corrosive medium resistivity, current in the passive state, and potential of the lower passive region bound. The tube configuration is shown and the dependence of the completely passive tube length on the tube radius at various medium temperatures is plotted. The exponent β in the dependence of the electric resistance on temperature is determined for sulfuric acid as the corrosive medium at various temperatures at a 10 m distance from the tube's end; assuming the resistivity to be equal to 3.5 Ω x cm at a 70° temperature, the plots can be approximated rather well by the experimental formula given β=0.02. It is shown that the passive segment length when the acid is cooled is greater under isothermal conditions and is lower in the case of heating. Figures 2; references 8: 7 Russian, 1 Western.

Potentiometric Sulfuric Acid Monitoring in Chemical Polishing Electrolyte

927D0167K Moscow ZASHCHITA METALLOV in Russian Vol 28 No 2, Mar-Apr 92 pp 319-321

[Article by A.I. Turashev, A.I. Samosova, Z.G. Belyayeva, Organic and Physical Chemistry Institute imeni A.Ye. Arbuzov at the Kazan Scientific Center of Russia's Academy of Sciences; UDC 621.794]

[Abstract] It is reported that in a chemical polishing electrolyte, pH is a function of not only H_2SO_4 concentration but also of the H_2O_2 concentration; consequently, despite its simplicity, potentiometric pH measurement is used to monitor the sulfuric acid concentration and establish a quantitative correlation between the electrolyte pH and the sulfuric acid and hydrogen peroxide concentration. The dependence of pH on the logarithm of the H_2SO_4 concentration in a H_2SO_4 solution with H_2O_2 and water at various hydrogen peroxide concentrations and the dependence of pH on the hydrogen peroxide concentration at a constant sulfuric acid concentration are plotted. The established patterns make it possible to determine the sulfuric acid concentration in the brass polishing solution at any measured pH during the electrolyte performance. A procedure for monitoring and correcting the electrolyte by using the sulfuric acid concentration as the independent variable is recommended. The proposed technique is tested and is proven effective. Figures 2; references 3.

Aluminum and TsAM4-1 Alloy Corrosion in Nickel-Plating Electrolyte

927D0167L Moscow ZASHCHITA METALLOV in Russian Vol 28 No 2, Mar-Apr 92 pp 321-322

[Article by V.P. Artamonov, Pavlodar Industrial Institute; UDC 620.193]

[Abstract] Corrosion of of A85 Aluminum and the TsAM4-1 alloy containing 4 percent Al, 1 percent Cu, and 95 percent Zn widely used in machine building for making parts by precision casting in the nickel plating electrolyte is investigated and the X-ray spectral analysis is carried out in a Simultex unit. To this end, the aluminum dissolution in the anode segments and nickel and hydrogen reduction in the cathode segments is examined. The hydrogen liberation rate on Al and the Ni precipitation rate on Al and the hydrogen liberation rate and nickel precipitation rate on the TsAM4-1 alloy are plotted. It is noted that Al corrodes slower than zinc and this is attributed to the fact that the Al-Ni galvanic cell's electromotive force (EDS) is 0.15 V lower than that of Zn-Ni. It is also demonstrated that although the TsAM4-1 alloy contains only 4 percent Al, its behavior is much closer to that of Al and not Zn; the alloy corrosion is slower and the cathode depolarization occurs predominantly due to the Ni ion discharge, so less hydrogen is liberated. Figures 2; references 4.

Effect of Iron Impurities on Electrolytic Nickel Precipitate Structure and Properties

927D0167M Moscow ZASHCHITA METALLOV in Russian Vol 28 No 2, Mar-Apr 92 pp 323-326

[Article by G.M. Yashina, Z.S. Martemyanova, V.F. Lazarev, N.G. Rossina, Urals Polytechnic Institute; UDC 620.193]

[Abstract] The effect of iron impurities in the Ni-plating electrolyte on the structure and quality of the nickel coat is examined using a sulfate electrolyte with a pH of 4.6-5.6 at a 50° temperature at a current density of 2 A/dm^2 with 100 μm thick nickel coats. In so doing, the background Fe concentration in the electrolyte is assumed to be equal to 0 while the iron addition concentration is manipulated within a 0-48 g/l range which corresponds to the actual contamination of commercial nickel plating electrolytes with steel St3 cathodes. The Fe concentration in the electrolyte is determine by photocolorimetry, the internal stresses are measured by the flexible cathode method, the coat thickness is measured by weighing and with the help of a thickness gauge, and the coat porosity is determined by N.M. Shmeleva's method. The Ni and Fe distribution in the 100 μm thick nickel coat precipitated from a sulfate electrolyte with a 0.48 g/l Fe addition is plotted and the Ni coat porosity at various Fe^{2+} and electrolyte concentrations after various electrolysis durations and the 100 μm thick Ni coat microhardness and lattice constant are summarized. The Ni precipitate structure is examined radiographically and by X-ray microspectral and metallographic analyses using DRON-3, Camebax, and Neophot-2. The findings reveal that Ni-plating electrolyte contamination with Fe ions sharply worsens the nickel-plating quality of electrolyzer parts and indicate that the Fe ion concentration must by strictly monitored; continuous electrolyte filtering and purification is required. It is established that the maximum permissible Fe concentration in sulfate electrolytes should not exceed 0.01 g/l. Figures 2; tables 2; references 11: 10 Russian, 1 Western.

Laser Stimulated Electrolytic Precipitation of Sn-Bi Alloy

927D0167N Moscow ZASHCHITA METALLOV in Russian Vol 28 No 2, Mar-Apr 92 pp 334-337

[Article by Yu.V. Seryanov, L.V. Aravina; UDC 621.793.14]

[Abstract] The study of laser stimulated electrolytic precipitation of metals (*Zashchita metallov* Vol. 24 No. 6, 1988, p. 1025 and Vol. 26 No. 4, 1990, p. 676) is continued and laser stimulated electrodeposition of a Sn-Bi alloy which is rather promising for rebuilding protective coats and applying local microamounts of solder to the topology elements of printed boards is investigated. To this end, a horizontally oriented Cu foil or an insulator with a chromium sublayer plated with copper are used as the cathode and tin is used as the anode; a saturated silver chloride reference electrode is used. The potentiostatic polarization curves of the Sn-Bi alloy precipitation from the acid sulfate electrolyte onto a local copper cathode with and without irradiation and the analytical dependence of the relative local laser precipitate spot on the relative radius and exposure duration under optimum electrolysis conditions are plotted. A formula is derived for calculating the local sediment spot thickness and mean precipitation rate of the Sn-Bi alloy in the focused laser beam spot. Total elimination of diffusion constraints on the process at the central zone of the heat affected area (ZTV) is experimentally confirmed. The results indicate that laser stimulated electrodeposition under optimal conditions, i.e., a -0.76 V potential, a 21 kW/cm^2 exposure, and a 1.06 μm wavelength, is suitable for rebuilding protective coat flaws or applying microscopic doses of solder on small hybrid integrated circuit (GIS) elements. Figures 2; references 6.

Principal Zinc Behavior Patterns in Blast Furnaces

927D0176A Moscow STAL in Russian
No 2, Feb 92 pp 5-9

[Article by Yu.P. Shchukin, V.S. Novikov, B.A. Marsuverskiy, Yu.V. Yakovlev, I.E. Kosachenko, A.D. Nikonorov, Urals Scientific Research Institute of Ferrous Metallurgy and Nizhniy Tagil and Magnitogorsk Integrated Iron and Steels Works; UDC 669.162.26]

[Abstract] The behavior patterns of zinc-containing iron ore materials of different origin in the blast furnace and the relationship between the type of blast furnace conditions and the properties of materials charged into it on the one hand and the zinc behavior in various blast furnace areas on the other are discussed. The zinc yield during the furnace blowing down as a function of the distance from the charge level in various Nizhniy Tagil (NTMK) and Magnitogorsk (MMK) Integrated Iron and Steels Works blast furnaces is plotted, the interaction of the zinc vapors with the blast furnace dust is investigated under a microscope, and the zinc distribution in the blast furnace is examined graphically. The study reveals that all zinc-containing charge materials have common zinc behavior patterns which are related to the process conditions and may explain the discrepancy observed between the inflow and outflow parts of the zinc balance. A number of measures for decreasing zinc's harmful effect are suggested on the basis of the relationship between the zinc behavior and the blast furnace process and it is noted that this range of measures is far from being complete. The need for further research is stressed, especially in regard to the effect of the charging system and the furnace cooling system and its parameters on the zinc behavior. The authors and the editors are hopeful that a broad range of experts will become involved in studying this problem. Figures 4; references 4: 3 Russian, 1 Western.

Development of Multijet Injectors of Natural Gas Into Blast Furnace Tuyere

927D0176B Moscow STAL in Russian
No 2, Feb 92 pp 9-12

[Article by Yu.P. Mityushin, Yu.V. Fedulov, V.P. Monastyrskov, V.M. Udilov, V.I. Moykin, Magnitogorsk Integrated Iron and Steel Works and All Union Scientific Research Institute of Metallurgical Heat Technology; UDC 669.162.22.2]

[Abstract] The possibility of enhancing the natural gas (PG) utilization efficiency at a high consumption rate in a blast furnace by improving the gas conversion without the soot formation and developing favorable H_2 radial distribution in the shaft are discussed and a formula is derived for the relative depth of jet penetration which characterizes gas feed conditions in the blast. A computer routine is developed for examining the effect of the natural gas injector designs and conditions on the gas jet penetration depth. The dependence of the relative natural gas penetration depth on the blast rate and natural gas pressure, the temperature distribution in the blast cross section at a 87 mm distance from the injection point, and the gas distribution in the furnace top radius in a Magnitogorsk blast furnace are plotted. The operation of conventional tuyeres and new tuyeres with multijet gas injection is compared and the operating indicators of the furnace with a new natural gas injection method are summarized. The use of the new tuyere design resulted in a change in the gas distribution character, a drop in the hydrogen content on the periphery, and an increase in the H_2 content in the axial zone, thus improving the mixing conditions. The ore utilization efficiency rose and the coke consumption decreased. A lesser effect is obtained after an extended furnace operation, probably due to its deterioration and the substitution of experimental tuyeres with standard designs. Figures 4; tables 1; references 5.

Development of 7KhNM Steelmaking Process in Open Hearth Furnaces

927D0176C Moscow STAL in Russian
No 2, Feb 92 pp 18-19

[Article by N.F. Bakhcheyev, A.F. Sarychev, Yu.A. Ivin, V.N. Bobkov, V.V. Pavlov, Magnitogorsk Integrated Iron and Steel Works; UDC 669.054]

[Abstract] A process for smelting steel 7KhNM in a single-runner open hearth furnace developed at the Magnitogorsk Integrated Iron and Steel Works and the difficulties of controlling the sulfur concentration are outlined and the mechanical properties and microstructure of the cold and hot rolled coils made from steel smelted by the new method are investigated. The metal part of the charge consist of 40 percent scrap and 60 percent molten pig iron. After the bath is fully melted, the slag is forcibly removed and the new slag is pumped in, then lime and crushed chamotte are added. The metal is alloyed with Mo and Ni in the course of the process. Pilot products are refined by the users and their properties are examined; the results show that the technical level of cold rolled coils from steel 7KhNM smelted in open hearth furnaces corresponds to the quality of the coil shipped by German companies. The resulting steel has a sulfur concentration of no more than 0.012 percent and meets the requirements of the TU 14-4-1411—87 specifications. The economic impact from implementing the new method exceeds 200 thousand rubles. Figures 1.

Argon Blasting of Ingot Header of Rimmed Chemically Capped Steel

927D0176D Moscow STAL in Russian
No 2, Feb 92 pp 19-20

[Article by G.P. Burakovskiy, V.P. Andreyev, L.I. Yeliseyev, N.M. Kolova, Magnitogorsk Integrated Iron and Steel Works; UDC 621.746.58]

[Abstract] A method of improving the quality of chemically capped ingots by decreasing its contamination with nonmetallic inclusions by lowering the deoxidizer rate for capping while improving its mixing with the metal is discussed and an experiment to blast the ingot header of chemically capped rimmed steel with argon carried out at the Magnitogorsk Integrated Iron and Steel Works is described. Rimmed steel is smelted in a two-bath steelmaking unit with a 300 t bath capacity while coke breeze is added to the ladle to control the metal oxidation. The metal macrostructure of 12 pilot and 10 conventional smeltings is examined and the chemical composition behavior of steel 08kp along the axis and periphery of a slab made from an ingot with argon blasting and wooden rod stirring is plotted. The findings indicate that the ingot head blasting with argon makes it possible to lower the aluminum consumption for capping and obtain a dense macrostructure at higher ingot layers as well as considerably to decrease the amount of aluminum oxide (Al_2O_3) and nonmetallic inclusions dissolved in the metal. As a result, it becomes possible to improve the ingot head quality and reduce the amount of top discards by 0.43 percent. Figures 1; tables 1; references 2.

Improving Killed Steel Ingot Quality

927D0176E Moscow STAL in Russian
No 2, Feb 92 pp 20-22

[Article by V.P. Vozhdayev, Yu.N. Selivanov, V.P. Prishedko, Magnitogorsk Integrated Iron and Steel Works; UDC 621.746.58]

[Abstract] A comparative study of ingots cast into big-end-up (UV) and small-end-up (UNT) ingots with hot tops insulated with fireclay brick and the relative volume of top discards led to the conclusion about the expediency of expanding the range of killed steel cast into small-end-up ingots; to this end, a study is carried out at the Magnitogorsk Integrated Iron and Steel Works aimed at finding ways of slowing down the solidified metal "bridge" formation under the ingot head and preventing the secondary shrinkage cavity development. The study shows that this can be attained by increasing the ingot cross section under the head by eliminating the planar mold segment and matching the insulation slab profile to that of the inside walls. Six ingots cast into UNT molds and six ingots cast into UV molds are examined and their macrostructure and chemical composition are analyzed. The axial carbon and sulfur distribution in pilot and regular ingots of steel 65G and the carbon distribution in the height of steel 45 ingot cast into small-end-up molds are plotted and the carbon segregation, its mean value, and spread in pilot and regular ingots are summarized. The findings show that the use of curvilinear insulating slabs makes it possible to increase the range of killed steel cast into UNT ingots and attain a 2 percent top discard gain and a 5 kg/t mold gain as well as improve the ingot surface quality. Figures 3; tables 2; references 2.

Improving Steel Quality for Cold Rolled Band by Degassing

927D0176F Moscow STAL in Russian
No 2, Feb 92 p 23

[Article by V.I. Frolov, V.F. Sarychev, N.F. Bakhcheyev, V.N. Bobkov, Magnitogorsk Integrated Iron and Steel Works; UDC 669.014.4]

[Abstract] The failure of the semifinished rolled stock shipped by the Magnitogorsk Integrated Iron and Steel Works to the Krasnaya Etna Plant for making cold rolled steel band to meet specifications prompted a decision to substitute rimmed steel with killed steel for making 08YuT in double-bath open hearth furnaces. To this end, rimmed semifinished product with $\leq$0.10 percent C at 1,620-1.635°C is deoxidized by ferromanganese in the ladle and transferred to a degassing machine, then cast into small-end-up molds with hot tops. The frequency distribution of the C, Mn, S, and P concentration in steel 08YuT and 08kp and Ti and Al content in steel 08YuT and the frequency distribution of the ultimate strength and elongation of steel 08YuT and 08kp are plotted. Tests of pilot metal at the client plant demonstrates that the strength and surface quality of the semifinished rolled stock improved while maintaining virtually the same ductility. The annual economic impact from implementing the new type of steel exceeds 300 thousand rubles. Figures 2.

Lowering Ferromanganese Outlays in Steelmaking

927D0176G Moscow STAL in Russian
No 2, Feb 92 pp 24-25

[Article by A.I. Blokhin, Yu.N. Volshchukov, A.I. Sergeyev, V.V. Pavlov, S.I. Voronin, Magnitogorsk Mining and Metallurgy Institute and Magnitogorsk Integrated Iron and Steel Works; UDC 669.054]

[Abstract] A system for analyzing the deoxidizer rate in steelmaking is developed and implemented by the Magnitogorsk Mining and Metallurgy Institute together with the Magnitogorsk Integrated Iron and Steel Works in order to find qualitative and quantitative correlations between the thermal and process conditions of blasting and the slag and metal oxidation during the smelting of steel 08kp, 11kp, B1kp, and B2kp in double-bath steelmaking vessels. All smelting are classified as a result of analyzing the experimental results. The dependence of the oxygen concentration in the metal and the iron oxide content in the slag on the carbon concentration is plotted and a flow chart of the system for determining the ferromanganese outlays is cited. Regression equations which connect the Mn loss to the metal overheating over the liquidus line are derived and analyzed. An examination of the bath's thermal condition and its effect on the ferromanganese consumption necessary for making steel with a specified Mn content in the ready metal shows that an annual economic impact of 108,106.87 rubles is attained while the ferromanganese outlays are decreased

from 7.8 to 7.19 kg/t. A P-100 programmable input/output chip is used in calculations. Figures 2; references 2.

Improving Rimmed Chemically Capped Steel Quality During Casting by Using Intensifying Briquettes

927D0176H Moscow STAL in Russian
No 2, Feb 92 pp 26-27

[Article by G.P. Burakovskiy, V.S. Ploshkin, A.I. Mitrokhin, L.I. Yeliseyev, R.I. Myachin, Magnitogorsk Integrated Iron and Steel Works; UDC 621.746.68]

[Abstract] Additions of intensifying briquettes to molten metal during the casting of 7-ton ingots into small-end-up molds in order to increase the boil intensity and decrease ingot tears is discussed and effect of these intensifying briquettes on the macrostructure quality, chemical uniformity, steel contamination with nonmetallic inclusions, and surface defects on the ingots is investigated. To this end, metal is smelted in 400 ton open hearth furnaces and deoxidized with ferromanganese in the furnace or the ladle while the intensifying briquettes are added during the casting. Granulated aluminum is also added in the case of molten metal shrinkage in the mold. The characteristics of the ingots cast with intensifying briquettes and by conventional technology, the nonmetallic inclusion composition of the ingots cast with intensifying briquettes and by conventional technology, and the quality of billets produced by rolling pilot and conventional ingots are compared. An analysis shows that the use of intensifying briquettes in smelting rimmed steel chemically capped with aluminum makes it possible to produce metal with a suitable macrostructure at higher ingot levels thus decreasing the steel contamination with nonmetallic inclusions and decreasing the volume of rejects due to tears. Tables 3.

Material Balance of Ferrosilicon Smelting With Vanadium

927D0176I Moscow STAL in Russian
No 2, Feb 92 pp 34-37

[Article by N.V. Tolstoguzov, S.S. Zhilyakov, V.N. Tolstoguzov, M.A. Solovyev, I.A. Selivanov, Siberian Metallurgical Institute and Kuznetsk Ferroalloys Plant; UDC 669.168.3:669.292'782]

[Abstract] The large number of stages involved in preparing vanadium concentrates for smelting their alloys by processing vanadium-containing converter slags, vanadium-rich ores, or concentrates and the resulting low vanadium recovery prompted the Chelyabinsk Integrated Iron and Steel Works and the Urals Branch of Russia's Academy of Sciences to develop a composition and technology for smelting of a vanadium alloying composition with 8-12 percent V and 10-20 percent Si directly from vanadium slag by silicothermic reduction and the Kuznetsk Ferroalloys Plant and the Siberian Metallurgical Institute to develop a technology for melting an alloying composition with 6-8 percent V and 45 percent Si by continuous carbothermy. The material balance of the ferrosilicovanadium smelting by carbothermy at the Kuznetsk Ferroalloys Plant (KZF) is examined and the vanadium and addition (Mn, Ti, Cr) concentrations and their ratios in vanadium slag, quartzite, coke, and iron chips are summarized. The effect of the iron concentration in the dump slag on the V_2O_5 concentration is plotted and the sources of V, Si, and additions and their distribution among the smelting products of ferrosilicon and vanadium are investigated. An analysis of the material balance shows that vanadium and its concomitant additions are reduced virtually completely and largely pass to the metal during the smelting. For example, the Ti and Mn recovery during the ferrosilicon smelting with vanadium reaches 90-92 percent. Figures 1; tables 3; references 9.

Making Steel 08Yu of Higher Drawability Classes

927D0176O Moscow STAL in Russian
No 2, Feb 92 pp 65-68

[Article by S.A. Bratus, V.A. Maslennikov, E.D. Nemkina, V.P. Gubchevskiy, A.A. Vostrikov, Magnitogorsk Integrated Iron and Steel Works; UDC 669.14.018.262]

[Abstract] The need to increase considerably production of cold stamping steel for complex drawing necessitated by the development of the automotive and tractor industry prompted an investigation of the behavior of strip metal structure and properties at all process stages, including the initial slab state. To this end, two smeltings of aluminum-killed low carbon steel 08Yu made by cycling degassing and deoxidation in a vacuum chamber are examined and their chemical composition is summarized. The microstructure parameters of two types of slabs—cooled in a stack and stripped manually—are analyzed and the character of cementite particle size distribution in annealed sheets made from the slabs is plotted. The mechanical properties and structure of hot rolled strips of top and bottom cast slabs, the microstructure parameters of cold rolled annealed strips, and the physical and mechanical properties of annealed strips made from top and bottom cast slabs. The study demonstrates that polymorphous transformations in slabs of steel 08Yu determine the excess phase, pearlite column, and nonmetallic inclusion distribution and the state of solid solution at all process stages while additional $(\alpha+\gamma)+(\gamma+\alpha)$ transformations suppress the development of the structurally free cementite grid on the ferrite grain boundaries and refine pearlite columns. Accelerated slab cooling makes it possible greatly to improve the stamping properties of steel 08Yu sheets. The study also underscores the urgency of controlling not only the nitride but also the carbide formation processes at the earliest process stages. The findings are corroborated by pilot and commercial tests at the Magnitogorsk Integrated Iron and Steel Works. Figures 1; tables 5; references 5: 3 Russian, 2 Western.

New Type of Steel Making Vessel

927D0175B Dnepropetrovsk METALLURGICHESKAYA I GORNORUDNAYA PROMYSHLENNOST in Russian No 4 (162), Oct-Dec 91 pp 10-11

[Article by N.M. Skorokhod, N.A. Antonov, V.A. Rybinov, Kommunarsk Integrated Iron and Steel Works; UDC 669.183.21.041.43:658.589]: [502.55:628.51]

[Abstract] After the sintering and blast processes, the open hearth plant at the Kommunarsk Integrated Iron and Steel Works is the principal source of pollution within the iron and steel plant itself and the city as a whole. This fact calls for substituting the open hearth process with a much cleaner and economically more efficient converter process, yet the plant lacks the necessary resources for such a step. After studying the experience of the Orsk-Khalilovo Integrated Iron and Steel Works where a two-bath open hearth furnace was upgraded, open hearth No. 10 was switched to the intermediate operating condition in 1989. Its success prompted the development of a new high-capacity unit during the overhaul of open hearth furnaces Nos. 1 and 2; the resulting steel-making vessel is a furnace with two melting chambers and one vertical gas exhaust channel located between the two baths at the center of the furnace. Each bath has three charging doors with aerodynamic curtains on them, thus completely eliminating gas discharges through the doors during all smelting phases. The new unit has two gas scrubbing systems operating in a parallel mode with a single exhaust channel. At the end of commercial tests the new unit will be certified by a special commission involving scientists, iron and steel works representatives, and state environmental authorities so as to make the decision whether to replace other open hearth furnaces with such units. Figures 2.

Confidence Coefficient of Blast Furnace Zone Balance Analysis Data

927D0175E Dnepropetrovsk METALLURGICHESKAYA I GORNORUDNAYA PROMYSHLENNOST in Russian No 4 (162), Oct-Dec 91 pp 28-30

[Article by K.M. Bugayev, Donetsk Scientific Research Institute of Ferrous Metallurgy; UDC 669.162.263. 046.5.012.34 .021.3.4.001.24]

[Abstract] The characteristic features of the zone balance analysis of blast furnaces are discussed and the procedure for analyzing the heat and mass transfer in each zone as well as for the blast furnace as a whole is outlined. The premise of the S-shaped temperature variation with the furnace height is checked and it is demonstrated both experimentally and analytically that the gas flow heat capacity is not constant along the blast furnace height but decreases in the intensive mass transfer zone, probably due to the tuyere gas on its path to the furnace top. The temperature on the thermal zone boundary varies as a function of the gas and burden mass flows. The decrease in the tuyere gas heat capacity in the intensive reduction zone is manifested at all melting parameters and at any arbitrary reduction course. The positions of the thermal zone boundaries are determined by the gas:burden mass ratio which correspond to changes in their heat capacity along the furnace height. It is suggested that all processes occurring in the blast furnace as well as the factors of gas flow variability in the furnace height and the temperature level in the delayed heat exchange zone be taken into account in order to increase the confidence level of the zone balance analysis and calculations. Figures 4; references 4.

Liquid Steel Treatment in Ingot Mold by Powder Wire

927D0175F Dnepropetrovsk METALLURGICHESKAYA I GORNORUDNAYA PROMYSHLENNOST in Russian No 4 (162), Oct-Dec 91 pp 31-32

[Article by V.A. Vikhlevshchuk, V.M. Chernogritskiy, V.A. Polyakov, V.I. Drachev, Yu.G. Badogin, N.M. Omes, Ferrous Metallurgy Institute and Zaporozhstal Integrated Iron and Steel Works; UDC 669.141.245.046.516:621.746.393]:621.762-426.001.5]

[Abstract] The efficiency of using powder wire with silicocalcium and an alloying composition of rare earth metals (RZM) for treating converter steel in the ingot mold developed by the Ferrous Metallurgy Institute together with Zaporozhstal Integrated Iron and Steel Works is investigated. To this end, samples of steel St3sp, 08YuT, 35, 45, and Sv-08G2S melted in 60 t converters are deoxidized during the tapping process and alloyed by adding ferroalloys and aluminum to the ladle. The type of wire filler and wire rate, the filler rate, the wire addition method, and mass fraction of elements in steel before and after the wire addition to the ingot mold are summarized as a function of the steel brand and the rare earth metal and calcium content distribution in the billet cross section as a function of the time of powder wire addition to the ingot mold during the casting is plotted. The conclusion is drawn that addition of powder wire immediately after the end of casting to metal with an aluminum content of at least 0.03 percent is optimal. The use of powder wire with SKZO silicocalcium and FS30RZM3O rare earth metal alloying composition for microalloying in the ingot mold makes it possible to lower the ferroalloy consumption by 2.5-3 times due to improving the assimilation of elements, resulting in an economic impact of 1-5 rubles per ton. Figures 1; tables 2; references 1.

Mastering Alloyed Steel Steel Smelting in 350 Ton Converters Using Liquid Alloying Compositions and Ladle Refining

927D0175G Dnepropetrovsk METALLURGICHESKAYA I GORNORUDNAYA PROMYSHLENNOST in Russian No 4 (162), Oct-Dec 91 pp 33-35

[Article by L.F. Kosoy, S.I. Yaburov, M.A. Pozhivanov, O.V. Nosochenko, S.G. Melnik, Central Scientific Research Institute of Ferrous Metallurgy and Azovstal Integrated Iron and Steel Works; UDC 669.15'26'24'28-194.046.516.523.54:621.746.32].001.5]

[Abstract] Success in bringing on stream a new oxygen converter plant with two DSP-12NZ arc furnaces and one RKZ-16.5 5FL-I1 slag melting furnace for melting alloying composition and synthetic slags opened the way for using a new technology of smelting alloyed steel in large capacity (350 ton) oxygen converters using liquid alloying compositions. The use of such compositions makes it possible to solve many converter steel making problems, such as greatly lowering the final blast and metal tap temperatures, decreasing the slag and metal oxidation, reducing the thermal load on the converter lining and the number of blasts, improving the steel deoxidation quality, and lowering the pig iron outlays. A schematic diagram of the converter plant with a synthetic slag and liquid alloying composition melting section is cited and the behavior of the chemical composition of the pilot melting metal during the argon blast as well as the mechanical properties of steel 02G2S made with a liquid alloying composition and with solid ferroalloys are outlined. Phase one of the assimilation process shows that it is rather efficient from the economic and quality viewpoints. Combined with ladle refining, this method of smelting steel 09G2S, 13G1SU, and 17G1SU also reduces the Mn and Si melting loss by 3.5 and 7 percent, respectively, and lowers the sulfur concentration in ready steel by 0.001-0.005 percent as well as increases toughness by 1.5 times. The economic impact from its implementation at the Azovstal reaches 900 thousand rubles per year. In addition, the level of harmful discharges does not exceed the maximum allowable concentration. Figures 1; tables 4; references 1.

Metal Desulfurization in Ladle by Active Slag Mixtures

927D0175H Dnepropetrovsk METALLURGICHESKAYA I GORNORUDNAYA PROMYSHLENNOST in Russian No 4 (162), Oct-Dec 91 pp 35-38

[Article by M.A. Pozhivanov, P.M. Semenchenko, S.V. Kazakov, O.A. Poshinov, A.G. Svyazhin, Azovstal Integrated Iron and Steel Works and Moscow Steel and Alloy Institute; UDC 669.184.046.587.6.004.12:621.746.32]

[Abstract] Various out-of-furnace metallurgy methods based on the sulfur redistribution between the metal and sulfur-free refining slag and their shortcomings are addressed and the need for additional metal refining for the purpose of sulfur removal in a ladle refining machine (UDM) is noted. The process of ladle sulfur-removal refining with the help of active slag mixtures is investigated at the Azovstal Integrated Iron and Steel Works where metal is melted in a 350 ton converter and cast at a 1,600-1,700°C temperature with a tap duration of 4.3-11 min; the temperature prior to ladle refining varies within 1,550-1,605°C while the inert gas blast duration varies within 4-20 min at a rate of 30-100 m^3/h of argon. The dependence of the distribution coefficient at the tapping moment on the CaO content in the slag, a change in the S concentration in the melt as a result of ladle refining, and the dependence of the total sulfur removal degree in the ladle on the product of the ladle slag's sulfide capacity (calculated from the value of the slag's optical basicity) by the lag layer thickness before the start of the UDM process are plotted. An analysis reveals that under existing active slag mix treatment conditions, the refining utilization of slag averages 10 percent for synthetic slag (SSh), 6.5 percent for solid slag-forming mixtures (TShS), and 3 percent without the mixture, whereas the desulfurizing process occurs mostly during the tapping. It is shown that the sulfur removal process can be controlled by manipulating the slag composition and amount. It is suggested that the slag be additionally stirred in the ladle in the UDM machine since blasting through the lance is inefficient. Figures 3; references 4.

Effect of Ion Irradiation on Composition and Atomic Structure of Fe-Ni System Alloys

927D0171H Moscow POVERKHNOST: FIZIKA, KHIMIYA, MEKHANIKA in Russian No 4, Apr 92 pp 113-121

[Article by M.A. Vasilyev, S.D. Gorodetskiy, Institute of Physics of Metals at the Ukrainian Academy of Sciences, Kiev; UDC 584.4;211;541;123]

[Abstract] The use of ion irradiation of the solid state surface as a means of surface measurements and surface layer diagnostics and the resulting changes in the surface properties are discussed and the effect of the low-energy irradiation of the surface of single crystal alloys of the Fe-Ni system with various crystallographic orientations with Ar^+ ions on the atomic structure and surface composition is investigated. To this end, measurements are taken in a combined slow electron diffraction/Auger electron (DME/EOS) superdeep vacuum spectrometer equipped with a four-grid quasispherical energy analyzer and a diffraction reflex photometer. The dependence of the Fe concentration on the surface of Fe-Ni alloys on the ion irradiation doze, the temperature dependence of the isothermal annealing time of $FeNi_3(100)$ after ion irradiation necessary for restoring the equilibrium surface concentration of components, and layer-by-layer curves of the percentage change in the intreplanar spacing on the $FeNi_3(100)$ surface at various ion energies are plotted. The annealing activation energy for various faces of Fe-Ni system alloys and the dependence of the lattice constant on the ion energy for various Fe-Ni

system alloys are summarized. An analysis shows that a large number of stable nonequilibrium vacancies forms in the near-surface area under irradiation which, in turn, stimulates the Ni atom diffusion. The mean surface destruction area per incident ion and a relative change in the interplanar distance are calculated and it is established that the above defect formation parameters are substantially anisotropic due to the difference in the atomic interaction force constants of the corresponding crystal faces. Figures 3; tables 2 references 25: 8 Russian, 17 Western.

Abnormal Mass Transfer in $Fe_{70}Ni_{27}Mn_3$ Alloy Under Low-Energy Proton Irradiation

927D0171I Moscow POVERKHNOST: FIZIKA, KHIMIYA, MEKHANIKA in Russian No 4, Apr 92 pp 122-124

[Article by V.A. Tsurin, A.M. Sorkin, N.P. Filippova, V.A. Pavlov, Institute of Physics of Metals at the Urals Branch of Russia's Academy of Sciences, Yekaterinburg; UDC 620.193+621.785]

[Abstract] The abnormal behavior of the real crystal structure in the near-surface layers extending from the surface to a distance much greater than the particle path length during the solid state interaction with a charged particle flux is discussed and the mixing effects as well as the surface phase penetration depth are investigated under the conditions of intense low-energy ion irradiation at low temperatures. To this end, a face-centered cubic lattice (GTsK) $Fe_{70}Ni_{27}Mn_3$ alloy enriched with ^{57}Fe by 25 percent is subjected to diffusion annealing for 100 h at 1,000° and irradiated with H^+ ions at a 12 keV energy with a 70 nm free path length at a current density of 100 $\mu A/cm^2$ with a 3×10^{19} cm^{-2} dose at 90K. The Moessbauer spectra of conversion ions of the 15 μm thick alloy foil with a 200 nm thick sprayed ^{57}Fe layer and the ratio of the surface phase subspectrum area to the total spectrum area as a function of the thickness of the removed layer are plotted. The analysis reveals mixing and interpenetration under proton irradiation and shows that α-Fe penetrates to a depth exceeding the sprayed layer depth by an order of magnitude; this is attributed to an elastic wave propagation. The experiment did not fully establish the other sources of the long-range effect. Figures 2; references 8: 6 Russian, 2 Western.

Blast Furnace Restart Blowing After Extended Shutdown

927D0170A Dnepropetrovsk METALLURGICHESKAYA I GORNORUDNAYA PROMYSHLENNOST in Russian No 1 (163), Jan-Mar 92 pp 8-10

[Article by G.G. Vasyura, V.N. Dementyev, G.P. Troitskiy, Kommunarsk Integrated Iron and Steel Works and Yenakiyevo Iron Works; UDC 669.162.261.2.267.33.002.26:[621.74:621.182.3.001.24]

[Abstract] A 1,719 m^3 blast furnace is restarted at the Kommunarsk Integrated Iron and Steel Works after an emergency six day shutdown without a preliminary preparation. The criteria used in selecting the blow-in restart pace and the charge composition are outlined and the blast furnace operating parameters during the blow-in restart period, such as the pressure, temperature, O_2 concentration, natural gas rate, number of tuyeres in operation, the amount of pig iron smelted, the amount of slag in the ladle, the Si and S concentration in the metal, the CO_2, CO, and H_2 concentration in the flue gas, and the CO utilization percentage, are summarized. An analytical procedure is developed for calculating the coke rate under nonstandard production conditions. The blast furnace blow-in restart method makes it possible to determine the coke rate with an accuracy sufficient for practical applications. Recommendations are developed for the blow-in restart conditions, e.g., to close down some tuyeres and increase the duration of charge stay in the furnace by 1.7-2 times. Tables 1.

Ferromanganese Smelting Using Burden With Decreased Manganese Content

927D0170B Dnepropetrovsk METALLURGICHESKAYA I GORNORUDNAYA PROMYSHLENNOST in Russian No 1 (163), Jan-Mar 92 pp 10-12

[Article by V.A. Gordiyenko, G.G. Vasyura, L.M. Rudakov, V.I. Varava, Kommunarsk Integrated Iron and Steel Works and Donetsk Scientific Research Institute of Ferrous Metallurgy; UDC 669.162.262-034.74:669.743.11]

[Abstract] In recent years, the Mn concentration in the ferromanganese smelting charge dropped by 5.1 percent due to a substitution of a part of oxide manganese concentrate with a 43-45 percent Mn content with a carbonate concentrate with a 28-29 percent Mn concentration. This necessitated a number of corrections in the temperature-blast, slag, thermal, and gas dynamic conditions in the ferromanganese smelting process. The resulting theoretical and practical studies helped to establish that a decrease in the metallurgical value of the manganese concentrates used in the process sharply reduces the blast furnace productivity and increases the coke consumption. Analyses show that in order to ensure technologically stable and emergency-free blast furnace operation with a somewhat Mn-depleted charge, it is necessary first of all to maintain the hearth in the active state and ensure the blast furnace smelting of ferromanganese using stable slags. Tables 4.

Assimilation of Commercial Plant for Measuring Coke Combustibility at Dneprovskiy Integrated Iron and Steel Works

927D0170C Dnepropetrovsk METALLURGICHESKAYA I GORNORUDNAYA PROMYSHLENNOST in Russian No 1 (163), Jan-Mar 92 pp 12-14

[Article by A.D. Dzhigota, F.N. Moskalina, A.P. Monarshuk, V.A. Danko, A.S. Romanenko, Ferrous Metallurgy

Institute and Dneprovskiy Integrated Iron and Steel Works; UDC 662.74:536.468].003.12.001.76]

[Abstract] The inadequacy of today's criteria for estimating the coke properties and their inconsistency with modern concepts of the functional role of coke in the blast furnace process prompted the development and assimilation of new methods of evaluating the metallurgical properties of blast furnace coke. Special attention is focused on the coke's high-temperature properties, primarily its chemical activity under the effect of oxidants, such as carbon dioxide (i.e., reactivity), and oxygen (i.e., combustibility). To this end, a procedure for determining the coke combustibility indices and progress in assimilating a pilot-commercial coke combustibility measuring plant designed by the Ferrous Metallurgy Institute (IChM) and assembled at the Dneprovskiy Integrated Iron and Steel Works is described and the combustibility index values of Bagleyskiy By-Product Coke Plant (KKhZ) during the assimilation period are summarized. A schematic diagram of the coke combustibility measurement plant is cited and a statistical analysis of the indicator stability is performed. It shows a high variability of this parameter under real commercial conditions and the resulting inevitable and uncontrollable blast furnace distortions. It is suggested that the coke combustibility be controlled within a narrow range so as to obtain data for making on the spot decisions on manipulating the blast furnace smelting parameters. Figures 1; tables 2; references 1.

Improving Quality of 8.5-Ton Killed Steel Ingots Cast With Hot Top Insulated by Heat Resistant Concrete

927D0170D Dnepropetrovsk METALLURGICHESKAYA I GORNORUDNAYA PROMYSHLENNOST in Russian No 1 (163), Jan-Mar 92 pp 16-17

[Article by M.Ya. Zavadskiy (deceased), A.Yu. Konoplyanik, N.M. Omes, V.I. Bashliy, V.A. Koshelev, Dnepropetrovsk Civil Engineering Institute and Krivorozhstal Integrated Iron and Steel Works; UDC 669.141.241.2-412.004.12:[621.746.464:666.974.2]

[Abstract] A mechanized plant for making two-layer feeder head hot top from heat resistant concrete built at the Krivoy Rog Integrated Iron and Steel Works is described and the quality of the metal cast into 8.5 ton ingots with hot tops lined with fireclay brick and heat resistant concrete is examined in order to estimate the effect of heat resistant concrete lining on the heat insulating ability of the hot top. Schematic diagrams of hot tops with chamotte and heat resistant concrete lining are cited and hot top specifications are summarized. An analysis of the metal quality demonstrates that shrinkage defects in ingots cast with hot tops lined with heat resistant concrete are located in the feeder head section rather than the ingot body while the liquid metal volume decreases by 0.026 m^3. The resulting improvement in the heat insulating capacity of the hot top with a heat resistant concrete over that with fireclay brick makes it possible to reduce the volume of top discards by 0.8 percent. Figures 2; tables 1.

Lowering Top Discards of 24-Ton Killed Steel Ingots Cast With Hot Top Insulated by Heat Resistant Concrete

927D0170E Dnepropetrovsk METALLURGICHESKAYA I GORNORUDNAYA PROMYSHLENNOST in Russian No 1 (163), Jan-Mar 92 pp 18-19

[Article by Ye.G. Gryzlov, A.I. Belkin, Ye.N. Agafonova, M.Ya. Zavadskiy (deceased), Mariupol Integrated Iron and Steel Works imeni Ilich and Dnepropetrovsk Civil Engineering Institute; UDC 669.141.241.2-412.004.12:[621.746.464:666.974.2]

[Abstract] The scarcity of experimental data on the effect of the hot top with heat resistant concrete lining and its advantages over fireclay brick lining and, consequently, the possibility of decreasing metal losses with top discards prompted additional studies of the quality of metal cast from steel 20SP into 24 ton ingots. To this end, an experiment is conducted whereby the ingots cast with hot tops lined with heat resistant concrete are regarded as experimental while those with a fireclay brick lined hot top—as a standard group. The macrostructure of the metal in the feeder head of the experimental and standard ingots is cited and the maximum positive C, S, and P segregation in the experimental and reference ingots and the slabs rolled from them are summarized. An analysis of the data indicates that shrinkage defects in the ingots cast with the heat resistant concrete hot top lining do not extend to the ingot body while the metal weight in the feeder head is lowered by 300 kg. Moreover, the experimental and standard ingots have almost the same chemical metal inhomogeneity, which is consistent with earlier findings. The use of the heat resistant concrete as hot top lining instead of the fireclay brick makes it possible to lower the top discards of 24 ton ingots made from killed steel by 1 percent. Figures 1; tables 2; references 1.

Successive Phase Transition Kinetics in InSb Films Made by Pulse Condensation

927D0189B Moscow ROSSIYSKAYA AKADEMIYA NAUK: NEORGANICHESKIYE MATERIALY in Russian Vol 28 No 5, May 92 pp 947-954

[Article by V.I. Petrosyan, O.I. Vasin, Radio Engineering and Electronics Institute at Russia's Academy of Sciences; UDC 548.526;538.9;536.425]

[Abstract] The sequence of solid phase transitions occurring after rapid condensation of thin films by the dielectric amorphous-metastable close packed metallic conduction-crystal semiconductor (A-M-K) mechanism is discussed and the importance of understanding the transformation kinetics for practical applications is stressed. The A-M-K phase transformation kinetics are studied by measuring the electric conductivity of InSb films within a 200-2,000 angstrom thickness range condensed at a rate of close to 1 μm/s at various temperatures on mica with film contacts applied beforehand. The dependence of the InSb film conductivity on the elapsed time since the end of condensation at various condensation temperatures, the experimental dependence of the metastable phases' volume fraction on the elapsed time, the temperature dependence of the interfacial boundary movement rate in the film, and the potential profile of A-M-K phase transitions are plotted. An analysis of the experimental findings shows that the "transit" metastable phase domain may exist in the sequential phase transition; as the temperature increases, the domain becomes thinner and eventually degenerates into an interfacial amorphous-crystalline boundary. The amorphous→crystalline transition discovered in InSb at $T \approx 400$K occurs in place of the A-M-K phase transition. The critical condensation temperature equal to one half of the InSb melting point is interpreted as the level below which Ostwald's rule is satisfied and above which it is not. Figures 5; tables 1; references 8.

Electrocapillary Phenomena on Liquid Lead in Chloride Melt With Lithium and Potassium Nitrate Additions

927D0183A Vladikavkaz IZVESTIYA VYSSHIKH UCHEBNYKH ZAVEDENIY: TSVETNAYA METALLURGIYA in Russian No 3, Jun 91 pp 26-28

[Article by T.V. Valuyeva, V.B. Patrov, Ye.P. Babiy, Leningrad Polytechnic Institute; UDC 669.2]

[Abstract] Earlier studies of electrocapillary phenomena on the liquid lead/salt melt interface (*Tsvetnaya metallurgiya* No 4 1983 and No 5 1989) are continued and the findings obtained in a study of electrocapillary phenomena on liquid lead in eutectic lithium and potassium chloride solutions with an addition of up to 7.5 percent mol. of potassium and lithium nitrites at a 723K temperature are discussed. The surface and interfacial tension and zero charge potential as a function of the component concentration in the eutectic LiCl-KCl melt are summarized and electrocapillary curves on liquid lead in the chloride melt with additions are plotted. An analysis of the curves and data shows that addition of up 7.5 percent mol of $LiNO_3$ and KNO_3 leads to a decrease in interfacial tension at the electrocapillary curve (EKK) maxima from 450 to 379 and 410 mJ/m^2, respectively, and a shift of the zero charge potential toward more electropositive values. This shift is consistent with the correlation of the electron work function of a metal when it is transferred from a vacuum to the salt melt, the affinity of alkali metal cations for electrons, and the alkali metal cation binding energy to anions. The effect of nitrates attests to their surface activity in the chloride salt melt. Figures 1; tables 2; references 3.

Optimization of Low-Temperature Guinea Bauxite Leaching Process

927D0183B Vladikavkaz IZVESTIYA VYSSHIKH UCHEBNYKH ZAVEDENIY: TSVETNAYA METALLURGIYA in Russian No 3, Jun 91 pp 62-68

[Article by V.M. Alkatseva, V.F. Kokayeva, T.N. Kudinova, L.K. Sizkova, North Caucasian Mining and Metallurgy Institute; UDC 669.712]

[Abstract] The process of Guinea bauxite leaching by Bayer's method and its shortcomings, primarily the excessive electric power outlays, are discussed and an attempt is made to optimize the process of low-temperature leaching of Guinea bauxite while the alumina recovery to the solution during the leaching process is selected as the objective variable. Given a constant milling size, the principal factors affecting the bauxite leaching are the recirculating solution temperature and concentration, the caustic moduli of the circulating and aluminate solutions, and the leaching duration. The chemical composition of the Gibbs-type Guinea bauxite is summarized and the experiment procedure is outlined. A leaching algorithm is developed and the equilibrium solution composition at a given leaching temperature, liquid:solid isolines at various caustic alkali concentrations in the recirculation solution, and the alumina extraction isolines are plotted. The experimental alumina recovery reaches 93.68 percent vs. the theoretical figure of 94.75 percent; thus, under optimal conditions, alumina recovery is close to theoretical. The replication error is calculated and is equal to 8.5583 percent. In contrast to the two-stage leaching process used abroad where the first stage pulp is sent to the second stage, it is suggested that the first stage pulp be sent to the second stage after separating if from the aluminate solution. Figures 3; references 11: 9 Russian, 2 Western.

Microstructure and Mechanical Properties of 20-100 kg Br013 Tin Bronze Ingots

927D0183C Vladikavkaz IZVESTIYA VYSSHIKH UCHEBNYKH ZAVEDENIY: TSVETNAYA METALLURGIYA in Russian No 3, Jun 91 pp 94-98

[Article by Yu.V. Yefimov, L.A. Ryabtsev (deceased), V.V. Tatarenko, T.M. Frolova, M.Ye. Savelyeva, N.N.

Litvinova, Metallurgy Institute imeni A.A. Baykov at Russia's Academy of Sciences and All-Union Correspondence Polytechnic Institute; UDC 669.35'6]

[Abstract] Extensive applications of bronze in various industries and a shortage of data on the structures and mechanical properties of large ingots prompted an investigation of the microstructure, phase composition, and some mechanical properties of double tin bronze ingots with a $\geq$20 kg mass. To this end, bronze ingots with 5-17 percent Sn with a 75-130 mm diameter are smelted from M1 copper and OV4000 tin by RF induction melting melting under a layer of carbonaceous flux or in an atmosphere of argon in graphite crucibles with two or three remeltings. The microstructure is examined in the cast state as well as after cold straining and annealing in a vacuum. The phase composition is estimated by diffraction patterns in Cu*K* radiation on a metallographic section or in a powder. The microhardness is measured in a PMT-3 gauge under a 50-100 gs force; the strength indicators and ductility are determined under tension at a 10^{-3} 1/s rate in an "Instron" unit at room temperature. An examination of the findings shows that in cast bronze ingots considerable specific gravity and dendritic Sn segregation are observed; as the ingot size and mass of bronze Br013 increase, the gravity Sn segregation becomes more pronounced. Cast inhomogeneity leads to a two-phase structure (with 1-3 percent of the second phase) while dendritic segregation drops somewhat with an increase in the number of remeltings. The cast material state inhomogeneity also leads to an increase in the limits of mechanical properties while the second phase precipitation on the grain boundaries leads to embrittlement. Extended diffusion annealing is recommended. Figures 1; tables 3; references 5.

Structural Recrystallization Detection During Titanium Alloy Heating in β-Region

927D0183D Vladikavkaz IZVESTIYA VYSSHIKH UCHEBNYKH ZAVEDENIY: TSVETNAYA METALLURGIYA in Russian No 3, Jun 91 pp 98-104

[Article by V.K. Portnoy, N.L. Anikanov, T.A. Ryabchikova, N.A. Kuksov, Moscow Steel and Alloy Institute; UDC 669.295:620.186.1]

[Abstract] Attempts to obtained a recrystallized β-structure in Ti alloys by annealing and the phenomenon of phase strain hardening are reported and the role of phase strain hardening during the structural recrystallization by deformation methods as well as thermal cycling is investigated. A popular martensitic VT3-1 (α+β)-Ti alloy is used as the source material. Cylindrical samples cut from the bottom part of a commercial ingot are tested by upsetting in a UME-10TM tester and after the tests the samples are cut in half along the generator line, polished in acid solutions, and the grain structure is examined under a Neophot-21 metallographic microscope; the β-structure parameters are estimated quantitatively by measuring the specific surface of the β-grain boundaries which is evaluated by the linear method. The recrystallization processes are studied by the load relaxation method during heating in the β-region; the experimental procedure is described. The dependence of the specific surface of the grain boundaries and straining rate (lnε) on the test temperature, the thermal cycling diagram, the dependence of the specific surface of β-grains on the number of cycles, and the β-grain size distribution under thermal cycling (TTsO) at various intermediate temperatures are plotted. The curves and macrostructure analyses show that the structural recrystallization of the VT3-1 alloy is detected not only by the grain refinement under heating within 1,275-1,300°C but may also be produced at lower temperatures in the β-region with the help of thermal cycling to room temperature at which the maximum extent of the two-phase interval is observed. Figures 6; references 5: 4 Russian, 1 Western.

On Morphology of α-Phase Plates in α+β-Ti Alloys

927D0183E Vladikavkaz IZVESTIYA VYSSHIKH UCHEBNYKH ZAVEDENIY: TSVETNAYA METALLURGIYA in Russian No 3, Jun 91 pp 104-107

[Article by T.N. Roshchina, L.A. Bunin, V.V. Shevchenko, B.A. Kolchayev, Moscow Aviation Engineering Institute; UDC 669.295.5.621.011]

[Abstract] The effect of flaky structure parameters on the mechanical and service properties of Ti alloys and the importance of understanding the patterns of microstructural transformations during heat treatments are noted and the behavior of the initial β-grain size, α-plate thickness and length and their ratio during the VT23 alloy reheating for hardening and aging are investigated in commercial rods with the initial flaky structure. The samples are hardened beforehand at various temperatures. The linear dimensions of the flaky structure elements (plates) are measured in microsections prepared for this purpose; the quantitative metallographic analysis is conducted under the Metaval and Neophot-21 optical microscopes. The microstructure after various types of heat treatment represents original β-grains surrounded with the α-phase. The dependence of the mean grain size of the original β-grain on the heat treatment conditions, the *l/b* parameter distribution density (the ratio of the maximum α-phase plate length to the maximum thickness), and the effect of the hardening heating temperature on the distribution frequency of the $l/b \approx 5$ parameter are plotted. The study reveals that after hardening within a 780-880°C temperature range, the flaky structure of the VT23 alloy is characterized by a predominant parameter ratio of five. A change in the aging temperature from 450 to 550°C has little effect on the flaky structure parameters. Moreover, the proportion of α-phase plates with a $l/b \approx 5$ ratio rises with an increase in the hardening reheat temperature. Figures 3; references 7.

Superplasticity of Al-Zn-Mg-Zr-Sc System Alloy

927D0183F Vladikavkaz IZVESTIYA VYSSHIKH UCHEBNYKH ZAVEDENIY: TSVETNAYA METALLURGIYA in Russian No 3, Jun 91 pp 107-110

[Article by A.M. Diskin, A.A. Alalykin, Moscow Steel and Alloy Institute and All-Union Light Alloy Institute; UDC 621.7.043:539.374]

[Abstract] The conditions necessary for realizing superplastic forming of alloys are discussed and the requirements imposed on a perfect thermally hardenable alloy for superplastic forming are outlined: the simplicity of sheet production, the possibility of air hardening after superplastic forming, and the preservation of ready product properties at the level of original sheets. As a consequence, an attempt is made to establish whether the new 01970 superhard alloy of the Al-Zn-Mg-Zr-Sc system meets these requirements. To this end, diffusion annealed alloy ingots are rolled first in the hot, then in the cold state to a 1 and 2 mm thickness without intermediate annealing; longitudinal and transverse samples are cut from the sheets in order to determine their superplasticity by tension tests at three temperatures while stepping up the straining rate within a 10^{-5}-10^{-1} s^{-1} and by tension under optimal conditions in order to determine their elongation at rupture. The dependence of the flow stress and its rate sensitivity indicator on the straining rate at various temperature and the thickness distribution in a "stiffness" part after superplastic forming are plotted and superplasticity indices of the 01970 alloy sheets at a 475°C temperature and a straining rate of 6 x 10^{-3} s^{-3} are summarized. The mechanical properties of samples cut from formed parts are examined. The tests demonstrate that the sheets display superductility within the above straining rate and temperature ranges and may indeed be used for making parts of a complex configuration by the superplastic forming method. After such forming and aging, the alloy has high mechanical properties while its yield strength and elongation remain at the level of the original sheets with a slight drop in ultimate strength. Figures 3; tables 2; references 6.

On Issue of Selecting Rotary Tube Kiln Diameter

927D0183G Vladikavkaz IZVESTIYA VYSSHIKH UCHEBNYKH ZAVEDENIY: TSVETNAYA METALLURGIYA in Russian No 3, Jun 91 pp 122-124

[Article by A.M. Davidson, M.I. Akatsev, North Caucasian Mining and Metallurgical Institute; UDC 666.3/041]

[Abstract] The importance of determining the inside diameter of rotary tube kilns for selecting the kiln parameters and Khodorov'a and Arefyev's internal methods are calculating the inside diameter are discussed and compared. Formulas are derived for calculating the inside diameter of rotary tube kilns which do not take into account the change in the kiln's thermal efficiency as a result of a change in the mass transfer conditions with a change in the kiln diameter; to remedy this problem, the inside diameter of the combustion zone is expressed as a function of the kiln output and its heat demand which are connected to its thermal efficiency. A regression equation is derived and the dependence of the kiln diameter on various process parameters is summarized and the alumina calcination kiln diameter is assessed and compared on the basis of the above three methods. Mathematical processing of the findings makes it possible to calculate the kiln diameter more correctly than on the basis of the earlier semiempirical formulas. Tables 2; references 2.

On One Erroneous Statement Made on Book on Molten Salt Electrolysis

927D0183H Vladikavkaz IZVESTIYA VYSSHIKH UCHEBNYKH ZAVEDENIY: TSVETNAYA METALLURGIYA in Russian No 3, Jun 91 pp 124

[Article by A.A. Revazyan, Armenian Ministry of Nonferrous Metals Industry]

[Abstract] Yu.V. Baymakov's and M.M. Vetyukov's assertion that "the fact that the CO concentration in the mixture of anodic gases (during the cryolite and alumina melt electrolysis) does not reach equilibrium is due to the fact that the $C+CO_2=2CO$ reaction does not occur at all since anode's carbon is polarized" citing other sources as evidence is refuted and it is stated that the chemical reaction of O_2 with C of the polarized anode demonstrates that the anode cannot be chemically inert for the $CO_2+C=2CO$ reaction reported in other publications and chemically active as the same time for the $O_2+C=CO_2$ reaction. References 4: 3 Russian, 1 Western.

Er(Tm)-Fe-Ge Systems

927D0172D Moscow ROSSIYSKAYA AKADEMIYA NAUK: SERIYA NEORGANICHESKIYE MATERIALY in Russian Vol 28 No 3, Mar 92 pp 493-497

[Article by O.I. Bodak, O.Ya. Oleksin, M.F. Fedyna, V.K. Pecharskiy, Lvov State University imeni I. Franko; UDC 541.123.3]

[Abstract] The need for systematic studies of the Er(Tm)-Fe-Ge system constitution diagrams and the high probability of the development of intermetallic compounds which can be used as new magnetic and resistive materials prompted an investigation of isothermal cross sections of the Er-Fe-Ge constitution diagrams at 1,070K and Tm-Fe-Ge constitution diagrams at 870K as well as the temperature and development mechanism of a number of ternary erbium germanates and the crystalline structure of the compounds. The melting point, melting type, and lattice constants of Er(Tm)-Fe-Ge system crystals are summarized. It is speculated that the composition shift (according to data of X-ray spectral and structural analyses) relative to the real compositions

parallel to the two-phase equilibrium line is due to the peritectoid character of intermetallic compound formation. Single crystals of two new ternary germanoids are discovered and a complete interpretation of their structure by the single crystal method made it possible to localize their compositions. A considerable similarity of the systems is noted: ternary compounds crystallize as the same crystal types and the isothermal cross section structure is similar. Figures 2; tables 1; references 11: 9 Russian, 2 Western.

Investigation of Electric Properties of Bi_2Te_3 Single Crystals Doped With V and Tm

927D0172G Moscow ROSSIYSKAYA AKADEMIYA NAUK: SERIYA NEORGANICHESKIYE MATERIALY in Russian Vol 28 No 3, Mar 92 pp 518-520

[Article by P.N. Sherov, Kh. Mukhiddinov, Ye.I. Shvedkov, Engineering Physics Institute imeni S.U. Umarov at the Tadzhik Academy of Sciences; UDC 537.531]

[Abstract] The high anisotropy of the electric and magnetic properties of lamellar compounds due to the specific features of their structure prompted an examination of the effect of V and Tm impurities on the electric properties of single crystals of bismuth and antimony telluride. The initial compounds are synthesized from bismuth and antimony telluride ingots and the samples are grown by the Bridgeman method. The hole concentration in antimony telluride is determined by measuring the Hall coefficient. A block diagram of the unit for measuring the specimen resistivity in a Dewar flask is cited, the temperature dependence of resistivity of Bi_2Te_3 single crystals with 1.0 percent V and with 0.5 and 1.0 percent Tm are plotted. In all samples except for antimony telluride, the dependence of resistivity on temperature is metallic while in antimony telluride single crystals doped with Tm, the dependence of resistivity on temperature displays anomalies: at low temperatures, these samples have metallic conduction while within a 90-95 to 215K range—semiconductor. As the temperature is further increased, the conduction character reverts back to metallic. The transition temperature shifts downward with an increase in the Tm concentration. Figures 4; references 5.

Niobium, Molybdenum, and Tungsten Diselenide Intercalation With Copper, Zinc, and Gallium

927D0172I Moscow ROSSIYSKAYA AKADEMIYA NAUK: SERIYA NEORGANICHESKIYE MATERIALY in Russian Vol 28 No 3, Mar 92 pp 525-530

[Article by L.M. Kulikov, A.A. Semenov-Kobzar, L.G. Akselrud, T.A. Lobova, Ye.A. Bogachev, Institute of Materials Science Problems imeni I.N. Frantsevich at the Ukrainian Academy of Sciences, Lvov State University imeni I. Franko, and Moscow Steel and Alloy Institute; UDC 23:548.5:669.15.39.2]

[Abstract] The outlook for using intercalated dichalcogenides of transition metals with semiconductor properties as antifriction materials in various friction units is discussed and the processes of intercalation of said chalcogenides with a 2*H* structure with Cu, Zn, and Ga are examined. Polycrystalline diselenides of Nb, Mo, and W are produced by an interaction of selenium vapors with metal powders at 1,000K in an inert gas current by an interaction of components in evacuated quartz vials (with <50 μm particles) are used as source materials. X-ray studies are carried out in DRON-2.0 and HZG-4A diffractometers while X-ray pattern interpretation is performed using CSD routines on an Elektronika-5 computer. The concentration dependence of the intercalate lattice cell parameters are plotted and compared to published data and the X-ray analysis results are tabulated. The formation of modulated structures is discovered for the first time and it is speculated that 2*H*-MoS_2 structure are more susceptible to the formation of modulated structures than 2*H*-TaS_2 structures. It is shown that for Cu_xNbSe_2, intercalation proceeds into different voids of the interlayer space: octahedral at $0<x<0.2$ and tetrahedral and proximate with a predominant copper atom distribution in the tetrahedral voids at $0.29<x<0.75$. Figures 1; tables 1; references 8: 4 Russian, 4 Western.

Low-Temperature Oxidation of Zinc Sulfide Phosphor

927D0189C Moscow ROSSIYSKAYA AKADEMIYA NAUK: NEORGANICHESKIYE MATERIALY in Russian Vol 28 No 5, May 92 pp 955-960

[Article by A.O. Dmitriyenko, L.V. Abramova, S.A. Bukesov, Saratov State University imeni N.G. Chernyshevskiy; UDC 535.376]

[Abstract] The behavior of polycrystalline zinc sulfides and their solid solutions activated with various crystals—crystal phosphors—during oxidation is discussed and the phase composition of oxidation products and the depth of surface oxidation of polycrystalline ZnS and the zinc sulfide phosphor made on its basis during isothermal annealing in the air are investigated. To this end, zinc sulfide phosphor samples produced by the hydrogen sulfide technology with a 1 μm mean particle size are used. The samples are oxidized within a 300-600°C temperature range under isothermal conditions. The X-ray phase analysis of the annealing products is carried out in a DRON-2.0 diffractometer in filtered Cu*K* radiation; the diffuse reflection spectra (SDO) are recorded by a Specord M40 spectrometer; the photoluminescence spectra are recorded by an MSD monochromator and a photomultiplier. Oxidation of the ZnS<Ag, Cl, Al> low-voltage cathodoluminescence phosphor (KL) with a blue glow (commercial brand KN-455-1) is also examined. The dependence of the ZnO and $ZnSO_4$ on the ZnS annealing temperature, the dependence of the ZnO and $ZnSO_4$ concentration on the KN-455-1 phosphor annealing temperature, and the diffuse reflection spectra of the initial ZnS powder and its oxidation products and the initial phosphor and its oxidation products at various annealing temperatures are plotted. A comparison of the curves and spectra shows that amorphous phases with a variable composition form in the near-surface phosphor grain layer ($ZnS_{1-x}O_x$) and that ZnO and $ZnSO_4$ are the principal oxidation products whose relative concentration depends on the oxidative annealing temperature. It is noted that the amorphous solid solution layer forming under the phosphor grain surface is "dead" since the nonequilibrium carrier recombination occurs in this layer by the nonradiative channel mechanism, thus lowering the efficiency of low-voltage cathodoluminescence excited by slow electrons. Figures 4; tables 1; references 11: 9 Russian, 2 Western.

New Crystalline Phase in Li_2O-Al_2O_3-SiO_2 System and Transparent Glass Crystalline Materials on its Basis

927D0189I Moscow ROSSIYSKAYA AKADEMIYA NAUK: NEORGANICHESKIYE MATERIALY in Russian Vol 28 No 5, May 92 pp 1006-1011

[Article by O.S. Dymshits, A.A. Zhilin, T.I. Chuvayeva, All-Union Scientific Center at the State Optics Institute imeni S.I. Vavilov; UDC 546.623.34 284]

[Abstract] The structure of the phases forming during the Li-Al silicate glass ceramic crystallization, particularly β-eucryptit, is discussed and a wide range of Li_2O-Al_2O_3-SiO_2 system compositions in the domain of Al_2O_3 excess over Li_2O is investigated using ZrO_3 in a 3 percent concentration (molar). The SiO_2 molar concentration varied within 30-78 percent. The constitution diagram of the Li-Al-Si oxide glass is shown and the X-ray patterns of crystallized glass of various compositions and their thermograms and X-ray patterns after the differential thermal analysis of vitreous samples are plotted. The linear thermal expansion coefficient of the original glass and glass ceramics on the basis of the γ-eucryptit solid solution measured within a 20-500°C temperature range is 65 x 10^{-7} and 134 x 10^{-7} deg^{-1}, respectively. It is speculated that the disappearance of solid solutions of γ-eucryptit and the solid solution precipitation of β-eucryptit reduces the linear thermal expansion coefficient to the vanishing point and leads to the sample cracking. Figures 3; tables 2; references 11: 4 Russian, 7 Western.

Effect of Hydrothermal Treatment and Subsequent Sintering on Strength of Titanium Dioxide Ceramics Prepared by Sol-Gel Method

927D0189P Moscow ROSSIYSKAYA AKADEMIYA NAUK: NEORGANICHESKIYE MATERIALY in Russian Vol 28 No 5, May 92 pp 1134-1136

[Article by V.M. Chertov, T.F. Makovskaya, V.V. Tsyrina, V.A. Kaganovskiy, Physical Chemistry Institute imeni L.V. Pisarzhevskiy at the Ukrainian Academy of Sciences; UDC541.182]

[Abstract] The effect of hydrothermal treatment and thermal sintering of TiO_2—one of the principal ceramics components which is also used as an adsorbent, catalyst, and carrier—on its porous structure and crushing strength of TiO_2-based ceramics is investigated. To this end, titanium dioxide is synthesized by the sol-gel method. The crushing strength of cylindrical samples is measured by crushing shanks between plane parallel supports with a force perpendicular to the cylinder axis in an MP-2S unit. A preliminary analysis of the findings shows that hydrothermal of the initial cryogel at 373-473K greatly activates its subsequent sintering and results in a sample growth. Hydrothermal treatment is leads to a decrease in the ceramic strength while heat treatment leads to an increase in the titanium dioxide ceramic strength. Hydrothermal treatment at 373-473K also increases the ceramic strength by more than two-fold. Tables 3; references 6.

Concrete Effectiveness and Reliability at Elevated Activated Coarse Aggregate Consumption

927D0188A Moscow BETON I ZHELEZOBETON in Russian No 5 (446), May 92 pp 6-7

[Article by V.I. Selivanova, G.I. Zharycheva, Ivanovo Civil Engineering Institute and Ivanovo Integrated House Building Factory; UDC 691.322.621]

[Abstract] A new method of preliminary mechanical activation of the aggregate at an elevated cement rate introduced at the Ivanovo Integrated House Building Factory (DSK) in order to save cement and its shortcomings revealed by industrial tests are outlined and the outcome of a study carried out by the Ivanovo Civil Engineering Institute and Ivanovo Integrated House Building Factory is presented. The study led to a new technology based on using coarse aggregates and increasing the mixing and slab setting duration on the conveyor. The resulting reinforced concrete structure is heavier and costs 0.92 ruble/m^3 more. Three series of industrial tests show that the crushing strength, spalling strength, axial tensile strength, and softening coefficient of the structures produced by the new technology are superior to known data. The economic efficiency of the new method is assessed and it is speculated that the earlier proposed gravel activation technology does not meet the composition optimization criteria nor the efficiency and quality criteria since the factory operates with aggregates which correspond to GOST 8736 and GOST 8267. Tables 1; references 2.

Crack Resistance and Strength of End Sections of Prestressed Elements With Cable Reinforcement

927D0188B Moscow BETON I ZHELEZOBETON in Russian No 5 (446), May 92 pp 13-15

[Article by N.A. Markarov, R.Sh. Sharipov, Yu.V. Petrenko, Scientific Research Institute of Reinforced Concrete; UDC 691.87:693.554:539.3/.4]

[Abstract] The issue of end section reinforcement and crack prevention and the absence of specific recommendations in Building Rules and Standards (SNiP) prompted the Scientific Research Institute of Reinforced Concrete to carry out an experimental-theoretical investigation of this issue in order to develop a procedure for analyzing the crack resistance and cross section area of oblique reinforcement. To this end, six batches of samples with the rectangular and H-shaped cross section are tested for the crimping force transfer and operation under load. The dependence of the end section cracking stress on the concrete transfer strength, protective layer thickness, and oblique reinforcement percentage is plotted and the analytical and actual cracking stress of the end sections and oblique reinforcement cross section area as well as the analytical and actual cross section areas of oblique reinforcement in standard batches of products are compared graphically. The study made it possible to eliminate longitudinal cracking at the design stage and in some cases, to decrease the steel outlays for oblique reinforcement. Figures 3; tables 1; references 4.

Practical Oblique Section-Based Reinforced Concrete Wall and Beam Strength Analysis Method

927D0188C Moscow BETON I ZHELEZOBETON in Russian No 5 (446), May 92 pp 15-17

[Article by K.G. Ashkinadze, Central Scientific Research Institute of Patent Information Monolit; UDC 624.072.2:539.4]

[Abstract] The effect of various design factors on the reinforced concrete element failure along oblique sections and the shortcomings of existing analytical techniques are discussed and a new practical procedure is proposed for analyzing the strength of reinforced concrete walls and beams on the basis of the oblique sections method. Although the proposed method is not a physical one in true sense of the word since it involves a certain abstract form of graphic representation of stresses in the compression zone and resorts to a phenomenological criterion of concrete strength, it reflects nevertheless the shear resistance structure of reinforced concrete elements while the use of abstracting methods makes it possible to simplify the analytical formulas and make them suitable for practical use. Nineteen samples of rectangular and H-shaped beams from heavy and light concrete are tested under the effect of offset compression with shear; the outcome shows a good consistency of the experimental and theoretical results with respect to the breaking load; ten samples reveal a <15 percent deviation. The proposed method can be recommended for implementation. Figures 3; references 4.

Effect of Colmating Water-Dispersing Film-Forming Compositions on Protective Pipe Coat Quality

927D0188D Moscow BETON I ZHELEZOBETON in Russian No 5 (446), May 92 pp 21-23

[Article by G.V. Topilskiy, V.I. Melikhov, V.P. Koretskiy, All-Union Scientific Research Institute of Reinforced Concrete and Ukrainian Scientific Research Institute of Hydraulic Engineering and Reclamation; UDC 691-462:666.657.205]

[Abstract] The effect of the protective concrete coat and its properties on the normal life and corrosion resistance of pipes and the shortcomings of existing methods of coat impregnation and application are discussed and a new colmating water-dispersing film-forming composition (VPS) developed at the All-Union Scientific Research Institute of Reinforced Concrete and Ukrainian Scientific Research Institute of Hydraulic Engineering and Reclamation together with the Belstroynauka Scientific Production-Technical Association is described and its effect on the quality of sprayed concrete is studied. The colmating compositions contain low-melting soft paraffin or petrolatum, emulsifiers, and functional additives, e.g., latex, corrosion inhibitors, and water repellent mixtures, and are nontoxic and environmentally safe. The results of comparative tests of the new colmating composition and other coat impregnating substances are summarized; the findings indicate the impregnation of sprayed concrete with the colmating composition at a temperature within a 45-60°C range makes it possible to lower the coat's water absorption and diffusive penetration by three- to fivefold, i.e., reduce them to a level of high-temperature petrolatum impregnation. It is noted that the concrete strength does

not increase as a result. The findings have been incorporated in a Building Rules and Standards reference. Tables 4; references 3.

Effect of Additives on Corrosion Resistance of Building Mortars in Man-Made Media

927D0188E Moscow BETON I ZHELEZOBETON in Russian No 5 (446), May 92 pp 23-25

[Article by V.V. Goncharov, A.M. Rozhanskaya, Kiev Civil Engineering Institute and IMV at the Ukrainian Academy of Sciences; UDC 679.69:620.193.8: 627:691.327]

[Abstract] The criteria used for evaluating the corrosive effect of natural and man-made media on concrete and building mortars and the difficulty of predicting the corrosive environment in media modified with various groups of microorganisms are discussed and the characteristics of the chemical and microbiological effect of various additives on the building mortars of various compositions is investigated. To this end, model tests are carried out using building mortar samples with a 1:3 composition and a water:cement ratio of 0.4, 0.6, and 0.6 with and without additives. The katamin AB, katapin KB, and polidim P organic compounds added together with water in making the concrete mix are used as the additives. Aqueous solutions of organic and inorganic substances are used as the nutrient medium for microorganisms. The dependence of the corrosion resistance coefficient KS_3on the amount of additives and water:cement ratio in various media is plotted. The additive's corrosion resistance is determined as the ratio of the bending strength of samples exposed to sterile tap water to the bending strength of samples exposed for six months to room conditions. The findings make it possible to trace the specific features of the protective actions of microbic corrosion inhibitors for concrete as a function of the corrosive process stimulants and develop practical recommendations for using the specific protective additives; it is noted that the use of additives must be preceded by a microbiological analysis for each specific type of reinforced concrete structure. Figures 1; references 3.

Tasks of Improving Domestic Structural Design Standards

927D0188F Moscow BETON I ZHELEZOBETON in Russian No 5 (446), May 92 pp 27-29

[Article by N.A. Markarov, V.D. Grinev, National FIP-YeKB Committee of the Former Soviet Union and Novopolotsk Polytechnic Institute; UDC 624.012.45[083.75]]

[Abstract] The proceedings of a joint session of the National Committees of FIP and YeKB of the Former Soviet Union held at the Novopolotsk Polytechnic Institute in October 1991 are described. The reports and papers presented by scientists from 30 cities and dozens of leading scientific research, design, and academic institutions dedicated to improving domestic regulatory documents for the design and analysis of reinforced concrete structures allowing for the YeKB-FIP standards (1990 edition, model code 90) are briefly summarized. A few suggestions for improving existing Building Rules and Standards (SNiP) were made at the sessions. The session addressed the specific issues of longevity, reinforcement, dynamic loads, prestressed structures, reliability, and precast structures among others. Plans to hold future FIP-YeKB sessions in Budapest in 1992, Kyoto in 1993, and Washington in 1994 were approved. The need to harmonize domestic standards and rules with international standards due to the integration of the FSU into the world community is stressed.

Joining of Ceramic Parts From Reaction-Bonded Silicon Nitride

927D0187A Moscow OGNEUPORY in Russian No 5, May 92 pp 2-3

[Article by V.V. Vikulin, I.N. Kurskaya, Tekhnologia Industrial Scientific Production Association; UDC 666.762.93:621.792]

[Abstract] The increasing use of ceramic materials in various branches of industry, particularly for making aircraft engines, prompted a study of the possibility of joining products of complex shape made from reaction-bonded silicon nitride. To this end, blanks are molded from thermoplastic bodies consisting of 82-83 percent semiconductor grade silicon (by mass) with a particle size of at least 10 μm and 17-18 percent wax-paraffin binder with a small amount of enhancing additives which accelerate the nitriding process. Then a gasoline suspension whose disperse phase has a similar composition to that of the molded blanks is applied to the sample surface. The blanks are then joined and locked for 15-20 min until a strong bond is formed. The samples are then heat treated in alumina and tested. The parts thus joined have a strength of up to 1,400-1,500°C while the seam has a shear strength of approximately 21 or 27 N/mm^2, depending on the joining method. The seam's bending strength reaches 200-300 N/mm^2 within a 20-1,400°C temperature range. Photographs of ceramic elements after shear tests, nozzle vanes after thermal cycling tests, and a nozzle vane block after thermal cycling tests are shown. The tests made it possible to develop a simple method of joining parts from reaction-bonded silicon nitride which ensures a high thermomechanical strength of ceramic assemblies and makes it possible to join simple parts into complex-shaped structures. Figures 3; references 3.

Sialon-Containing Silicon Carbide Refractories

927D0187B Moscow OGNEUPORY in Russian No 5, May 92 pp 6-8

[Article by N.V. Pitak, R.M. Fedoruk, T.P. Khmelenko, T.N. Vdovitchenko, N.G. Privalova, L.K. Savina, M.Ya.

Shpirt, L.A. Sinkova, N.N. Novikova, Ukrainian Scientific Research Institute of Refractories and Combustible Fossils Institute; UDC 666.762.852.022.69]

[Abstract] The use of sialon in various mechanisms and devices and as a lining material for furnaces and plants and the most accessible materials for making β-sialon are discussed and the production method and properties of sialon-containing silicon carbide refractories are investigated. To this end, coal dressing byproducts and the products of their roasting are used in a 82:18 ratio to synthesize sialon. The chemical composition of the source materials and the charge composition of silicon carbide refractories with a sialon binder are summarized and the dependence of open porosity, compressive strength, and apparent density on the mass fraction of sialon in the silicon carbide sialon-containing refractory roasted at 1,450°C and the dependence of open porosity, compressive strength, and apparent density on the roasting temperature are plotted. The study shows that an addition of 5 percent MgO and 5-10 percent Al_2O_3 yields the best results, especially with byproducts of rare earth element oxides; these additions increase the strength of refractories and improve their quality. Sialon-bonded silicon carbide refractories are characterized by their high resistance to slags and are recommended for use as lining in the lower part of blast furnace shafts, bosh, and lower inwall. Figures 2; tables 2; references 5: 1 Russian, 4 Western.

Resistance of Silicon Nitride-Based Hot Compacted Materials to High-Temperature Oxidation

927D0187C Moscow OGNEUPORY in Russian No 5, May 92 pp 8-10

[Article by V.D. Borzilova, I.I. Tkacheva, Tekhnologia Industrial Scientific Production Association; UDC 666.762.93:621.777.016.2]

[Abstract] The resistance of of ceramic materials on the basis of the Si_3N_4-Y_2O_3 system to oxidation which largely determines their applicability as structural materials makes it necessary to study the behavior of these ceramic materials under the specific oxidation conditions. To this end, oxidation of the OTM-906 and OTM-914 hot compacted Si_3N_4-Y_2O_3-based structural materials in an air medium with 8+/-1 and 13+/-1 percent Y, respectively, is examined within a 1,200-1,500°C temperature range. In so doing, ultradisperse powders produced by plasma chemical synthesis at the Inorganic Chemistry Institute at the Latvian Academy of Sciences is used. The phase composition before and after high-temperature oxidation of hot compacted materials during 50 h, the percentage mass loss, and the specific oxidation features are summarized and the structure and surface of hot compacted ceramic materials before and after oxidation is examined under a microscope. Kinetic curves of the OTM-906 and OTM-914 hot compacted material oxidation at various temperatures are plotted. An analysis of the findings demonstrates that hot compacted silicon nitride-based materials made from ultradisperse powders are characterized by high stability to extended oxidation and thermal cycling regardless of the phase composition and crystallinity differences and maintain their strength, making it possible to use them in thermally loaded structures in an oxidizing medium. Figures 6; tables 1; references 7: 2 Russian, 5 Western.

Grinding of Certain Composition Particles in (Al_2O_3-ZrO_2)-Y_2O_3 System Produced by High-Speed Melt Quenching

927D0187D Moscow OGNEUPORY in Russian No 5, May 92 pp 11-12

[Article by Yu.S. Vilk, Ye.A. Ilin, A.Yu. Timofeyev, S.S. Semenov, V.S. Niss, Yu.G. Alekseyev, V.N. Kovalevskiy, Central Scientific Research Institute of Metallurgy and Belarussian Polytechnic Institute; UDC 666.762.11+666.762.52]:[66.022:621.926]

[Abstract] Compounds of zirconium dioxide, partially stabilized by Y_2O_3, with aluminum oxide are investigated near their eutectic composition. To this end, a special unit is developed for producing rapidly solidified particles from such melts (VZR) with a large number of defects. The resulting samples are then melted in a molybdenum crucible using graphite electrodes; the melt is then let out onto two horizontally positioned discs with activating beaters; the lower disc is spinning at a 8,000 RPM speed while the upper one is stationary. The melt is water quenched on the lower disc and the resulting particles multiply collide with each other and the activating beaters. The resulting particles are generally spherical in shape; the spherical particle fraction size distribution, the sedimentation curves of powders after vibration milling of the granules produced by rapid quenching, the mean particle size distribution as a function of the attrition milling duration, and the effect of the milling duration on the specific surface of the powder are plotted. An analysis of the relative efficiency of various types of milling demonstrates that powders with a specific surface of under 20 m^2/g and an equivalent diameter of approximately 95 nm from high-strength granules crystallized by the rapid quenching technology can be produced only by combining vibration milling for up to 60 h, subsequent attrition milling for up to 3 h, shock treatment, and another milling in a high-energy attrition mill. Figures 6; references 1.

Making Products of Complex Configuration With Expanded Polystyrene Cores

927D0187E Moscow OGNEUPORY in Russian No 5, May 92 pp 23-25

[Article by V.A. Ustichenko, V.V. Primachenko, L.V. Belik, G.B. Goryushko, Ye.V. Devishev, Ukrainian Scientific Research Institute of Refractories and Special Design Office of Foundry and Forging; UDC 666.76-478]

[Abstract] The difficulties of making products of complex configuration from refractory materials with internal through and dead end cavities in the ferrous and nonferrous metals industry prompted an examination of the process of making products with complex cavities of any configuration which virtually eliminates rejects and gas liberation. The process is developed on the basis of a known vibratory casting technology from bodies of various compositions; expanded polystyrene cores are used as void-forming mandrels. The cores are made by a two-stage technology: first the granules are partially foamed, then caked in a mold by the autoclave method. The core fabrication indices, i.e., the yield of usable products, open porosity, and compressive strength of the metal and expanded polystyrene technologies are compared. The results show that the use of such cores makes it possible to simplify the production technology and attain a smooth and nondeformed inner cavity as well as increase the yield of ready products, improve their quality, decrease the volume of manual operations, increase productivity, and improve the working conditions. Figures 5; tables 1; references 10.

Certification Track Record of Refractory Enterprise Technologies

927D0187F Moscow OGNEUPORY in Russian No 5, May 92 pp 27-30

[Article by S.G. Dolgikh, A.K. Karklit, All-Union Refractories Institute; UDC 666.762:331.108.43]

[Abstract] The results of a drive to certify the production methods conducted by the All-Union Refractories Institute at a number of refractory enterprises in response to a decree "On Urgent Measures of Environmental Remediation in the Country" adopted in 1990 by the USSR Supreme Council and the introduction of an environmental certification procedure for all operating enterprises developed by the All-Union Scientific Research Institute of Ferrous Metallurgy are outlined. The three principal criteria for analyzing each production process—environmental impact, waste generation, and secondary raw material utilization—are summarized. Production methods are evaluated at the following enterprises: VZOI, ZOZ, KondOZ, NMOZ, NLMK, PZOI, BKO, and VOK. Production methods are then classified by the product type and by individual criteria. Recommendations are developed for each enterprise for improving base technologies and methods under design. It is recommended that methods of decreasing the fly dust and improving dust recovery, especially for use in other refractory production be developed, raw material storage facilities be improved and expanded, and raw material consumption standards be reexamined. Tables 3; references 4.

Mullite-Silica Glass Fiber Refractories Production and Application Analysis and Outlook for Increasing Their Output at Seversk Dolomite Plant

927D0187G Moscow OGNEUPORY in Russian No 5, May 92 pp 33-36

[Article by I.G. Subochev, L.A. Dergaputskaya, I.V. Yeremina, Yu.I. Stoyanov, V.V. Churilov, S.Ye. Alekseyev, Ukrainian Scientific Research Institute of Refractories, Stalproyekt, and Seversk Dolomite Plant; UDC 666.762-486]

[Abstract] The production and use of mullite-silica glass fiber refractories are analyzed and the outlook for increasing their production volume at the Seversk Dolomite Plant (SDK) is assessed. Tentative data on the anticipated demand for fibrous refractory materials in ferrous and nonferrous metallurgy, construction and erection enterprises, the electrical engineering industry, the power generating industry, the automotive industry, chemistry and petrochemistry, and the building materials industry are summarized and uses of fibrous refractories are illustrated by comparing the designs of heat insulation in the ferrous metallurgy industry. The mean annual demand for various types of fibrous refractories is summarized. It is noted that the annual demand for fibrous refractories is expected to rise from 44,000 tons in 1990 to 67,000 tons in 2000 while the most popular fibrous refractories are the MKRP-340 mullite silica slabs, the MKRV-200 mullite silica felt, and the ShVP-350 heat treated slabs with a clay binder. The expediency of setting up production of fibrous heat insulating materials operating within a 600-1,400°C temperature range is noted. Tables 3.

Thermal Power Plant Ash Waste-Based Facing Glass Materials

927D0186A Moscow STEKLO I KERAMIKA in Russian No 5, May 92 pp 2-3

[Article by O.A. Golozubov, N.G. Kisilenko, V.V. Vinogradova, Ye.I. Gavrilov, L.S. Pokrovskaya, State Scientific Research Glass Institute and Power Engineering Institute imeni G.M. Krzhizhanovskiy; UDC 666.24.002.68:662.613.11]

[Abstract] The urgency of fossil fuel power plant (TES) ash waste utilization in the national economy is considered from the environmental and economic viewpoints and the low volume of ash waste applications in concrete filler, binders, and ceramic wall facing materials is stressed; it is noted that to date, ash waste has not been used for making glass-like wall facing tiles. A study jointly carried out by the State Scientific Research Glass Institute and Power Engineering Institute imeni G.M. Krzhizhanovskiy aimed at investigating the ash waste from three coal deposits—Kansk-Achinsk, Kuznetsk, and Ekibastuz—is reported and the chemical composition of the thermal power plant ash waste is summarized. Glass compositions are developed while trying to maximize the ash utilization and minimize charge preparation. Soda ash, sulfate, chalk, dolomite, and phosphates are used as charge materials. The presence of calcium oxide in the Kansk-Achinsk ash made it possible to synthesized opaque glass; due to their decorative properties, the resulting types of glass are recommended for use as facing materials. The glass tiles are characterized by a low temperature coefficient of linear expansion (TKLR) and a high softening temperature; they are also water and wear resistant. The density, thermal coefficient of expansion, glass transition temperature, water resistance, and wear resistance of glass products from the three deposits are summarized. It is shown that commercial production of ash waste-based facing tile glass may be set up using conventional glassmaking technology by rolling in a single roll mill; the cost of production is much lower than that of glass made from traditional raw materials. Tables 2; references 5.

Interrelation of Thermal and Mechanical Soda-Lime Sheet Glass Properties and Molding Parameters

927D0186B Moscow STEKLO I KERAMIKA in Russian No 5, May 92 pp 7-8

[Article by V.F. Solinov, T.V. Kaplina, A.V. Gorokhovskiy, NITS, Tekhstroysteklo Scientific Production Association, and Saratov Polytechnic Institute; UDC 666.11.01:539.213.1:620.193.23]

[Abstract] The effect of the glass surface state, i.e., the degree of the silicon-oxygen frame cohesion in the surface layers and the presence of defects, on the thermal and mechanical properties of glass which determine the mechanical strength, microhardness, and thermal stability of sheet glass and the relationship between the thermal and mechanical properties and the process parameters which determine the state of the surface are discussed. The central symmetric bending strength, thermal resistance, and microhardness of sheet soda-lime glass are investigated and the differential curves of soda-lime sheet glass strength distribution under central symmetric bending tests are plotted. Three clear strength levels are clearly seen in the curves for the upper surface and two levels for the lower surface. The relationship between the mechanical properties, microhardness variation, and thermal stability and the glass body temperature and hydrogen content as well as the molding temperature and sampling location are summarized. An analysis of the findings indicates that in making thermally polished sheet glass, its thermal and mechanical indicators can be improved and their spread narrowed by increasing the glass body temperature before forming; it is also noted that by lowering the hydrogen concentration in the shielding atmosphere we can increase the microhardness of both surfaces; this is accompanied, however, by a decrease in bending strength. Thus, the thermomechanical properties of glass can be controlled by manipulating the glassmaking parameters. Figures 1; Tables 2; references 4.

Characteristics of Inelastic Strain of Glass Band on Molten Metal

927D0186C Moscow STEKLO I KERAMIKA in Russian No 5, May 92 pp 10-11

[Article by V.B. Seltser, V.S. Guryanov, Tekhstroysteklo Scientific Production Association and Saratov Polytechnic Institute; UDC 666.1.036.4:539.37/.38]

[Abstract] The use of glassmaking on the surface of molten metals for producing high-quality flat glass and decorative architectural glass prompted an investigation of the characteristic features of inelastic strain to which glass is subjected during molding on the metal melt surface. Schematic diagrams of viscoelastic glass band rolling on a metal melt and inelastic strain of glass submerged into the melt by a molding toll are cited and the heat exchange process and the forces applied to the glass surface by the metal melt (tin) are described. The assumptions made for analyzing the inelastic strain in this case allowing for all thermal and mechanical factors are summarized. A complete mathematical procedure which makes it possible tentatively to analyze the magnitude of inelastic strain in the glass band on the surface of molten tin during molding with the necessary accuracy is cited. It is noted that the findings have been used to develop a new process of making structural glass for decorative and architectural purposes. Figures 2; references 2: 1 Russian, 1 Western.

Temperature- and Strain-Induced Optical Element Shape Distortions During Machining

927D0186D Moscow STEKLO I KERAMIKA in Russian No 5, May 92 pp 12-13

[Article by A.A. Frolov, Optika Scientific Production Association; UDC 666.1.053.525:535.8.813:539.38]

[Abstract] The importance of taking into account numerous physical and mechanical phenomena which occur during the optical element machining for designing the grinding and polishing machine tools is stressed and the heat release phenomenon accompanying the machining of glass parts and the heating and thermoelastic strain in optical elements as well as the effect of the heat exchange system on the temperature-induced distortions—the factors which significantly affect the shape accuracy—are investigated. The findings of a theoretical study of the effect of heat release during the machining of blanks by disc and cylinder wheel tools on the heating and shaping of optical surface are summarized, the spatial structure of temperature-induced

deformations in the optical element surface at the end of the machining process is examined, heat conduction equations with the corresponding boundary value conditions are solved, and a cooling system whereby the heat is removed from the heated element by a lubricant-coolant liquid (SOZh) is considered. The resulting equations may be used for estimating thermal surface shape distortions and controlling the shaping processes. References 2.

Elasticity of Silicon Nitride-Based Ceramics

927D0186E Moscow STEKLO I KERAMIKA in Russian No 5, May 92 pp 19-20

[Article by V.N. Yakovkin, V.A. Kuzmenko, Institute of Materials Science Problems at the Ukrainian Academy of Sciences; UDC 666.792.6]

[Abstract] The elasticity characteristics of ceramics on the basis of MK-2, MK-3 (with 2 percent magnesium oxide), and NKM-2 (with 40 percent silicon carbide) silicon produced by the Makeyevka Branch of the Institute of Materials Science Problems at the Ukrainian Academy of Sciences are investigated. To this end, elasticity moduli are determined from the resonance frequencies of flexural or longitudinal vibrations while Poisson's ratio and shear modulus are determined from the velocity of longitudinal and surface ultrasonic pulses. The density is determined by hydrostatic weighing and the porosity is calculated from the difference of the experimental and theoretical densities. The relationship between the Young modulus, Poisson ratio, and porosity of the MK-2 and MK-2 ceramics and the temperature dependence of the Young modulus of the MK nitride and NKM nitride-carbide ceramics made by two different methods are plotted. The effect of porosity on various ceramic characteristics is classified into four categories. It is noted that the Poisson ratio changes linearly with porosity. The findings demonstrate that the rate of the $E(\theta)$ decrease during heating is determined by the energy of atomic bonds and virtually does not depend on the presence of voids while cracks and pores may lower the sample's strain resistance as a whole. The study also shows that in refining the ceramic production methods, it is necessary to take into account the dependence of the elasticity moduli on porosity. Figures 2; tables 1; references 1.

Silicon Nitride Milling Media for Fine Grinding of Ceramic Materials

927D0186F Moscow STEKLO I KERAMIKA in Russian No 5, May 92 pp 20-21

[Article by B.I. Kislov, L.V. Vodopyanova, All-Union Scientific Research Institute of Electronic Reagents; UDC 666.792.6:666.3.022.2]

[Abstract] The stringent requirements imposed on the impurity content of ball mills used for fine grinding of ceramic materials which makes it rather difficult to use easily available and inexpensive steel drum mills and balls and the advantages of ceramic steel drums lined with ceramics or rubber and nonmetallic milling media—the only alternative to steel mills and balls—are outlined and the quality of silicon nitride milling media as likely successors to chalcedony balls used today for fine wet grinding of insulating materials is assessed. To this end, milling media shaped as regular hexahedral prisms (TU 147M-21-50—90 specifications) are examined in a 10 dm^3 mill with 3.6 kg of balls. A batch of ceramic glass cement is ground in the mill during the experiment during a specified time and the milling media mass loss is measured. An analysis of the findings indicates that other things being equal, the wear of silicon nitride milling media is lower than that of chalcedony by an order of magnitude. It is noted that before using milling media from silicon nitride, they must be spun for at least 200 h in order to remove the relatively soft surface layer. Thus, silicon nitride milling bodies may be recommended as substitute for chalcedony balls for fine milling of ceramic materials. Tables 1; references 2.

Porcelain Cullet as Filtering Material

927D0186G Moscow STEKLO I KERAMIKA in Russian No 5, May 92 p 29

[Article by B.U. Barshchevskiy, V.M. Logvinov; Gzhel Production Association and IONKhR at Russia'a Academy of Sciences; UDC 666.5.004.8]

[Abstract] The outcome of preliminary studies of the porcelain industry cullet and waste utilization whereby glazed crushed porcelain is ground in a mill for increasing its utilization efficiency and grinding down the glazing is summarized. A loose material with a varying dispersivity (from 0.1-7.0 mm to "porcelain flour" with 1-50 μm particles) is prepared from the porcelain cullet by milling with subsequent separation into fractions; the particles are irregular in shape and have a rough surface, making it easier to trap the particles suspended in the water. Various uses of porcelain cullet as filer materials and the results of their filtering efficiency tests are described. The porcelain cullet efficiency as a filtering material exceeds that of sand, especially for domestic and industrial waste water treatment. The use of porcelain cullet may yield considerable environmental benefits and economic savings and is a new step toward developing waste-free technologies.

Characteristics of GaAs Deposition on Si Substrates From Superthin Liquid Phase in Temperature Gradient

927D0173A Moscow ROSSIYSKAYA AKADEMIYA NAUK: SERIYA NEORGANICHESKIYE MATERIALY in Russian Vol 28 No 4, Apr 92 pp 715-719

[Article by V.V. Dorogan, V.A. Kosyak, V.G. Trofim, S.K. Raylyan, Chisinau Polytechnic Institute imeni S. Lazo; UDC 621.315.592]

[Abstract] The difficulty of growing low-deficiency GaAs layers on Si substrates due to the considerable difference between the Si and GaAs lattice parameters, particularly

their coefficient of thermal expansion (KTR), and the problem of growing GaAs layers on Si substrates by liquid phase epitaxy prompted a study of the method of GaAs deposition on Si substrates from the liquid phase using space and time temperature gradients. The method is based on the principle that the liquid phase is confined between two Si and GaAs substrates while the resulting "sandwich" is placed into a spatial temperature gradient. The GaAs substrate serves as the liquid phase saturation source and the Si substrate serves as the seed during the deposition. The sandwich structure during heat treatment and the morphology of the etched Si surface are shown. The necessary additional dissolution of the Si substrate as well as predominant GaAs deposition from the liquid phase on the Si substrate may be controlled by proper selection of solvents, the temperature values which determine the temperature gradient, and the length of active phase interaction in the course of epitaxial deposition. It is shown that irregularities on the etched surface of the Si surface serve as crystallization centers; as a result, the process starts with an islet-type GaAs growth. Individual single crystals are intergrown into a solid GaAs layer. The difficulties of ensuring uniform temperature fields and the low accuracy of the temperature parameter measurements are noted. Figures 2; references: 2 Western.

Tl_4AsS_2-As_2S_3 System, Constitution Diagrams, and Vitrification in Some Chalcogenide Systems

927D0173B Moscow ROSSIYSKAYA AKADEMIYA NAUK: SERIYA NEORGANICHESKIYE MATERIALY in Russian Vol 28 No 4, Apr 92 pp 720-725

[Article by Yu.I. Vorobyev, N.G. Velikova, V.V. Kirilenko, General and Inorganic Chemistry Institute imeni N.S. Kurnakov at Russia's Academy of Sciences; UDC 546.683'23'19':541.123.3]

[Abstract] Polythermal cross sections of the Tl_4AsS_2-As_2S_3 system are discussed, the characteristic points of the Tl_4AsS_2-As_2S_3 polythermal cross section are summarized, the constitution diagram of the Tl_4AsS_2-As_2S_3 system as well as partial VII and VIII constitution diagrams of ternary Tl-As-S systems are plotted, and their extremal points are analyzed. The melting points of $A^IB^VX_2$ chalcogenides are measured. The issues of glass formation in the ternary A^{III}-B^V-X and A^{III}-B^V-X chalcogenide systems where A^{III} is Al, Ga, In, or Tl, B^V is As, Sb, or Bi, X is the chalcogen, and A^I is Li, K, Na, Cu, Ag, or Au are considered and it is shown that vitrification in these systems depends on the ternary phase melting point, the central atom coordination, the covalent radius, and the structural geometry of the crystalline phases. It is noted that the character of the physical and chemical interaction in the Tl-As-X' systems in which vast vitrification areas are observed and Tl-Sb-X' systems in which glass can be produced only by iced water quenching correlate with each other, thus attesting to the importance of not only their constitution diagrams but also the equilibrium phase structure geometry. Figures 3; tables 4; references 10.

Single Crystal Growth and Photoelectric Properties of New Lamellar $AgGa_{2.5}In_{2.5}S_8$ Compound

927D0173C Moscow ROSSIYSKAYA AKADEMIYA NAUK: SERIYA NEORGANICHESKIYE MATERIALY in Russian Vol 28 No 4, Apr 92 pp 726-730

[Article by N.A. Moldovyan, Applied Physics Institute at Moldova's Academy of Sciences; UDC 546.784'231]

[Abstract] A new lamellar phase which exists within a rather wide range of component ratio near the $AgGa_{2.5}In_{2.5}S_8$ composition discovered while searching for new lamellar sulfides with octahedral and tetrahedral cation coordinations (SKhOTKK) is reported and the growth conditions of $AgGa_{2.5}In_{2.5}S_8$ crystals from the vapor phase, their photoelectric properties, and the optical absorption edge are described. The method of chemical transport reactions in an enclosed iodide system is used for growing the crystals and a mixture of elementary especially pure components in a stoichiometric ratio is used as the initial charge. The structure of coplanar sandwich specimens, photoconduction spectra of two types of samples at a +4 V bias, and the spectral distribution of the surface barrier structure sensitivity in the photovoltaic mode for various crystal thicknesses, the voltage-current characteristic of samples of the Pt-$AgGa_{2.5}In_{2.5}S_8$-In system at 300K and a positive potential on the blocking electrode for various crystal thicknesses, and the optical absorption edge of the single crystal of $AgGa_{2.5}In_{2.5}S_8$ at 300 and 80K are plotted. X-ray studies show that the $AgGa_{2.5}In_{2.5}S_8$ compound crystallizes as a hexagonal lattice with the 0.38 (4) and 3.07 (5) nm constants. A study of the $AgGa_{2.5}In_{2.5}S_8$ single crystals with *n*-conduction reveals the presence of localized states below the conduction band bottom exponentially distributed in energy with a characteristic distribution energy of 65 meV. The forbidden gap width is equal to 2.63 eV at 80K and 2.57 eV at 300K. An addition, photosensitive centers with a 2.1 eV depth are discovered. Figures 3; references 8: 7 Russian, 1 Western.

Photoelectric and Optical Properties of $Mg_{0.5}Ga_2InS_5$ Single Crystals

927D0173D Moscow ROSSIYSKAYA AKADEMIYA NAUK: SERIYA NEORGANICHESKIYE MATERIALY in Russian Vol 28 No 4, Apr 92 pp 731-734

[Article by N.A. Moldovyan, Applied Physics Institute at Moldova's Academy of Sciences; UDC 546.784.231]

[Abstract] The outlook for using lamellar chalcogenide in solid state wide-band ultraviolet radiation detectors and the existence and properties of lamellar phases with a substantially different crystal structure some of which are quite stable are discussed and the growth conditions of single crystals of $Mg_{0.5}Ga_2InS_5$ and their photoelectric properties and optical absorption edge are described.

The single crystals are grown by the chemical transport reaction method in an enclosed iodide system. X-ray studies show that $Mg_{0.5}Ga_2InS_5$ crystallizes as a hexagonal lattice with the 3.8 (1) and 12.1 (1) angstrom parameters. Photoconduction spectra of $Mg_{0.5}Ga_2InS_5$ single crystals, the photoresponse spectra of the surface barrier structure in the photovoltaic mode at 300K and, the optical absorption edge of $Mg_{0.5}Ga_2InS_5$ at 300 and 80K are plotted. The forward forbidden gap width is equal to 3.05 eV at 80K and 1.96 eV at 300K. The latter value is consistent with the quantity obtained from the photostimulated electromotive force spectrum of Pt-$Mg_{0.5}Ga_2InS_5$-In samples. The photosensitive centers are found at a depth of 2.3 eV below the conduction zone bottom. Figures 2; references 4: 3 Russian, 1 Western.

Determining Solid Solution Single Crystal Composition of Bi_2Te_3-Sb_2Te_3-Bi_2Se_3 System

927D0173E Moscow ROSSIYSKAYA AKADEMIYA NAUK: SERIYA NEORGANICHESKIYE MATERIALY in Russian Vol 28 No 4, Apr 92 pp 759-763

[Article by L.D. Ivanova, Yu.V. Granatkina, N.V. Polikarpova, Ye.I. Smirnova, Metallurgy Institute imeni A.A. Baykov at Russia's Academy of Sciences; UDC 54-165]

[Abstract] The use of Bi_2Te_3-Sb_2Te_3 alloys as *p*-branches of thermoelectric devices and the difficulties of finding the composition of alloys grown by the oriented crystallization method and the resulting need to establish the effective distribution coefficients of both dopants and antimony and bismuth tellurides are discussed and single Czochralski-grown from melts containing 25-50 percent Bi_2Te_3 (molar) and doped with 2 and 4 percent (molar) of Bi_2Se_3 are investigated. The Sb and Bi composition in the crystals and in the charge is determined by the atomic absorption spectrometry method with the help of a Perkin-Elmer 303 spectrometer in an air-acetylene flame while LSP-2 hollow cathode lamps are used as radiation sources. The dependence of the Bi_2Te_3 concentration on the crystallize proportion of the $Bi_{0.8}Sb_{1.2}Te_3$ melt containing various Bi_2Se_3 concentrations, the behavior of the lattice cell constants in Bi_2Te_3-Sb_2Te_3 and Bi_2Te_3-Sb_2Te_3-Bi_2Se_3 solid solutions, and the dependence of the solid solution density on composition at various Bi_2Se_3 concentrations are plotted and effective Bi_2Te_3 and Sb_2Te_3 distribution constants in single crystals of Bi_2Te_3-Sb_2Te_3-Bi_2Se_3 solid solutions are summarized; the effective distribution coefficients calculated experimentally are equal to approximately 0.9 and 1.1, respectively. The indentations in solid solution cleavages at various indentor loads are shown and the dependence of the microhardness on the load on the (0001) face of single crystals of solid solution is calculated. It is shown that when $Bi_2Se_3$is added to the solid solutions, the lattice cell constants decrease while density decreases; on the other hand, an addition of Bi_2Te_3 increases the crystal density. The microhardness on the spalling planes of solid solutions increases with the amount of Sb_2Te_3 and decreases with an addition of Bi_2Se_3. Figures 4; tables 3; references 4: 3 Russian, 1 Western.

Production of Disperse Silicon Carbide Powders by Carbothermy Method

927D0173G Moscow ROSSIYSKAYA AKADEMIYA NAUK: SERIYA NEORGANICHESKIYE MATERIALY in Russian Vol 28 No 4, Apr 92 pp 782-788

[Article by A.P. Petrov, V. Kevorkian, D. Kolar, Moscow Institute of Fine Chemical Engineering imeni M.V. Lomonosov; UDC 669.762]

[Abstract] The requirements imposed on the β-SiC powder for producing high-density sintered products from it, such as MHD generators, turbine parts, internal combustion engines, etc., are summarized and a method of producing a disperse β-SiC powder with a high activity under sintering for this purpose is investigated. SiO_2, glucose, active carbon black (with a 113 m^2/g specific surface) and phenol formaldehyde resin are used as the source materials. The chemical analysis for total and free carbon, oxygen, and nitrogen is carried out by standard methods, the X-ray phase analysis is conducted according to Ruska, Gauckler, *et al*, the shape of the particles and the presence of sinter in the SiC powder is studied under a SEM microscope made by Leitz (Germany), and the particle size distribution is measured in a sedigraph. Hot compaction is performed in a Gegussa (Germany) unit. The effect of the synthesis temperature on the oxygen concentration in silicon carbide produced from a $C:SiO_2$=1.3:1 mix relative to the stoichiometric composition, the integral size distribution curve of SiC powder produced at various temperatures and pressures and different exposure durations, and the X-ray pattern of the SiC powder produced from the 1.3:1 mix are plotted. The silicon carbide particle morphology at various magnification factors is cited. The findings indicate that the SiC powder synthesized by the carbothermy method has a low amount of impurities. A 1,450-1,500°C synthesis temperature with a 4 h duration and a 20 kPa residual argon pressure and a 1,550-1,600°C synthesis temperature at a 4 h exposure and an atmospheric argon pressure are identified as the optimum conditions. The optimum conditions of SiC purification to remove oxygen and free carbon are determined: 1,300-1,400°C. Figures 5; references: 6 Western.

Solid Solution Formation in SiC-BeO System During Hot Ceramics Compaction

927D0173H Moscow ROSSIYSKAYA AKADEMIYA NAUK: SERIYA NEORGANICHESKIYE MATERIALY in Russian Vol 28 No 4, Apr 92 pp 789-792

[Article by G.K. Safaraliyev, Yu.M. Tairov, V.F. Tsvetkov, Sh.Sh. Shabanov, A. Kamara, Dagestan State University imeni V.I. Lenin; UDC 541.123.2:666.3]

[Abstract] The properties of SiC-BeO high-resistance ceramics with an elevated thermal conductivity and the role of the diffusion processes in these ceramics occurring both on the grain boundaries and in the bulk which may lead to the development of polycrystalline solid solutions highly sensitive to the beryllium oxide concentration are discussed and the formation mechanism and existence conditions of solid solutions in the SiC-BeO system during the hot compactions of ceramics on its basis is investigated. The ceramics for the study is produced by hot compaction at a 35 MPa pressure and a 2,370-2,420K temperature in a nitrogen atmosphere. The 6*H* modification SiC and BeO powder dispersivity does not exceed 2 μm. The structure of the resulting ceramics is studied in Cu*K* radiation in a DRON-2.0 diffractometer at a 20 kV accelerating voltage while microhardness is examined by the Vickers prism indentation method; thermal conductivity is measured by the steady-state heat flux method. The dependence of the lattice constant in the SiC-BeO ceramics composition, the concentration dependence of of the SiC-BeO ceramics microhardness and thermal conductivity, and the area of the SiC-BeO solid solution immiscibility are plotted. The results of the radiographic analysis and other data show that in the hot compacted SiC-BeO ceramics, microhardness and thermal conductivity increase in the SiC+BeO composition of 2.3-2.5 percent (molar). The limit of the BeO solubility in SiC is approximately 3 percent (molar). It is also established that a limited ordered solid solution forms in the SiC-BeO system at a temperature below 2,500K. Figures 3; references 10: 5 Russian, 5 Western.

Using Mechanical Activation for Synthesizing High-T_c Semiconductors

927D0173L Moscow ROSSIYSKAYA AKADEMIYA NAUK: SERIYA NEORGANICHESKIYE MATERIALY in Russian Vol 28 No 4, Apr 92 pp 840-846

[Article by N.G. Khaynovskiy, Yu.T. Pavlyukhin, V.V. Boldyrev, Institute of Solid State Chemistry and Mineral Raw Materials Processing at the Siberian Department of Russia's Academy of Sciences; UDC 542.9]

[Abstract] The problems often encountered in synthesizing yttrium-barium cuprite high-T_c semiconductors (VTSP), particularly the low reaction rate, and the need to improve traditional mechanical activation methods are discussed and it is speculated that by using mechanical activation in HTSC synthesis, one can accelerate the solid-phase synthesis rate. An attempt to examine the behavior of barium nitrate, peroxide, and hydroxide under the mechanochemical synthesis conditions is described. Mechanical activation is performed in APF1-M3 activators designed as a planetary ball mill while X-ray patterns are recorded in the air at room temperature using DRON-3 and DRON-3M diffractometers in Co*K* radiation. Diffractometry studies are carried out using synchrotron radiation at a 1,445 angstrom wavelength with a 2 min frame exposure. Moessbauer spectral studies are conducted by Psavlyukhin's method with a chemical shift relative to α-Fe while derivation curves are plotted using a Setaram instrument. The samples' conductivity is measured by the four-electrode method and their temperature is measured by a Pt resistance thermometer. X-ray and Moessbauer spectra of the original and activated powder mixture, the temperature dependence of electric resistivity of an YBaCuO sample produced with mechanical activation, and diffraction patterns of the initial and activated mixtures prepared in synchrotron radiation at various YBaCuO HTSC production stages are plotted. The findings indicate that the use of traditional mechanical activation is still rather promising for improving the synthesis of ceramic materials: preliminary mechanical activation accelerates the synthesis process and makes it possible to use nonstandard chemical reagents and lower the synthesis temperature. Figures 4; references: 6 Western.

Thermal Stability of Y-Ba-Cu-O System High-T_c Semiconductor Ceramics in Amorphous State

927D0173M Moscow ROSSIYSKAYA AKADEMIYA NAUK: SERIYA NEORGANICHESKIYE MATERIALY in Russian Vol 28 No 4, Apr 92 pp 847-852

[Article by V.D. Okunev, Z.A. Zamoylenko, Donetsk Engineering Physics Institute at the Ukrainian Academy of Sciences; UDC 539.213]

[Abstract] The effect of the intermediate amorphous state forming during the preparation of high-T_c superconductors shaped as a ribbon or thin film on the properties of the resulting HTSC ceramics forming during heat treatment and the lack of data on the structure and properties of HTSC in the amorphous state are discussed and the effect of annealing on the structure of amorphous films of the Y-Ba-Cu-O system is investigated; in so doing, special attention is focused on the initial crystallization stage. The 0.1-5 μm thick films are produced by spraying ceramic superconducting targets in an argon atmosphere and depositing the atomized material onto planar and cylindrical glass substrates. The phase composition of the two types of targets and films is summarized in order to determine the effect of the sprayed material structure on the film properties. Diffraction patterns of both types of Y-Ba-Cu-O system samples in the initial state and after isochronous annealing (1 h) at various temperature and the optical absorption spectra of amorphous Y-Ba-Cu-O films are plotted. Clusters of amorphous structure forming in the film which contain at least two (001) basal planes with an interfacial spacing which corresponds to the interfacial spacing of the corresponding lattice planes are examined; it is shown that interfacial distances of the superconducting and nonsuperconducting clusters differs by a factor of 1.5. X-ray phase and optical absorption analyses indicate that amorphous films inherit the two-phase state of the targets and that the heterophase structure is manifested on the mesoscopic scale as truncated planar areas (the clusters) and on the short-range order scale in the intercluster medium. The existence of two amorphous

phases complicates the development of crystallization processes: the development of the orthorhombic superconducting phase is suppressed at high Y_2BaCuO_5 concentrations. Figures 3; tables 1; references 13: 11 Russian, 2 Western.

Interaction of $YBa_2Cu_3O_{7-\delta}$ Ceramics With $SrTiO_3$, MgO, ZrO_2 Substrates at 1,170-1,470K

927D0173N Moscow ROSSIYSKAYA AKADEMIYA NAUK: SERIYA NEORGANICHESKIYE MATERIALY in Russian Vol 28 No 4, Apr 92 pp 853-856

[Article by A.Yu. Musatenko, R.B. Turovskiy, Ye.V. Blagov, Ya.M. Mukovskiy, N.A. Kozlovskaya, A.S. Nigmatulin, Stabilizatsiya *ad hoc* Scientific and Engineering Group and Moscow Steel and Alloy Institute; UDC 538.945]

[Abstract] Production of textured bulk Y-Ba-Cu-O ceramics with a high current density in the magnetic field by oriented crystallization is discussed and the interaction between the components of $YBa_2Cu_3O_{7-\delta}$ ceramics with the material of $SrTiO_3$, MgO, and ZrO_2 substrates—the most stable to chemical interaction with the ceramics at high temperature—during partial melt crystallization is investigated. Single crystal $SrTiO_3$, MgO, and ZrO_2+Y_2O_3 substrates are used in order to eliminate the effect of porosity on the phase stratification during partial melting of $YBa_2Cu_3O_{7-\delta}$ ceramics. The superconducting transition in $YBa_2Cu_3O_{7-\delta}$ ceramics after annealing at 1,470K on a MgO substrate is plotted and the structure of the transition layer between the $SrTiO_3$ substrate and $YBa_2Cu_3O_{7-\delta}$ ceramics and the microstructure of a $YBa_2Cu_3O_{7-\delta}$ sample annealed in the air on a ZrO_2 substrate at 1,470K for 20 min are shown. The X-ray microanalysis is performed under a CAMSCAN scanning electron microscope. The study reveals that the ZrO_2+Y_2O_3 substrate has the least effect on the superconducting properties of $YBa_2Cu_3O_{7-\delta}$ ceramics and that a MgO substrate has certain advantages over $SrTiO_3$ and ZrO_2+Y_2O_3 in that there is no noticeable chemical interaction between the $YBa_2Cu_3O_{7-\delta}$ components during the annealing process at temperatures above 1,300K. Figures 3; references: 5 Western.

Effect of Growth Buildup Conditions on Stoichiometry in GaAs-Autoepitaxial Layer Boundary Area

927D0173O Moscow ROSSIYSKAYA AKADEMIYA NAUK: SERIYA NEORGANICHESKIYE MATERIALY in Russian Vol 28 No 4, Apr 92 pp 878-879

[Article by A.A. Krasnov, A.A. Akmarov, V.A. Ivanov, V.A. Uskov, Salyut Scientific Production Association; UDC 621.793.162:546.681.191.1]

[Abstract] The behavior of crystal perfection of the substrate's boundary with the epitaxial layer in autoepitaxial structures produced in a $Ga(CH_3)_3$-AsH_3-H_2 system at various $AsH_3/Ga(CH_3)_3$ ratios (α) is discussed and the origin of the changes occurring on the boundary area as a function of the growth buildup conditions is investigated. Cr-doped GaAs substrates with a (100) orientation are used in the study. The distribution of the As and Ga atom ratio in the depth of heteroepitaxial structures at various temperatures and α is plotted. Enrichment of the interface with As or Ga atoms on the substrate side as a function of α and time is discovered and it is noted that an increase in the As content in the substrate boundary area correlates with a deviation from the epitaxial layer stoichiometry toward a Ga concentration increase and vice versa. It is speculated that the As or Ga excess in the substrate's boundary area is due to diffusion of one of the components from the substrate bulk to the interface. In growing epitaxial GaAs of nonstoichiometric composition, the boundary area enrichment with Ga or As atoms may worsen the structural perfection of the substrate's boundary area. Figures 1; references 2.

Certain Optical Properties of $YbGa_2S_4$ Single Crystals

927D0173P Moscow ROSSIYSKAYA AKADEMIYA NAUK: SERIYA NEORGANICHESKIYE MATERIALY in Russian Vol 28 No 4, Apr 92 pp 889-891

[Article by G.M. Niftiyev, O.B. Tagiyev, F.B. Askerov, Physics Institute at the Azeri Academy of Sciences; UDC 548.55]

[Abstract] The photo-, electro-, and cathodoluminescence properties of semiconductor materials with unfilled 4*f* inner electron shells are discussed and the fundamental absorption and luminescence edge in $YbGa_2S_4$ single crystals is investigated on the basis of analyzing the optical absorption spectrum within a 130-300K temperature range and a 2.1-2.3 eV energy range. The absorption spectra of $YbGa_2S_4$ single crystals, the dependence of absorptance on $h\nu$ at various temperatures, the temperature dependence of the forbidden gap width, the photoluminescence spectrum, and the temperature dependence of the luminescence intensity of $YbGa_2S_4$ single crystals are plotted. It is shown that the fundamental absorption edge shifts to the lower energy area with an increase in temperature; the forbidden gap curves are parallel to each other, indicating that the fundamental absorption edge is formed by the nondirect allowed transition. The activation energy of $YbGa_2S_4$ single crystals is equal to 0.12 eV. It is noted that the photoluminescence band in $YbGa_2S_4$ single crystals is due to $5d \rightarrow 4f$ transitions of the Yb^{2+} ions. Figures 2; references 7: 4 Russian, 3 Western.

Bi-Containing Oxide High-T_c Semiconductors

927D0172A Moscow ROSSIYSKAYA AKADEMIYA NAUK: SERIYA NEORGANICHESKIYE MATERIALY in Russian Vol 28 No 3, Mar 92 pp 453-471

[Article by G.Ye. Nikiforova, V.B. Lazarev, I.S. Shaplygin, General and Inorganic Chemistry Institute imeni N.S. Kurnakov at Russia's Academy of Sciences; UDC 537.312.62]

[Abstract] The search for new bismuth- and copper-containing oxide high-T_c semiconductors (VTSP) prompted by the discovery of superconductivity in the Bi-Sr-Cu-O system and the subsequent discovery of two such superconductors with a T_c of 85 and 110K are discussed and numerous published sources dealing with this subject matter are surveyed. The structural characteristics of bismuth-containing high-T_c superconductors, their syngony, pseudotetragonal and rhombic structure and modulated Bi-type structure as well as the dependence of the volume fraction of superconducting phases on the initial phase component is summarized. The characteristic features of the Bi-containing high-T_c semiconductor synthesis, the behavior of substituted systems, and thermal properties of Bi-containing high-T_c semiconductors are examined and the temperature dependence of electric resistivity and the dependence of critical temperature on the rare earth element (RZE) concentration in the compound are plotted. The physical and chemical properties of bismuth-containing high-T_c semiconductors indicate that in contrast to conventional superconductors in which the electron contribution is dominant, in HTSC the principal heat transfer occurs due to phonons. At low temperatures, a decrease in the electron-phonon scattering is more significant that the freezing out of electrons; this is reflected in a decrease in their heat conductivity with a decrease in temperature. Figures 10; tables 1; references 117: 13 Russian, 104 Western.

Epitaxial Si Layers Grown by Crystallization From Sn-Based Solution Melts

927D0172B Moscow ROSSIYSKAYA AKADEMIYA NAUK: SERIYA NEORGANICHESKIYE MATERIALY in Russian Vol 28 No 3, Mar 92 pp 472-475

[Article by D.I. Brinkevich, N.M. Kazyuchits, V.L. Kryukov, V.V. Petrov, G.P. Furmanov, Belarussian State University imeni V.I. Lenin; UDC 542.65:536.28]

[Abstract] Structural defects in epitaxial layers (ES) of *n*- and *p*-type silicon grown by crystallization from tin-based (Si:Sn) solution melts are investigated. The epitaxial layers are grown in graphite cells using the shift technology within a 1,170-1,420K temperature range on KDB-80 and KEF-5 substrates and the defect containing layer is examined by the methods of low-temperature photoluminescence (FL) and optical microscopy in combination with selective etching. Microphotographs of the angle lapping of epitaxial Si layers before and after etching and photoluminescence spectra are presented. An analysis of the spectra and photographs shows that structural perfection of the epitaxial layers grown by this method is close to that of single crystal silicon and generally does not depend on the growth conditions. A new defect distribution in these epitaxial layers whereby the defect area boundaries become blurred when Yb is added to the solution melt is discovered. It is demonstrated that the process impurity concentration in the epitaxial layers is much lower than in the substrate. Figures 2; references 4.

Effect of Ge on Defect Formation Processes in Si

927D0172C Moscow ROSSIYSKAYA AKADEMIYA NAUK: SERIYA NEORGANICHESKIYE MATERIALY in Russian Vol 28 No 3, Mar 92 pp 480-483

[Article by D.I. Brinkevich, N.I. Gorbachev, I.I. Kolkovskiy, V.V. Petrov, V.V. Shusha, Belarussian State University imeni V.I. Lenin; UDC 546.28:621.315.592]

[Abstract] The process of radiation-induced and thermally stimulated defect generation in Si(Ge) and control materials without an addition of isovalent impurity (IVP) grown under identical conditions is investigated. To this end, dislocation-free *n*-Si(Ge) single crystals doped with an isovalent impurity while being Czochralski-melt-grown (*Cz*-Si) and crystals subjected to zone fining (*Fz*-Si) are examined. The dependence of the radiation variation coefficient on the Ge concentration in the *Cz*-Si and *Fz*-Si crystals and the dependence of the initial injection rate (NSV) and the maximum attainable concentration (MDK) of high-temperature thermal donors on the Ge concentration in the initial and heat treated (for 250 h at 450°C) samples are plotted. The efficiency of defect injection depends nonmonotonically on the isovalent impurity content; it is speculated that its presence facilitates the drop in the concentration and dimensions of the defect-impurity interstitial clusters which serve as annihilation centers for radiation-induced defects and nucleation centers of thermally stimulated donors. The authors are grateful to P.F. Lugakov for interest in the effort and V.V. Borshchenskiy for help with the experiment. Figures 2; references 12.

Effect of Growth Reagent Ratio in Vapor Phase on Nucleation Process During Epitaxial GaAs Growth on Si in $Ga(CH_3)_3$-AsH_3-H_2 System

927D0172E Moscow ROSSIYSKAYA AKADEMIYA NAUK: SERIYA NEORGANICHESKIYE MATERIALY in Russian Vol 28 No 3, Mar 92 pp 498-501

[Article by A.A. Krasnov, R.V. Kudryavtseva, V.A. Ivanov, A.E. Ovsetsina, Yu.V. Chkalova, Salyut Scientific Production Association; UDC 621.315.592:2:546]

[Abstract] The issue of growing heteroepitaxial GaAs layers with a high structural perfection on Si in an organometallic compound (MOS) hydride system and the effect of high-temperature annealing in an AsH_3 atmosphere directly before the growth on the heteroepitaxial GaAs layer properties are discussed and the effect of such annealing on the formation character of GaAs layers in a $Ga(CH_3)_3$-AsH_3-H_2 system is investigated. The (100)- and (111)- oriented Si substrates are used in the experiment and the specimen morphology is examined under an EM-200 electron microscope by the replica method. The epitaxial layer structure is also examined by reflection electron diffraction pattern analysis at an 80 keV accelerating voltage. GaAs electron diffraction patterns on Si at a 5.2 and 72 growth reagent ratio and the change in the GaAs nuclei concentration on the

Si surface as a function of the growth reagent ratio are cited and the distribution of GaAs nuclei size at various growth reagent ratios is plotted. An increase in the AsH_3 concentration in the vapor phase facilitates the stable GaAs nucleation on Si substrates whereby the nucleation process is the most active on (111) Si substrates. A temperature increase in the reactor prolongs the incubation period of the stable nuclei formation. Figures 4; references 7: 2 Russian, 5 Western.

Epitaxial Growth of $InAs_{1-x-y}Sb_xBi_y$ on InSb Substrates From Bismuth Solutions

927D0172F Moscow ROSSIYSKAYA AKADEMIYA NAUK: SERIYA NEORGANICHESKIYE MATERIALY in Russian Vol 28 No 3, Mar 92 pp 502-506

[Article by R.Kh. Akchurin, T.V. Sakharova, A.V. Tarasov, V.B. Ufimtsev, Moscow Institute of Fine Chemical Engineering imeni M.V. Lomonosov; UDC 621.315.592]

[Abstract] The use of thin film $InAs_{1-x}Sb_x$-based epitaxial heterostructures as photodetector materials for the ~14 μm band made possible by advances in molecular beam epitaxy and vapor phase chemical deposition is discussed and the growth conditions of epitaxial layers (ES) on InSB substrates using Bi as the solvent metal are investigated. The effect of Bi-doping of $InAs_{1-x}Sb_x$ on the misalignment of the epitaxial layer and substrate lattice constants is estimated assuming that there is isovalent atom substitution in group V element sublattice. Formulas are derived for calculating the lattice constants. The analytical dependence of the lattice constant on the $InAs_{1-x}Sb_x$ and $InAs_{1-x-y}Sb_xBi_y$ solid solution content, the dependence of the h_k lattice parameter on the epitaxial layer composition, the dependence of the forbidden gap width on the InAsSb and InAsSbBi composition, the dependence of the epitaxial layer content on the initial liquid phase supercooling, and optical transmission spectra of epitaxial layers are plotted. An analysis of the curves shows that when an indium solvent is substituted with a bismuth solvent, the arsenic distribution coefficient increases from 33 to 47.5 while the intrinsic optical absorption edge of the epitaxial layers shifts to $\lambda_{77K} \geq 6.8$ μm. Figures 4; references 12: 6 Russian, 6 Western.

Production and Properties of $CuInS_3$ Semiconductor Films

927D0172H Moscow ROSSIYSKAYA AKADEMIYA NAUK: SERIYA NEORGANICHESKIYE MATERIALY in Russian Vol 28 No 3, Mar 92 pp 521-524

[Article by V.P. Panov, O.G. Movchan, S.B. Lomovtseva, G.D. Panova, Krivoy Rog Mining Institute; UDC 621.315.592]

[Abstract] The outlook for using the $CuInS_3$ ternary compound as a material for solar energy converters and the lack of data on the methods of $CuInS_3$ production prompted an examination of the technological conditions of $CuInS_3$ production by the spray deposition method. To this end, $CuInS_3$ films are deposited onto glass substrates made from X-ray slides which are treated beforehand. The films are deposited at an air pressure of 7×10^4 Pa, a solution rate of 8 ml/min, an outlet diameter of 0.6 mm, a distance from the nozzle to the substrate of 25 cm, a deposition duration of 20-25 min, and a film thickness of 1-4 μm. Spray solutions contain CuCl or $CuCl_2$ as a copper ion source, thiourea as a sulfide ion source, and $InCl_3$ as an indium ion source. The film properties, such as the substrate temperature, conduction type, conductivity, and ion sources, are summarized and X-ray patterns and transmission spectra of the films are plotted. A study of the spraying conditions and compositions for making *n*- and *p*-type films shows that the initial solution composition affects both the conduction type and transmission and conductivity of the films while *p*-type films also contain traces of $Cu_{1.765}S$ and CuS. On the other hand, *n*-type films also contain In_2S_3 and InS phases in addition to the principal phases. Figures 2; tables 2; references 8: 2 Russian, 6 Western.

Microstructure and Superconducting Properties of $YBa_2Cu_3O_{7-x}$ Fused Ceramics With Silver Additions

927D0172N Moscow ROSSIYSKAYA AKADEMIYA NAUK: SERIYA NEORGANICHESKIYE MATERIALY in Russian Vol 28 No 3, Mar 92 pp 652-659

[Article by B.P. Mikhaylov, G.Ye. Nikiforova, E.A. Tishchenko, A.R. Kadyrbayev, I.S. Shaplygin, V.B. Lazarev; General and Inorganic Chemistry Institute imeni N.S. Kurnakov at Russia's Academy of Sciences; UDC 537.312.62]

[Abstract] The relation between the current carrying ability of oxide high-T_c superconductors (VTSP) and the state of their microstructure, i.e., the presence of pores, cracks, and impurity phases localized on the superconducting crystal grain boundaries as well as the absence of strong pinning centers is discussed and the need to optimize the heat treatment temperature, liquid state exposure length, and crystallization rate of fused $YBa_2Cu_3O_{7-x}$ ceramics is emphasized. The microstructure of an YBaCuO pellet cross section after infrared (IK) heating and annealing in oxygen and the microstructure of pellets with Ag additions after surface fusing and annealing are cited and the transition of the initial powders synthesized by the nitrate technology with Ag additions into the superconducting state is plotted. The behavior of the resistivity of YBaCuO samples with Ag additions after infrared irradiation and annealing in the temperature domain is examined and the phase composition of the pellets with 20 percent Ag after infrared heating is summarized. An analysis of the effect of heat treatment on the electric properties of fused HTSC ceramics shows that under brief infrared heating (5 s), the rhombic structure of the original $YBa_2Cu_3O_{7-x}$ is maintained while the critical current density increases by 3.5-5.5 times. An exposure to infrared irradiation for 10 s leads to a specimen overheating and a phase transition in the original rhombic material into tetragonal accompanied with a considerable T_c drop and the

appearance of additional phases due to the compound decomposition. Figures 7; tables 1; references 7: 1 Russian, 6 Western.

Effect of Surface Phases and Critical State Occurrence on Ceramic Formation

927D0172O Moscow ROSSIYSKAYA AKADEMIYA NAUK: SERIYA NEORGANICHESKIYE MATERIALY in Russian Vol 28 No 3, Mar 92 pp 647-651

[Article by Yu.P. Korostikov, V.S. Strykanov, Pozitron Scientific Production Association and Center of Physical and Chemical Research and High Precision Measurements; UDC 621.315.612:546.83]

[Abstract] The decisive effect of surface phases on the so-called kinetic of ceramic materials, i.e., sintering, recrystallization, reactivity, catalytic activity, conductivity, and corrosion resistance is discussed and the need to obtain data on the composition and grain boundary structure and to develop adequate models which fully reflect the characteristic features of the impurity segregation phenomenon and the specially added dopants as well as the conditions and patterns of the surface phase and compound formation and their effect on the properties of ceramic materials in order to outline paths of technological development in this field is identified. Theoretical models which described the impurity segregation or adsorption on the surface are reviewed and the dependence of the chemical potential of the surface phase on the added dopant concentration is plotted. The conclusion is drawn that at a low impurity concentration, an impurity distribution in the ceramics in the form of surface phases is preferable. An increase in the impurity concentration leads to a transition from the heteroepitaxial system to a mechanical mixtures. The extremal character of the concentration dependence of the oxides' kinetic properties is due to the occurrence of critical state in the surface phase/bulk phase system. Figures 1; references 22: 11 Russian, 11 Western.

Use of Cd-Containing Fused Silica Glass in High-Temperature Thermodynamic Studies by Electromotive Force Method

927D0172P Moscow ROSSIYSKAYA AKADEMIYA NAUK: SERIYA NEORGANICHESKIYE MATERIALY in Russian Vol 28 No 3, Mar 92 pp 643-646

[Article by V.A. Leybov, Moscow Steel and Alloy Institute; UDC 539.21.213]

[Abstract] The use of the electromotive force (EDS) method with a fused silica glass-based electrolyte with various potential-forming component oxide compositions in studies of the thermodynamic properties of compounds and the difficulty of producing glass containing less than 20 percent of oxides of heavy bivalent metals are discussed and an attempt to use fused silica glass with a low cadmium oxide concentration as the solid electrolyte for measuring the thermodynamic properties of cadmium telluride by the electromotive force method is described. Chemically pure grade cadmium oxide and Spectrosil quartz are used as source materials; a finely disperse mixture of CdO and SiO_2 powders in an equimolar ratio is carefully mixed and loaded into a quartz vial which is evacuated and heated at 973K, exposed to this temperature for 2 h, then heated to 1,170K. A block diagram of the solid electrolyte resistance measurement cell is cited and the temperature dependence of Cd-containing glass resistivity and the temperature dependence of the electromotive force of Cd-Te samples with 55 percent Te are plotted. An analysis of fused quartz glass with 1.58 percent Cd by mass within a 1,000-1,450K temperature range shows that the dependence of the logarithm of resistivity on temperature is approximated by a linear function while the dependence of the EMF on temperature is also linear. The cadmium vapor pressure and the cadmium activity on the tellurium boundary of cadmium telluride homogeneity are calculated within a 1,253-1,330K range. Figures 3; tables 1; references 6: 4 Russian, 2 Western.

Luminescence of Cadmium Diarsenide Single Crystals

927D0172Q Moscow ROSSIYSKAYA AKADEMIYA NAUK: SERIYA NEORGANICHESKIYE MATERIALY in Russian Vol 28 No 3, Mar 92 pp 674-676

[Article by S.F. Marenkin, A.V. Mudryy, V.A. Leontyeva, A.M. Raukhman, M.G. Solovyeva; General and Inorganic Chemistry Institute imeni N.S. Kurnakov at Russia's Academy of Sciences; UDC 546.196+546.681]

[Abstract] Discovery of luminescence in $CdAs_2$ crystals in the near infrared spectrum at low temperatures is reported and two types of crystals are examined: one grown from the vapor phase and one melt-grown by Bridgeman's method. The samples are made from *n*-$CdAs_2$ single crystals and oriented in the [001] direction. The photoluminescence spectrum of *n*-$CdAs_2$ crystals at 4.2K is plotted and it is demonstrated that the luminescence spectra, regardless of the growth method and the degree of structural perfection, are characterized by the presence of a rather intense line with a 0.869 eV maximum (14,260 angstrom). An analysis of the findings obtained in doped and intrinsic $CdAs_2$ crystals reveals the presence of a deep 0.30-0.35 eV energy level within the forbidden gap through which the radiative recombination of nonequilibrium charge carriers occurs. It is speculated that this energy level is related to point defects in $CdAs_2$ crystals. Figures 1; references 12: 9 Russian, 3 Western.

Stimulated Emission Under Electron Excitation of $ZnAs_2$ Single Crystals

927D0172R Moscow ROSSIYSKAYA AKADEMIYA NAUK: SERIYA NEORGANICHESKIYE MATERIALY in Russian Vol 28 No 3, Mar 92 pp 677-678

[Article by S.F. Marenkin, D.I. Pishchikov, M.V. Chukichev, A.S. Artemov, General and Inorganic Chemistry Institute imeni N.S. Kurnakov at Russia's Academy of Sciences; UDC 546.196+546.681]

[Abstract] Optical and emission properties of $ZnAs_2$ crystals are discussed and the possibility of generating stimulated emission in melt grown $ZnAs_2$ crystals is investigated. The single crystal technology is based on the vertical oriented Bridgeman crystallization method made it possible to produce large perfect single crystals with a 20-25 mm diameter and 100-120 mm length. Both transverse and longitudinal electron beam excitation configurations are tested for generating stimulated emission. Cathodoluminescence spectra of a $ZnAs_2$ cavity under different excitation conditions are plotted. The findings indicate that in melt-grown crystals at 78K, stimulated emission can be attain with both longitudinal and transverse cavity geometry and that in the direction perpendicular to the *c*-axis, stimulated emission is linearly polarized. Figures 1; references 7: 5 Russian, 2 Western.

Deformation Effect in Exoemission of Dielectric Glass With Modified Surface

927D0171E Moscow POVERKHNOST: FIZIKA, KHIMIYA, MEKHANIKA in Russian No 4, Apr 92 pp 52-60

[Article by L.B. Glebov, A.F. Zatsepin, V.S. Kortov, N.V. Nikonorov, V.V. Tykov, G.B. Cherlov, Urals Polytechnic Institute, Yekaterinburg; UDC 537.533.2+539.319]

[Abstract] The effect of elastic stresses and deformations on the electric and physical properties of solids, particularly their near-surface layers, and the micromechanism of the effect of the field of elastic stress on the electron emission by an excited solid state surface are discussed and earlier studies (*Poverkhnost* No. 12, 1988 and *Fizika i khimiya stekla* Vol. 15 No. 1, 1989) are continued. To this end, the mechanism of the deformation effect on the emission of exoelectrons from the modified surface of dielectric glass under photo- and thermal stimulation is examined. In so doing, the results of simulating the transport process and electron escape from elastically deformed bodies are employed. Thermally stimulated electron emission (TSEE) of K8 glass samples after the glass surface excitation with electrons, the time dependence of the photostimulated electron emission (FSEE) of K8 glass samples with diffusion stresses, the dependence of the time constants of exponential photostimulated electron emission attenuation on the ion exchange treatment duration, and the energy distribution of the exoelectrons emitted from the glass surface within the thermally stimulated electron emission range at 420K are plotted. The results of the exoelectron energy and start depth distribution are summarized and plotted. The movement of electrons in the elastically deformed layers and their emission from the surface are simulated by the Monte Carlo method. It is shown that the deformation effect under photo- and thermal stimulation is general in nature and is determined by the characteristics of the electron transport mechanism in the strained layers. Elastic stresses affect the photoemission properties of excited surfaces in that they change the scattering efficiency of delocalized electrons by the strained lattice vibrations. The deformation effect is enhanced in an irradiated surface due to the dependence of the structure and magnitude of the deformation charge on the mechanical stress sign. Figures 4; references 20: 17 Russian, 3 Western.

Surface Periodic Structures in Polycrystalline Silicon Layers Recrystallized by Nanosecond Pulsed Laser Radiation

927D0171G Moscow POVERKHNOST: FIZIKA, KHIMIYA, MEKHANIKA in Russian No 4, Apr 92 pp 85-90

[Article by A.V. Demchuk, V.A. Labunov, Minsk Radio Engineering Institute; UDC 621.315.592]

[Abstract] The specific surface periodic structures (PPS) forming on the solid state surface under the effect of coherent optical emission are outlined and the surface periodic structure development during the recrystallization of polycrystalline Si layers by nanosecond pulses of nonpolarized laser radiation is investigated. The study is carried out in 0.45 μm thick polycrystalline Si layers produced by the vapor phase chemical deposition at a reduced 80 Pa pressure and a 625+/125° temperature onto pure and oxidized single crystal wafers with a 0.1 μm SiO_2 layer. Some samples are amorphized by ionic implantation with P. The surfaces are exposed to a single pulse of the first and second harmonic radiation of a neodymium glass laser at a 1.06 and 0.53 μm wavelength with a 50 ns pulse duration. Three types of periodic surface structures revealed by etching and the surface morphology of polycrystalline Si layers amorphized by ionic implantation are shown. A periodic change in the surface structure is confirmed in the area of threshold effects. This change in the crystal structure of the recrystallized layers is attributed to the laser radiation intensity modulation due to the radiation diffraction and interference both by the optical irregularities of the irradiated surface and optical inhomogeneities of the medium. Figures 2; references 11: 8 Russian, 3 Western.

Thermal GaAs Oxidation in 'Dopantless' and Dopant Atmosphere

927D0189A Moscow ROSSIYSKAYA AKADEMIYA NAUK: NEORGANICHESKIYE MATERIALY in Russian Vol 28 No 5, May 92 pp 917-927

[Article by I.Ya. Mittova, Voronezh State University; UDC 546.681.19:621.794.64]

[Abstract] The difficulty of predicting and studying the kinetics and mechanism of GaAs thermal oxidation under the effect of various factors, e.g., controlled dopants, is addressed and an attempt is made to establish common patterns and individual characteristic features of new GaAs thermal oxidation processes under the effect of controllably added dopants, compare them to dopant-free oxidation, and develop a classification based on the character of the defining process and its limiting stage. GaAs oxidation proper and the concomitant processes are identified as follows: oxidant diffusion toward the inner interface side, As oxidation with oxide formation, exchange interactions of As oxides with Ga in the substrate leading to the oxide film formation, and secondary interaction for the former and competing arsenic oxide evaporation from the outer interface side, Ga diffusion to the film, As diffusion to the film, component oxidation on the outer interface side and in the layer, and direct Ga oxidation by oxygen on the inner interface side for the latter. The rate characteristics of GaAs oxidation processes are characterized against a "dopantless atmosphere" standard and thermal oxidation processes are similarly classified. An analysis of the kinetic data and a study of grown layers by infrared spectroscopy, X-ray spectral analysis, electron Auger spectroscopy, X-ray electron spectroscopy, secondary ion mass spectrometry, and mass spectrometry analysis and the resulting classification make it possible to predict the methods for preparing high-quality insulating layers at a high rate on GaAs. Tables 2; references 27: 21 Russian, 6 Western.

Production and Study of Electrophysical Properties of $CuInSe_2$ Crystals and Films

927D0189D Moscow ROSSIYSKAYA AKADEMIYA NAUK: NEORGANICHESKIYE MATERIALY in Russian Vol 28 No 5, May 92 pp 961-964

[Article by M.A. Abdullayev, Dzh.Kh. Amirkhanova, A.K. Akhmedov, R.M. Gadzhiyeva, M.-R.A. Magomedov, P.P. Khokhlachev, Dagestan Department of the Physics Institute at Russia's Academy of Sciences; UDC 621.315.592:546.0.5.22]

[Abstract] The electrophysical properties of the $CuInSe_2$ semiconductor are examined from the viewpoint of its practical applications in solar photoelectric power generation; to this end, copper-indium diselenide crystals and films are prepared and their galvanomagnetic properties, thermal conductivity, and optical absorption edge are investigated at various temperatures. Bulk crystals are produced by direct fusion of the initial components in a stoichiometric ratio with subsequent oriented crystallization while films are prepared by thermal evaporation from two sources and by vacuum flash deposition on glass and thin mica substrates. The phase composition is examined by a DRON-2 diffractometer. The temperature dependence of the electric conductivity of crystals and films, the temperature dependence of Hall's charge carrier mobility in the crystals and films, the temperature dependence of the thermal conductivity of the crystals and films, and the dependence of the $(\alpha h\nu)^2$ parameter on the photon energy $h\nu$ at 300K where α is absorptance are plotted. The diffraction pattern analysis shows that the film contains only one phase of a stoichiometric composition with a chalcopyrite crystal structure. The forbidden gap is equal to 0.98+/-0.02 and 1.08+/-0.02 eV for single crystals and films, respectively. The difference in the values is attributed to the deviation from stoichiometry in films prepared with a shortage of Se. It is shown that deviations from stoichiometry and the impurity zone conductivity lead to a decrease in the charge carried mobility and thermal conductivity and a shift in the fundamental absorption edge. The authors are grateful to I.K. Kamilov and Yu.V. Rud for support. Figures 4; references 14: 8 Russian, 6 Western.

Thermal and Laser-Thermal Titanium Oxidation Within 773-973K Temperature Range

927D0189J Moscow ROSSIYSKAYA AKADEMIYA NAUK: NEORGANICHESKIYE MATERIALY in Russian Vol 28 No 5, May 92 pp 1019-1021

[Article by L.V. Bareukova, A.M. Khoviv, V.Z. Anokhin (deceased), Voronezh State University; UDC 546.82:542.943.4]

[Abstract] The failure of recent empirical data on thermal and laser oxidation of titanium to draw an unambiguous conclusion about the structure of the oxide film forming on Ti prompted a qualitative evaluation and comparison of the structure of oxide films on Ti produced under thermal and laser-thermal oxidation conditions; the latter is defined as a thermal oxidation condition under the effect of laser irradiation. A 773-973K temperature is selected due to the fact that a thin, transparent dense film is formed within this range which is necessary for subsequent ellipsometric measurements; the chemical and mechanical polishing is used as the optimal surface treatment condition while the surface standardization is monitored by the optical response. The VT 1-0 Ti, mostly consisting of α-Ti, is used as the source material. The 20 x 20 mm samples are irradiated by a continuous wave YAG laser (OKG) at a wavelength of 1.064 μm, a quantum energy of 1.17 eV, a maximum power of 60 W, and a beam diameter of 3.5 mm. The oxide film thickness after growth under both thermal and laser-thermal conditions is measured and summarized and the results of electron diffraction analyses of the oxide film structure after both oxidation methods are presented. The growth rate patterns indicate that the specific features of laser irradiation amount to speeding up the film growth rate while its mechanism is similar to

that of thermal oxidation; the oxide has a rutile structure according to data of X-ray phase analysis. If that the oxidation process is conducted for 10-60 min, TiO_2 films are grown. Tables 3; references 6.

Magnetic Material Films Grown by Molecular Beam Epitaxy Method

927D0189N Moscow ROSSIYSKAYA AKADEMIYA NAUK: NEORGANICHESKIYE MATERIALY in Russian Vol 28 No 5, May 92 pp 1122-1123

[Article by Ye.P. Vasilyeva, L.I. Vershinina, V.P. Kononov, S.G. Ovchinnikov, A.Ye. Khudyakov; UDC 539.234]

[Abstract] Fe (99.99 percent pure) and 99.99 percent pure FeNi films with 17 percent Fe and 83 percent Ni spray deposited in an Angara three-chamber molecular beam epitaxy (MLE) unit at a 1 x 10^{-8} Pa pressure with two-crucible deposition chambers one containing six and the other—two thermal evaporators and an electron beam gun are investigated. The film growth parameters are monitored and controlled by MX-7304 and PGA mass spectrometers, a fast electron diffractometer, an SNA-2 gas leak-in system, and a quartz film thickness gauge. Electron microscope photographs of 540 angstrom thick FeNi films before and after annealing at a 300°C temperature for 5 h are shown. The films have a ferromagnetic resonance line width of 795-955 A/m at a 400-800 angstrom thickness at a 3 GHz frequency. A study of the ferromagnetic resonance line width and other magnetic and magnetooptical parameters of FeNi films indicates that their coercive force is equal to 238-246 A/m at a 400-700 angstrom thickness and their magnetooptical Kerr rotation is equal to 1'. It is shown that annealing leads to a 79.6-159.2 A/m increase in the coercive force and an increase in Kerr's magnetooptical rotation to 4'. Annealing also increases the ferromagnetic resonance line width to 1,035-1,194 A/m. Figures 1; references 1.

Continuous Wave 3-μm Stimulated Emission of BaY_2F_8-Er^{3+} Crystals at Room Temperature With Semiconductor Laser Pumping

927D0189O Moscow ROSSIYSKAYA AKADEMIYA NAUK: NEORGANICHESKIYE MATERIALY in Russian Vol 28 No 5, May 92 pp 1130-1133

[Article by A.A. Kaminskiy, D. Wandt, I. Kropke, H. Schmidt, T.V. Uvarova, Crystallography Institute imeni A.V. Shubnikov at Russia's Academy of Sciences and Laser Zentrum Hannover, Germany; UDC 547.641-31:546.623-31:546.65-535.33]

[Abstract] The importance of 3 μm laser radiation with heterolaser pumping in today's medicine and engineering is discussed and excitation of CW 3 μm stimulated emission (SI) in BaY_2F_8-Er^{3+} fluoride crystals by a new inter-Stark $^4/_{11/2} \rightarrow {}^4/_{13/2}$ channel transition and in their activator ions with the help of GaAlAs semiconductor lasers is reported. The nonpolarized absorption spectrum of Er^{3+} ions in the Ba-Y-F crystal at 300K and the nonpolarized luminescence spectrum and multiplet splitting diagram are plotted and the energy parameters of stimulated emission of monoclinic crystal at 300K with laser pumping is summarized. It is speculated that the stimulated emission conditions could be further improved by using laser diodes with an emission spectrum in the 0.795 μm region, i.e., the maximum absorption band of the excitation channel, as well as optimizing the activator ion concentration and active element configuration, thus increasing the 3 μm stimulated emission efficiency. Figures 2; tables 1; references 19: 6 Russian, 13 Western.

$La_{1.8}Sr_{0.2}CuO_{4-\delta}$ Hydrothermal Treatment at 200-300°C and 10-70 MPa

927D0189K Moscow ROSSIYSKAYA AKADEMIYA NAUK: NEORGANICHESKIYE MATERIALY in Russian Vol 28 No 5, May 92 pp 1026-1030

[Article by E.N. Korytkova, N.I. Nesterchuk, L.N. Pivovarova, D.P. Romanov, Ye.A. Vasilyeva, R.G. Grebenshchikov, Silicate Chemistry Institute imeni I.V. Grebenshchikov at Russia's Academy of Sciences; UDC 538.945]

[Abstract] The high efficiency of hydrothermal treatment of the $La_{1.8}Sr_{0.2}CuO_{4-\delta}$ superconducting oxide (LSCO) for the purpose of increasing the cuprate stability and preventing its degradation is noted and an examination of the LSCO behavior (*Zhurnal prikladnoy khimii* Vol 64 No 1, 1991) is continued. To this end, La-Sr cuprate produced by conventional ceramic technology is exposed to hydrothermal treatment by water and NaOH and KOH solutions in a 200-300°C temperature range at a 10-70 MPa pressure and the treatment products are studied by X-ray phase, crystal optics, and electron microscope analyses. Diffraction patterns of the initial LSCO and after aqueous and alkali treatment are plotted and the LSCO microstructure is presented. The findings demonstrate the efficiency of refining the LSCO structure by the above treatment thus ensuring the compound stability. In addition, the optimum hydrothermal treatment parameters necessary for stabilizing the superconductor structure by injecting OH^- ions into vacant oxygen positions are established: 200°C at 10-70 MPa for 30 min for alkali solutions and 200°C at 70 MPa for up to 3 h for aqueous solutions. Figures 4; references 3: 2 Russian, 1 Western.

Development and Implementation of New Wide Strip Hot Rolling Process

927D0176J Moscow STAL in Russian No 2, Feb 92 pp 37-41

[Article by A.I. Starikov, V.M. Salganik, I.G. Gun, A.M. Tilvak, V.N. Girenko, A.V. Povarich, Magnitogorsk Integrated Iron and Steel Works, Magnitogorsk Mining and Metallurgy Institute, and Magnitogorsk State Institute of Metallurgical Plant Design; UDC 621.771.237]

[Abstract] New trends in the development of wide strip hot rolling mills (ShSGP) and the shortcomings of the coil box device (PPU) invented by the Stelco Co. in Canada prompted the Magnitogorsk Integrated Iron and Steel Works, Magnitogorsk Mining and Metallurgy Institute, and Magnitogorsk State Institute of Metallurgical Plant Design to develop a new hot strip rolling process which makes it possible to position long work pieces on a short intermediate roller table by forming a loop on the outlet from the last roughing stand. Schematic diagrams of strip rolling with looping on the intermediate roller table and of a new strip rolling method with free work piece looping are cited and its implementation experience is described. The method makes it possible to decrease considerably the intermediate roller table length when building new rolling mills, reduce heat losses, and position elongated work pieces on a short roller table by upgrading existing mills. The free looping version is tested and considered to be the simplest and most reliable. The method is implemented in the wide strip hot rolling mill 2500 at the Magnitogorsk Integrated Iron and Steel Works. Figures 3; references 3.

Automation of Continuous Cold Rolling Mills

927D0176K Moscow STAL in Russian No 2, Feb 92 pp 41-46

[Article by S.I. Belov, I.V. Zalesskiy, V.S. Senichev, All-Union Scientific Research Institute of Metallurgical Machine Building and Magnitogorsk Integrated Iron and Steel Works; UDC 621.771.06-114:658.012.011.56]

[Abstract] The development of computer-aided process control systems for rolling mills since bringing on stream the country's first continuous cold rolling mill 1200 (NSKhP) at the Magnitogorsk Integrated Iron and Steel Works in 1956 is reviewed and a block diagram of a computer-aided process control system (ASUTP) with a hierarchical architecture used for tandem cold mills is presented and its principal components are discussed. The ASUTP system is a multiply connected system where control actions on the roll speed and stand screwdown mechanisms are formed on the basis of data from process control pickups. Several system design concepts are considered. A mathematical model of the mill control system parameter adjustment analysis is derived and oscillograms of a strip of steel 65G reduced from a 3.2 to a 2.2 mm thickness in an automatically controlled mill are cited. The methods of adapting the mathematical model by a recursive formula is addressed. A.G. Mirer made the principal contribution in developing the automatic control algorithms. Figures 3; references 7: 5 Russian, 2 Western.

Lateral Strain in Thin Strip Rolled in Twenty-High Mill

927D0176L Moscow STAL in Russian No 2, Feb 92 pp 46-48

[Article by P.I. Denisov, R.V. Fayzullina, A.Kh. Belalov, M.S. Bronnikov, R.Ya. Kutuyev, Magnitogorsk Mining and Metallurgy Institute and Magnitogorsk Integrated Iron and Steel Works; UDC 621.771.23:621.77.014]

[Abstract] The diversity of views on the lateral strain in a thin strip during rolling and its effect on the strip stability due to the difficulty of directly demonstrating the existence of metal displacement in the deformation focus in the width direction is noted and the need for additionally studying the transverse metal flow on the outlet from the deformation center in order to determine the reason for the compressive stresses which lead to herringbone defects in strips with different types of

nonflatness is recognized. For this purpose, an experimental examination is conducted whereby 0.3 mm wide and 0.2 mm deep notches are made on the roll barrel of a twenty-high mill 700-E and measurements are taken by an IMTsL 150 x 150 instrument microscope pursuant to GOST 8074-82. The study of lateral strain at the exit from the mill made it possible to derive a formula for calculating the lateral strain in the width direction and establish the correlation between the strip broadening at the outlet from the deformation center and the herringbone defect formation. It is speculated that the compressive stresses leading to the defect formation appear due to the strip relaxation. Data obtained in the experiment make it possible to predict the appearance of defects. References 6.

Decreasing Metal Losses During Rolled Stock Cutting in Section Mills

927D0176M Moscow STAL in Russian
No 2, Feb 92 p 58

[Article by A.G. Averchenko, A.P. Khamlov, Ye.A. Krupskiy, V.L. Kornilov, A.P. Morozov, Magnitogorsk Integrated Iron and Steel Works; UDC 621.771.251.004.18]

[Abstract] Metal losses during the hot rolling of carbon and low alloyed steel ingots are classified as irreversible and preventable and a production method developed as a result of studies of metal losses due to discrepancies between the rolled metal length and specified values is described. The new procedure of cutting rolled stock in section mills involves measuring the blank length before rolling, sending metal blanks of the same length to the furnace, and installing air-operated pushers for evening the rear ends of the blanks. A schematic diagram of the pneumatic pusher is cited and the operating principle of its components is explained. The proposed design is intended for all types of steel made at the section mill plant. Its implementation makes it possible to decrease ready rolled product discards by 4,000 tons per year, improve the working conditions, and quicken the rolling pace. Figures 1.

Making Drilling Pipes With Welded Tool Joints From Low Carbon Steel

927D0176N Moscow STAL in Russian
No 2, Feb 92 pp 59-61

[Article by V.A. Rodnikov, I.G. Pogorelova, Scientific Production Association of the All-Union Scientific Research Tube Institute and Taganrog Metallurgical Plant; UDC 621.774:622.23/24:669.141.24]

[Abstract] The difficulties of using low carbon steel—a material which combines ductility and strength—for crucial parts of machines and mechanisms prompted the experts at the Taganrog Metallurgical Plant (TMZ) to develop a method of making drilling pipes with welded-on tool joints from low carbon steel 10 and 20. The structure of this steel in the normalized and hot rolled state consists of ferrite and pearlite and its strength is mostly determined by the carbon concentration and differs little from steel 10 to steel 20. The mechanical properties of low carbon steel 10 and 20 after hardening, hardening and tempering, and normalizing treatment and in the hot rolled state is plotted and the microstructure of the welded joints of steels 40KhMFA and 20 is examined. The results of the structural analyses of low carbon steel after heat treatment are summarized. The findings show that drilling pipes from low carbon steel 20 after hardening at 900°C and tempering at 530°C meet the requirements of the TU 14-3-1571—88 specifications for pipes with group-E strength and in addition to their excellent mechanical characteristics, are highly resistant to dynamic loads at subzero temperatures. The welded joint has a safety margin of 1.46. Figures 2; tables 1; references 3.

Crack Resistance Analysis of Steel for Cold Upsetting and Extrusion

927D0176P Moscow STAL in Russian
No 2, Feb 92 pp 72-73

[Article by V.N. Urtsev, V.A. Maslennikov, V.P. Gubchevskiy, L.P. Sarycheva, Ye.V. Radyukevich, Magnitogorsk Integrated Iron and Steel Works; UDC 669.14.018.265:621.771.019]

[Abstract] The rising need for steel rolled stock for sold upsetting and extrusion pursuant to GOST 10702-78 with upsetting groups 66 and 75 prompted an investigation of the causes of the so-called 45-degree cracks and a search for principally new designs for making semifinished rolled products which are not susceptible to these types of defects under compressive stress. Attention is focused on 45-degree cracks because the cracks caused by the presence of brittle nonmetallic inclusions as well as the cracks developing at mechanical surface defects are sufficiently well researched. To identify the structural inhomogeneity formation, the crystallographic texture of the surface layer of semifinished rolled stock is examined by DRON-1UM and DRON-3M diffractometers using the method of direct (PPF) and inverse (OPF) pole figures. An analysis of the findings reveals that 45-degree cracks develop during cold upsetting and extrusion of round steel samples due to the structural inhomogeneity of the semifinished rolled stock surface layer while ausforming which includes twisting deformation in the hot state makes it possible to control the surface layer texture within a broad range. Steel samples with an axial texture whose (110) axis is perpendicular to the rolling direction is characterized by a much lower susceptibility to cracking and withstand cold compressive strain better by 15-20 percent on the average. Figures 1.

Comparing Requirements for Vehicle Cardan Shaft Pipes and Ways of Improving Their Quality

927D0175I Dnepropetrovsk METALLURGICHESKAYA I GORNORUDNAYA PROMYSHLENNOST in Russian No 4 (162), Oct-Dec 91 pp 44-45

[Article by G.I. Gulyayev, K.I. Shkabatur, V.I. Mizera, A.I. Derevyanko, T.P. Rodionova, All-Union Scientific Research and Design Tube Industry Institute; UDC 006.44.001.36:[621.774.21:621.791.7]:621.825.6]

[Abstract] Due to the constantly increasing vehicle speed and power, especially stringent requirements are being imposed on cardan shafts which spin at a high speed under considerable alternating loads; this factor and the diversity of the foreign and domestic standards prompted an investigation of the requirements imposed on cardan shaft pipes under foreign and domestic standards. To this end, the requirements imposed on domestic pipes pursuant to GOST 5005-82 and Japan's JASOC 301-77 standard are compared. The choice of the Japanese standard is due to the fact that production of high-quality pipes for the automotive industry, including cardan shaft pipes, is highly developed in Japan. The tube-making technology is both countries is examined; an analysis of the findings made it possible to recommend the following steps for producing high-quality pipes at the level of the best world indicators and increasing the production volume: using a new generation of electric tube welding machines; using a dressed coil made from rimmed steel with a 0.25-0.30 carbon concentration with a twisting factor of no more that 5 mm per 10 m of length; and revising GOST 5005-82 so as to expand the range of tube products and add a clause for the possibility of making electric resistance welded nonstrained pipes with pipe end machining as well as expanding the standard by mandating tube tests for alternating loads with a specific minimum permissible number of cycles to failure. Tables 1; references 7: 4 Russian, 3 Western.

Study of Possibility of Railroad Wheel Roll Surface Laser Hardening. In Two Parts. Part 1. Pulsed Laser Treatment

927D0175K Dnepropetrovsk METALLURGICHESKAYA I GORNORUDNAYA PROMYSHLENNOST in Russian No 4 (162), Oct-Dec 91 pp 51-53

[Article by Yu.N. Taran, V.P. Yesaulov, S.I. Gubenko, L.S. Kalashnikova, V.N. Varavka, V.A. Poluyanov, O.A. Demidova, Dnepropetrovsk Metallurgical Institute; U D C 669.14.018.294.3:[621.785.5:621.375.826]:620.18]

[Abstract] The effect of the roll surface profile wear and the flange ridge shouldering on the railroad wheel service life and, consequently, the rolling stock ride stability and smoothness is discussed and the use of laser hardening of the roll surface for increasing the reliability and normal life of wheels is considered. To this end, the roll surface is hardened by pulse laser radiation without trying to attain a record hardness (due to the rail hardness limitations). The roll surface is irradiated by 20.5, 17.5, 15.5, 13.5, 12.0, and 10.0 J pulses of a Kvant-16 laser with a heating and cooling rate of 10^5 and 10^6°C/s, respectively and a close to 10^{-3} s pulse duration. The microstructure of the hardened roll surface is shown, the steel microhardness behavior throughout the depth of the laser-affected zone is plotted, and the effect of the laser pulse energy on the steel's micro- and fine structure parameters and its microhardness and hardness are summarized. The findings show that the wheel surface hardness resulting from laser irradiation exceeds the 350 HB maximum value attained to date for the roll surface, indicating that the problem of laser hardening of wheels must be solved together with the problem of increasing the rail hardness so as to attain an optimum hardness ratio and thus increase their wear resistance. It is noted that the possibility of hardening the entire roll surface using a CW laser should be further examined. Figures 2; tables 1.

Computer Simulation of Certain Problems of Electrochemical Machining to Size

927D0174A Chisinau ELEKTRONNAYA OBRABOTKA MATERIALOV in Russian No 6 (162), Nov-Dec 91 pp 4-8

[Article by L. Dambrowski, E. Kozak, Warsaw Polytechnic Institute, Poland]

[Abstract] The use of electrochemical machining to size (REKhO) in mechanical engineering is examined from a viewpoint of microcomputer (IBM PC) applications and the new possibilities opened up by personal computers are investigated. The problem of designing cathode tools, analyzing and computing the machining accuracy, and determining the optimum process parameters is considered and it is speculated that the use of microcomputers at the design stage will make it possible to take into account a larger number of factors which affect the principal machining indicators, thus reducing labor outlays and cost of setup operations. The problem of computer simulation of such problems is formulated and a mathematical model of electrochemical forming is developed. Algorithms of the precision analysis, cathode tool design, and machining condition selection are developed and a formula is derived for the physical condition distribution in the interelectrode gap. The anode surface configuration, the effect of the electrode voltage on the shape error under various machining conditions, the microsurface evolution during the machining, and the roughness profile behavior during the machining are plotted. The electrochemical machining-accuracy-tool-conditions (ECM-ATC) simulation routine is compiled in the Fortran, Turbo-Pascal, and Assembler languages. The routine is a part of a CAD/CAM system for electrochemical machining to size being developed at the Institute of Mechanical Engineering. Figures 10; references 2: 1 Russian, 1 Western.

Behavior of Quartz and Phenakite Crystals' Exoemission Properties During Radiative Transformation of Surface Structure

927D0171D Moscow POVERKHNOST: FIZIKA, KHIMIYA, MEKHANIKA in Russian No 4, Apr 92 pp 43-51

[Article by A.F. Zatsepin, V.S. Kortov, V.I. Ushkova, V.A. Kalentyev, Urals Polytechnic Institute, Yekaterinburg; UDC 537.533+539.213.26]

[Abstract] The relationship between the study of the crystal surface and an investigation of the defects typical of the amorphous state of substances is discussed and the exoemission properties of oxide crystals with various degrees of surface disordering are examined; in addition, the characteristics of the emission-active centers of similar origin in crystalline and amorphous matrices are examined and the possibility of investigating the process of radiation-stimulated transformations on the surfaces of solids by the method of exoelectronic emission is assessed. The thermally stimulated exoelectronic emission from the a quartz crystal surface after electron bombardment in a vacuum, thermally stimulated exoelectronic emission (TSEE) of fused silica glass after electron bombardment in a vacuum, and thermally stimulated exoelectronic emission from the quartz crystal surface before and after fast neutron irradiation are plotted. The dose dependence of the thermally stimulated exoelectronic emission intensity of adsorption centers and of the concentration of bulk paramagnetic centers and the dose dependence of the thermally stimulated exoelectronic emission from the surface of the neutron irradiated phenakite surface after excitation are examined. The peculiar features of exoemission centers of the adsorption origin on the crystalline and amorphous surface of SiO_2 and Be_2SiO_4 are identified and the development of an intermediate crystalline phase under the radiation-stimulated surface structure transformation in α-quartz into the amorphous state is demonstrated. The effect of the isothermal annealing temperature with a 10 h exposure on the adsorption and emission active center concentration in neutron-irradiated phenakite is studied. The findings show that the exoelectronic spectroscopy method is suitable for examining the radiation-induced phase transitions in thin near-surface layers. Figures 6; References 11: 10 Russian, 1 Western.

Study of Possibility of Railroad Wheel Roll Surface Laser Hardening. Part 2: Continuous Wave Laser Emission

927D0170H Dnepropetrovsk METALLURGICHESKAYA I GORNORUDNAYA PROMYSHLENNOST in Russian No 1 (163), Jan-Mar 92 pp 33-35

[Article by Yu.N. Taran, V.P. Yesaulov, S.I. Gubenko, L.S. Kalashnikova, V.A. Poluyanov, V.N. Varavka, O.A. Demidova, All-Union Scientific Research Tube Industry Institute; UDC 669.14.018.294.3: [621.785.5: 621.375.826]: 620.18]

[Abstract] The structural transformations occurring in the roll surface of railroad wheels made from wheel steel under the effect of continuous wave laser radiation are investigated. To this end, wheel samples are laser treated, i.e., surface hardened, in an LG-710 Kardamon installation using laser radiation with an approximately 600 W power; the beam travel rate on the surface determines the degree of treatment. The beam is moved at three rates: 1, 2.5, and 6 mm/s. The microstructure of the wheel steel surface in the laser irradiation zone is examined in metallographic sections under an optical microscope. The surface microhardness in various structural zones as a function of the laser beam rate and the effect of the laser beam velocity on the parameters of the heat affected area are summarized. An analysis of the findings reveals that the steel structure in the surface hardening zone under CW exposure is preferable to that produced by pulse irradiation. CW laser surface hardening makes it possible to attain a surface hardness of close to 350 HB or more. The resulting surface structure increases the wheel's wear resistance. The need to incorporate relevant experience gained by laser hardening of rails in the wheel treatment procedure is stressed. Figures 1; tables 2.

Thin-Walled Electric-Welded Tubes for Automotive Cardan Shafts

927D0170G Dnepropetrovsk METALLURGICHESKAYA I GORNORUDNAYA PROMYSHLENNOST in Russian No 1 (163), Jan-Mar 92 pp 29-31

[Article by K.I. Shkabatur, F.D. Davydov, V.I. Mizera, A.I. Derevyanko, T.P. Rodionova, All-Union Scientific Research Tube Industry Institute; UDC 621.774.21: 621.791.7]:621.825.6]

[Abstract] The reasons for using electric-welded thin-walled tubes for making cardan shafts, both at home and abroad, are reviewed and data on existing and proposed tube dimensions and drawing formulas are summarized. It is recommended that the wall thickness be reduced by 20 percent as a first step toward mastering production of new tubes and reducing the volume of imports. The effect of the total tube deformation after cold mandrel drawing and the optimal combination of deformation along the wall thickness and diameter on the tube's endurance strength is evaluated and it is shown that the optimum total deformation falls within a 25-30 percent range while the wall thickness deformation should exceed that along the diameter. The use of coil steel 20, 25, and 08GSYuT is recommended. Production of thin-walled tubes for vehicle cardan shafts makes it possible to maintain the present production level while increasing the metric tube output by 17 percent and reducing outlays of foreign exchange. Tables 1; references 4.

Transfer Hopper Charge Level Control System of Sinter Machine

927D0175D Dnepropetrovsk METALLURGICHESKAYA I GORNORUDNAYA PROMYSHLENNOST in Russian No 4 (162), Oct-Dec 91 pp 24-26

[Article by I.M. Salnikov, V.D. Getalo, A.T. Getalo, Zaporozhstal Integrated Iron and Steel Works; UDC 622.786.36.002.5:622.693.23]-52:669.162.262]

[Abstract] Stage-by-stage implementation of a charge level control system in the transfer hoppers of six sinter machines (SAR) made with standard "AND Logic" integral logic elements which uses the proportionate-integral (PI) control law of the charge level is described. The system consists of two contact electrodes, a logic control module, and power supply unit, and an amplifier. The operating principle and operating modes of the charge level control system are outlined and a schematic diagram of the contact electrode placement in the transfer hopper is cited. The effect of the charge moisture content and chemical composition on the level-gauging process is eliminated by using discrete inputs from two electrode level gauges while the charge level is maintained within 200 mm. Automatic control system implementation in six sinter machines makes it possible to regulate the sintering process and sinter quality while saving solid fuel used for sintering. The economic impact from the system reaches 20,900 rubles per year. Figures 2.

Ways of Improving Deep Floor Mining Efficiency at Ingulets Ore Dressing Combine Quarry

927D0175L Dnepropetrovsk METALLURGICHESKAYA I GORNORUDNAYA PROMYSHLENNOST in Russian No 4 (162), Oct-Dec 91 pp 53-55

[Article by A.V. Krivosheyev, Ingulets Ore Dressing Combine; UDC 622.341.1: [622.012.3: 622.221.3]: [622.647: 65.011.46]

[Abstract] A new trend towards increasing the utilization of cyclical flow-line technology at ore dressing combines, particularly at the Ingulets Ore Dressing Combine in the Krivoy Rog Basin (Krivbass) which produces close to 140-150 million tons of iron ore per year is considered and it is shown that the use of cyclical flow-line technology alone makes it possible to maintain the high ore yield of collieries while stripping 150-250 m deep levels. Mining techniques which make it possible to lower labor outlays by using vehicles and conveyor for transferring ore and utilizing gravity feed for the rock mined at the upper level and conveyors for hauling ore from lower levels in relation to a stationary transfer station are outlined. The method also makes it possible to reduce the volume of truck haulage. Experience shows that iron ore colliery stripping depth may be increased to 10-12 or more levels by using the new procedures with a crushing and transfer station at mid point in the zone. It is speculated that the trends is toward using more conveyor transport in the quarries and thus decreasing harmful discharges into the atmosphere. M.S. Chetverik and V.P. Shportko participated in the study.

Using Biolocation in Mining in Krivoy Rog Basin

927D0175M Dnepropetrovsk METALLURGICHESKAYA I GORNORUDNAYA PROMYSHLENNOST in Russian No 4 (162), Oct-Dec 91 pp 55-57

[Article by G.A. Libster, A.I. Chirva, Krivoy Rog Mining Institute; UDC 622.341.1:[528.481:550.87].001.5 (477.63)]

[Abstract] The use of extrasensory perception (biolocation) in various human endeavors, e.g., mining, since the prehistoric days are reviewed and biolocation applications in the United States, Western Europe, and Australia for geological exploration in general and mining in particular are discussed. The history of biolocation in the USSR since N.N. Sochevanov's experiments in the 1960's and the results of biolocation studies aimed at locating and outlining underground cavities in the Krivbass are summarized. The physical essence of the phenomenon is addressed and credit is given to A.F. Okhatrin for pioneering work in this field. The findings obtained to date attest to the fact that biolocation is mostly a subjective phenomenon and is definitely reproducible, i.e., does not belong in the domain of superstitions, miracles, and mysticism. It is noted that the lack of sound physical interpretations should not stop biolocation experts from pursuing the subject further since available experience shows that the method is by far the cheapest prospecting technique. References 7: 6 Russian, 1 Western.

Detonation Wiring Network Which Expands Short-Delay Blasting Capabilities

927D0175N Dnepropetrovsk METALLURGICHESKAYA I GORNORUDNAYA PROMYSHLENNOST in Russian No 4 (162), Oct-Dec 91 pp 57-59

[Article by V.R. Dyadyushko, V.A. Zayarnyuk, Yu.N. Kireyev, S.A. Kovrigin, A.G. Lukashenko, Dnepropetrovsk Mining Institute and Sokolovsko-Sarbayskiy Ore Dressing Production Association; UDC 622.235.432.352.001.76:621.316.1.014.2]

[Abstract] The shortcoming of the electric detonators for short-delay massive explosion methods used in mining are discussed and a special distribution wiring network (SRS) developed by the authors which makes it possible to use short-delay electric detonators in groups of charges whose operation error does not exceed the tolerated error is described. The new network's principal function is to distribute the current in the explosion circuit so as to ensure that the first group of electric detonators is set off first, then the second one after a

certain specified time interval. The special distribution network consists of two groups of electric detonators (ED), a controlling electric detonator, adjustable series resistors, and a shunting resistor. The purpose and operating principle of network elements are outlined and the conditions which the distribution network parameters must satisfy to ensure correct detonation timing and conform to the Unified Safety Rules (YePB) are derived. The specific features of the special distribution network wiring are summarized. The detonation wiring network for alternate priming of two groups of charges with the same set of delay factor makes it possible to increase the number of delay steps while the detonation network parameter analysis procedure increases the charge detonation safety and efficiency. The device passed commercial tests and was certified by the USSR State Engineering Inspection Service for use in underground mines with electric detonation circuits. Figures 1.

Ways of Improving Mining Surveys of Ore Deposits Under Cost Accounting Conditions

927D0170I Dnepropetrovsk METALLURGICHESKAYA I GORNORUDNAYA PROMYSHLENNOST in Russian No 1 (163), Jan-Mar 92 pp 44-46

[Article by B.Ye. Povnyy, Krivoy Rog Mining Institute; UDC 622.013.362:622.271].001.24:681.3:[338.244.018]

[Abstract] The old instruction from the metallurgy ministry governing the procedure for mining surveys of ore reserves and movements and the need to reevaluate the approaches to estimation and exploitation of ore reserves in the light of new economic conditions are discussed and it is suggested that existing mining survey procedures be amended. This would call for taking into account explored, blocked-out, prospected, extrapolated, inferred, and stripped reserves and determining and standardizing mineral extraction indicators. A sample form for reporting the state and movement of commercial ore reserves is designed and the impact of implementation of a computer-aided system of calculating actual reserves in each category is summarized. The new surveying procedure makes is possible objectively to analyze the development of mining operations, compare actual mining reserves in all categories to standards, establish optimum strip mining parameters and regulate the loss, depletion, and contamination characteristics, predict the volume of work and outlays for future mining operations, and automate all computations. Tables 1; references 4.

On Using Draglines for Hoisting Rock in Deep Quarries

927D0170J Dnepropetrovsk METALLURGICHESKAYA I GORNORUDNAYA PROMYSHLENNOST in Russian No 1 (163), Jan-Mar 92 pp 47-49

[Article by L.M. Solodovnik, S.A. Stepchenkov, I.I. Lelyakov, N.P. Benko, V.A. Gontsul, OPPRE ITM at Ukraine's Academy of Sciences, Dnepropetrovsk Mining Institute, and Poltava Ore Dressing Combine; UDC 622.271:622.693]:621.879.323]

[Abstract] The falling technical and economic indicators of the trucks used to haul rock in deep quarries with an increase in the stripping depth, e.g., over 100-150 m, and the resulting need for intraquarry transfers prompted the use of draglines at transfer stations for hoisting the rock. The resulting increase in the strip mining efficiency, especially in steep dipping deposits, is analyzed and the specific factors are identified: distribution and mobility of the transfer stations and the resulting shortening of the rock hauling distance and the possibility of hauling rock without crushing it beforehand. A schematic diagram of rock hoisting in a quarry by draglines is cited and the dependence of economic efficiency on the dragline height over the quarry floor is plotted. The parameters necessary for feasible dragline operation are derived. It is shown that at a rock's specific gravity of ¾ t/m^3, the annual operational yield is 3.4 million t/year for the ESh-6/45, 4.8 million t/year for the ESh-10/70, and 5.3 million t/year for the ESh-15/90 draglines. The conclusion is drawn about the expediency of using the ESh-10/70 draglines for hoisting rock in deep quarries. Figures 2; references 1.

Underground Ore Dressing Mill Under 'Gigant' Mine Conditions

927D0170K Dnepropetrovsk METALLURGICHESKAYA I GORNORUDNAYA PROMYSHLENNOST in Russian No 1 (163), Jan-Mar 92 pp 49-50

[Article by V.I. Karamzin, S.G. Borisenko, V.N. Bespalko, V.A. Sirotyuk, Dnepropetrovsk Mining Institute; UDC 061.5:622.7](24):502.55(477.63)]

[Abstract] The severe environmental impact of the mining and metallurgy industries and the increasing demand for waste and tailings dump areas prompted a feasibility study of ecologically clean metal mining technologies whereby ferrous quartzites are transferred underground and the principal body of waste is buried underground in the worked space. The principal premises of such an enterprise developed at the Dnepropetrovsk Mining Institute for the Kremenchug Iron Ore Deposit are outlined and the "Gigant" mine in Krivbass is used as an example. A block diagram of the prospective underground ore dressing mill in the "Gigant" mine is cited and it is demonstrated that its implementation will make it possible to produce high-quality concentrate and lay the groundwork for the development of coke-free metallurgy. Utilization of this mill's experience by other enterprises in the industry will make it possible to increase the nonferrous metallurgy production efficiency and make a radical change in the industry's environmental impact. The pilot mill is expected to have a 2 million t/year output. Figures 1.

Ecology of Massive Explosions in Collieries

927D0175A Dnepropetrovsk METALLURGICHESKAYA I GORNORUDNAYA PROMYSHLENNOST in Russian No 4 (162), Oct-Dec 91 pp 5-6

[Article by E.I. Yefremov, V.D. Petrenko, IGTM at the Ukrainian Academy of Sciences; UDC 622.233.012.3: 622.235.023.22]: 628.511]

[Abstract] The environmental impact of the dust and gas released during explosions in the mining industry, especially today when the volume of strip mining is constantly increasing, is considered and its is noted that a plume of a gas and dust mixture ejected by explosions in collieries rises up to 1.5 km into the atmosphere and its volume reaches millions of cubic meters with a dust concentration of up to 2 g/m^3. Consequently, the principal factors responsible for upsetting the ecological balance as a result of massive explosions in strip mines are investigated on a scientifically sound basis and quantitative estimates of the fraction composition of the blast hole drilling products which determine the dust formation patterns are derived. An analysis shows that the volume of dust and gas effluents may be decreased considerably by reducing the drill hole diameter. Engineering measures for decreasing the environmental impact of explosions by using spacing the explosive charges or using explosives (VV) with a zero oxygen balance are examined and substitution of today's explosives with the less harmful ones, e.g., grammonite, is considered. The study shows that removal, utilization, or binding and wetting of the drilling mud and blasting of wide benches as well as the use of new explosion procedures are the principal trends in lowering the harmful effect of massive explosions. References 4.

Effect of Sociopsychological Factors on Occupational Safety

927D0175C Dnepropetrovsk METALLURGICHESKAYA I GORNORUDNAYA PROMYSHLENNOST in Russian No 4 (162), Oct-Dec 91 pp 20-22

[Article by V.T. Britan, Yu.Ye. Shulga, P.V. Girich, Dnepropetrovsk Metallurgical Institute and Zaporozhstal Integrated Iron and Steel Works; UDC 621.771.23.016.3:[614.8:65.013.001.5]

[Abstract] The causes of occupational injuries in the metallurgical industry, primarily due to human errors, are discussed and the effect of the sociopsychological factors on the occupational safety at integrated iron and steel works is considered. To this end, the social and psychological factors which negatively affect the behavior, physical condition, and working fitness of workers and occupational safety are investigated for the purpose of making practical recommendations for lessening this effect. The following methods are used: administering questionnaires to workers, both injured and uninjured; testing the healthy workers; interviewing the workers, foremen, team leaders, shift supervisors, and section chiefs; and analyzing documents dealing with the occupational safety and safety engineering issues. The study is carried out in the specific setting of cold sheet rolling mill No. 1 (TsKhP-1) since 13-17 percent of accidents recorded at the integrated iron and steel works occur there. Recommendations are produced for lowering the injury rate and setting up an efficient occupational safety and safety engineering system. It is suggested that economic and morale incentives be used to stimulate safe working conditions and that a new safety engineering dissemination system be used.

New Diode-Pumped CW Lasers Based on Compounds With Structure of Calcium Gallogermanate With Nd^{3+} Ions

927D0150K Moscow IZVESTIYA AKADEMII NAUK SSSR: SERIYA NEORGANICHESKIYE MATERIALY in Russian Vol 28 No 1, Jan 92 pp 141-145

[Article by A.A. Kaminskisy, H.R. Verdun, B.V. Mill, A.V. Butashin, Crystallography Institute imeni A.V. Shubnikov at the USSR Academy of Sciences, Fibertek, USA, and Moscow State University imeni M.V. Lomonosov; UDC 546.654:548.55+535.371]

[Abstract] Stimulated emission (SI) of gallogermanate crystals with Nd^{3+} ions and their lasing, optical, nonlinear, dielectric, elastic, and piezoelectric properties are discussed and the results of the fist successful experiment to excite continuous wave and quasicontinuous stimulated emission of Nd^{3+} ions in six laser crystals of calcium, lanthanum, and strontium gallogermanates, which belong to the same structural family of inorganic laser materials, at a 300K temperature ($^4F_{3/4} \rightarrow {}^4I_{11/2}$ channel) are presented. The single crystals for the study are grown by Czochralski's method in platinum crucibles in the third axis direction. A fragment of the crystal lattice is cited, absorption spectra of Nd^{3+} in the six gallogermanate crystals are plotted, and the cation distribution in the oxygen coordinates in trigonal Ca-gallogermanate structured crystals is determined. The principal luminescent and laser parameters of trigonal Ca-gallogermanate structured crystals activated with Nd^{3+} ions which emit in the CW and quasicontinuous mode at 300K under diode pumping are summarized; a 1 W Spectra Diode Lab SDL-2460-C diode laser structure is used as a pump. It is speculated that better results can be obtained in disordered oxide laser crystals. The authors are grateful to V. Koeschner for support and Ti-Chuang for help with measurements. Figures 2; tables 2; references 23: 13 Russian, 10 Western.

Spectral-Luminescent Properties of Laser-Active Phosphorus Oxide Chloride Based Fluids Under Excitation by Nuclear Reaction Products

927D0150L Moscow IZVESTIYA AKADEMII NAUK SSSR: SERIYA NEORGANICHESKIYE MATERIALY in Russian Vol 28 No 1, Jan 92 pp 162-169

[Article by Ye.A. Seregina, P.P. Dyachenko, V.V. Kalinin, O.D. Shevchuk, O.N. Gilyarov, Yu.I. Krasilov, B.N.

Kulikovskiy, T.L. Novoderezhkina, Obninsk Energy Physics Institute and General and Inorganic Chemistry Institute imeni N.S. Kurnakov at the USSR Academy of Sciences; UDC 535.376:546.657]

[Abstract] The spectral-luminescent properties of inorganic laser liquids (LNZh) on the basis of $POCl_3$-$SnCl_4$ activated by Nd^{3+} and Eu^{3+} or coactivated by Nd^{3+}, UO_2^{2+}, Nd^{3+} and Eu^{3+} under excitation by nuclear reaction products are investigated. The measurements are taken in the KG-0.3 accelerator at the Obninsk Energy Physics Institute operating both in the pulse and continuous mode using 10 samples. The luminescent characteristics of $POCl_3$-$SnCl_4$-based inorganic laser liquids are summarized and the luminescence photon and accelerator target neutron time distribution, the spread function of the luminescence photon count by wavelengths under nuclear reaction product excitation and optical pumping, the accelerator target neutron count distribution, and the dependence of the luminescence conversion efficiency on the Nd^{3+} concentration are plotted. The Eu^{3+} luminescence spectrum under nuclear reaction product excitation and optical pumping is recorded. Despite the luminescence quenching and the low fraction of sensitized luminescence photons, the discovery of the sensitization phenomenon is valuable for assessing the possibility of developing inorganic laser liquids on the basis of oxide-chlorides of two-center active systems. The maximum conversion efficiency of 0.95+/-0.08 percent is recorded at a Nd concentration of 2.9×10^{20} cm^{-3}. Figures 6; tables 1; references 8.

$Cu_4Rb_{0.5}K_{0.5}Br_3I_2$ Superion Conductor

927D0150M Moscow IZVESTIYA AKADEMII NAUK SSSR: SERIYA NEORGANICHESKIYE MATERIALY in Russian Vol 28 No 1, Jan 92 pp 182-183

[Article by V.V. Ivanov, Novocherkassk Polytechnic Institute imeni S. Ordzhonikidze; UDC 541.133: 537.311.3]

[Abstract] The possibility that a number of new isostructural compounds with a univalent copper ion conduction mechanism exists in superion conductors indicated by crystallochemical analysis of known superion conductors prompted an examination of the properties of superion conductors produced by isovalent isomorphous rubidium substitution with potassium. The concentration curve of the lattice constant and electric conductivity at 473K of solid solutions of $Cu_4Rb_{1-x}K_xBr_3I_2$ and the temperature dependence of the solid solution's electric conductivity at various x are plotted. Radiographic analyses of samples made by solid phase synthesis are carried out within a 297-480K temperature range; an X-ray analysis of powder sample data confirms the development of isostructural solid solutions; the lattice constant is equal to 1.041+/-0.001 nm. The reversible α - β phase transition at x=0.5 is accompanied by a change in the conductivity activation energy and a conductivity jump; the α-phase activation energy is 0.1 eV and the ionic conductivity at 473K is equal to 0.97 siemens/cm; the extrapolated value at 298K is 0.41 siemens/cm. Figures 2; references 3.

NTIS
ATTN PROCESS 103
5285 PORT ROYAL RD
SPRINGFIELD VA 22161

Foreign Broadcast Information Service (FBIS) and Joint Publications Research Service (JPRS) publications contain political, military, economic, environmental, and sociological news, commentary, and other information, as well as scientific and technical data and reports. All information has been obtained from foreign radio and television broadcasts, news agency transmissions, newspapers, books, and periodicals. Items generally are processed from the first or best available sources. It should not be inferred that they have been disseminated only in the medium, in the language, or to the area indicated. Items from foreign language sources are translated; those from English-language sources are transcribed. Except for excluding certain diacritics, FBIS renders personal names and place-names in accordance with the romanization systems approved for U.S. Government publications by the U.S. Board of Geographic Names.

Headlines, editorial reports, and material enclosed in brackets [ ] are supplied by FBIS/JPRS. Processing indicators such as [Text] or [Excerpts] in the first line of each item indicate how the information was processed from the original. Unfamiliar names rendered phonetically are enclosed in parentheses. Words or names preceded by a question mark and enclosed in parentheses were not clear from the original source but have been supplied as appropriate to the context. Other unattributed parenthetical notes within the body of an item originate with the source. Times within items are as given by the source. Passages in boldface or italics are as published.

SUBSCRIPTION/PROCUREMENT INFORMATION

The FBIS DAILY REPORT contains current news and information and is published Monday through Friday in eight volumes: China, East Europe, Central Eurasia, East Asia, Near East & South Asia, Sub-Saharan Africa, Latin America, and West Europe. Supplements to the DAILY REPORTs may also be available periodically and will be distributed to regular DAILY REPORT subscribers. JPRS publications, which include approximately 50 regional, worldwide, and topical reports, generally contain less time-sensitive information and are published periodically.

Current DAILY REPORTs and JPRS publications are listed in *Government Reports Announcements* issued semimonthly by the National Technical Information Service (NTIS), 5285 Port Royal Road, Springfield, Virginia 22161 and the *Monthly Catalog of U.S. Government Publications* issued by the Superintendent of Documents, U.S. Government Printing Office, Washington, D.C. 20402.

The public may subscribe to either hardcover or microfiche versions of the DAILY REPORTs and JPRS publications through NTIS at the above address or by calling (703) 487-4630. Subscription rates will be provided by NTIS upon request. Subscriptions are available outside the United States from NTIS or appointed foreign dealers. New subscribers should expect a 30-day delay in receipt of the first issue.

U.S. Government offices may obtain subscriptions to the DAILY REPORTs or JPRS publications (hardcover or microfiche) at no charge through their sponsoring organizations. For additional information or assistance, call FBIS, (202) 338-6735,or write to P.O. Box 2604, Washington, D.C. 20013. Department of Defense consumers are required to submit requests through appropriate command validation channels to DIA, RTS-2C, Washington, D.C. 20301. (Telephone: (202) 373-3771, Autovon: 243-3771.)

Back issues or single copies of the DAILY REPORTs and JPRS publications are not available. Both the DAILY REPORTs and the JPRS publications are on file for public reference at the Library of Congress and at many Federal Depository Libraries. Reference copies may also be seen at many public and university libraries throughout the United States.